A Dissertation

entitled

Examination of Oxidation Sites for Electrolytic In-Process Dressing (ELID) Grinding using SEM

by

Bader Mushabbab Alqahtani

Submitted to the Graduate Faculty as partial fulfillment of the requirements for the Doctor of Philosophy Degree in Engineering

_____

Dr. Ioan Marinescu, Committee Chair

_____

Dr. Sorin Cioc, Committee Member

_____

Dr. Mansoor Alam, Committee Member

_____

Dr. Sarit Bhaduri, Committee Member

_____

Dr. Matthew Franchetti, Committee Member

_____

Cyndee Gruden, PhD, Dean
College of Graduate Studies

The University of Toledo

May 2019

An Abstract of

Examination of Oxidation Sites for Electrolytic In-Process Dressing (ELID) Grinding using SEM

by

Bader Mushabbab Alqahtani

Submitted to the Graduate Faculty as partial fulfillment of the requirements for the Doctor of Philosophy Degree in Engineering

The University of Toledo
May 2019

Electrolytic in-process dressing (ELID) is a grinding technique used to generate high quality surfaces on hard and brittle material such as ceramics and sapphires. Compared to the use of conventional wheel sharpening techniques (dressing), ELID greatly reduces grinding wheel wear and grinding forces, while improving surface quality and dimensional accuracy. Oxide layer formed on grinding wheel during ELID grinding heavily influences the surface roughness of the workpiece. To study the microscopic structure of the oxide layer and model the thickness of it, we conducted a previously reported study on metallic bonded prism samples with major adjustments and implementations. The parameter studied are voltage, electrode-grinding wheel gap, and coolant flow rate. Scanning Electron Microscopy (SEM) images of cross-section of the oxidation sites were captured and compared and oxide layer thickness was accurately measured. The voltage, gap, and coolant flow pattern were found to significantly affect the forming of the oxide layer. SEM images provide evidence that ELID grinding can achieve high levels of surface finish.

Acknowledgements

I believe that we should always give honor to where honor is due. So I would like to thank my parents for their undying and consistent support over the years. You've loved and cared for me. You've instilled a strong passion for learning in me, and you've taught me that my success and greatness is limitless. I will forever remember the values you have passed down to me, especially that of perseverance and honesty. There simply aren't enough words to describe what you mean to me.

Undoubtedly, I have to show gratitude to my lovely wife, Hanan Abutaleb, and our 4 children: Mushabbab, Yahya, Yoseph and Mohammed. You each have loved me and encouraged me, especially when I needed it most. And this would have never been done without you. You are my inspiration and you are the reason why I work so hard. Thank you for staying by my side and for putting up with ALL of me. I'm beyond proud to be your husband and father. I appreciate every sacrifice, every ounce of encouragement, and every inch of patience. To Abdullah Alsaab, Mohammed Therwan, Abdulaziz Alshareef, and all my friends, I appreciate the positive influence you've had on my life. Thank you for your concern and useful advice. I'll be forever grateful.

I would like to thank my advisor, Dr. Ioan Marinescu. Your patience and friendship over the last several years have endowed me with great guidance and inspiration.

I would also like to thank Dr. Sarit Bhaduri, Dr. Sorin Cioc, Dr. Mansoor Alam, and Dr. Matthew Franchetti for serving on my committee and for all of their help and support.

The experimental work wouldn't have been accomplished without the assistance of Mr. John Jaegly, MIME Laboratory Supervisor, and Mr. Tom Jacob, EECS Electronic Tech.

And a very special thanks to Dr. Kristin Kirschbaum, Director of Instrumentation Center at The Department of Chemistry and Biochemistry, as well as Dr. Burckel Pannee, Instrumentation Scientist, for the permission and training to use the Scanning Electron

Microscopy (SEM). You all have made this moment possible. And I am forever grateful for you being intricate parts of my life. Again, thank you!

Table of Contents

List of Tables

List of Figures

Chapter 1

Introduction

The main findings of this study have previously been published by the International Journal of Advanced Manufacturing Technologies in 2019 under the title of "Microscopic characterization and modeling of oxide layer for electrolytic in-process dressing (ELID) grinding with focus on voltage, electrode-wheel gap, and coolant flow" Permission has been granted by publisher and co-authors for its use in this dissertation. The abstract and part of chapter 1 originally appeared in the journal paper.

Electrolytic in-process dressing technology (ELID) signifies the process which a metal bond super abrasive wheel is used with in-process dressing through the usage of electrolytic actions. The use of this technique shows a tremendous impact in surmounting the challenges of the normal grinding on the hard and brittle metals. Though the procedure can provide a continuous and even utilization of the metal bonded wheel throughout the grinding process, it also at the same time helps in maintaining the sharpness of these super abrasives wheels. This technology was invented by the Murat whereby he used the method to grind the ceramics using a metal wheel bonded with diamonds of the grit dimension smaller than 400 [Zhang, Ohmori, Li 2000]. In 1990,

Japanese researchers Ohmori and Nakagawa used ELID grinding to generate high-quality surfaces on hard and brittle materials [Ohmori, Nakagawa 1990]. Since then, this technique has been developed to generate mirror surfaces using ultrafine grain metallic bonded wheels [Ohmori, Nakagawa 1995]. As described by Ohmori [Marinescu, Ohmori, Katahira 2011].

Previous studies indicate that grinding of ductile material with smoother surfaces and lower surface damage was realized on silicon slices by applying super abrasive and the ELID technology [Chen, Li 2000]. Irrespective of these improvements that were done, the developments of the surface finishes were present where there was production of a layer of oxides on the exterior of that grinding disk. This layer that was introduced acted as a spring damper in which it resides the grit extent of penetration and embodies the vibrations in the ELID grinding technology [Zhang, Ohmori, Li 2000]. This method continuously exposes the new sharp abrasives grains in which they dissolve the metallic bind that is around the super abrasive grains which help to sustain a high substance removal rating and be able to achieve a uniform surface roughness.

Usually, the ELID contains a power supply, metallic bond grinding wheel, and a coolant which contains a high electrolytic characteristic. In this system, it usually has two electrodes whereby the metal bonded disk is attached to the positive terminal while the copper brush is connected to the negative terminal. Normally the power source is provided through the two electrodes. Normally the length between the electrodes is maintained at 0.1 to 0.3 mm. Given that the ELID provides the in-process dressing; as a

result, the time required for dressing is eliminated; further, dressing costs are also minimized. Additionally, the layer of oxides that is produced on the surface of the grinding wheel significantly leads to the reduction of the grinding force which is normal to the surface as compared to the convention grinding as a result through this method has a capability to achieve a high-quality surface finish.

1.1 Scope

The technique of grinding has helped in the removal of unwanted material in engineering, especially hard, brittle and tough parts formed through electrolytic action. Therefore, the material for the bonding surface is consumed gradually. The nature of the materials used determines the rate of consumption. Some materials accelerate the formation of this layer. For instance, iron has ability to form an added oxide (iron oxide) which increases the layer. However, other materials form very thin layer which is difficult to measure especially when the precision of the components undergoing electrolysis is the necessity. In addition, the rate of the layer's formation is directly proportional to the current and voltage supplied during the ELID grinding process. To achieve high precision and accuracy, a better research should be conducted to determine the best materials to be used for the wheel instead of using diamond, which is hard and can alter the surface of the work pieces. Nevertheless, the ELID components and variables used during measurements of the oxide layer formed should be optimized. Therefore, an investigation on the best amount of voltage and current applied, the gap between two electrodes, and velocity of the wheel should be conducted to obtain the best

products. There are various aspects as to why we study ELID since the current machining process for sapphire is majorly done by fine lapping, grinding and through the usage of the polishing.

1.2 Objective

The objectives of the research are summarized below:

- Investigation of the mechanism of ELID in relation to the factors that affects the oxide layers.
- A study on the ELID grinding using materials for the cast iron metal-bond other than diamond and stainless steel for the cathodes.
- Determine the effects of parameters on the oxide layer: parameters include voltage, coolant flow rate, the geometrical distance between the anode and cathode.
- The use of SEM Microscope to observe the state and measure the thickness of the oxide layer and to study the extensive comparison of the morphology of the cross-section of oxide layers.
- To study for the best alternative way for ELID grinding to avoid the conventional machining process for sapphire which majorly done by fine lapping, grinding and through the usage of the polishing.

1.3 Process overview

There are various aspects as to why we study ELID since the current machining process for sapphire is majorly done by fine lapping, grinding and through the usage of the polishing. By comparing the two processes for polishing and lapping, fine grinding can be efficiently used in the generation of geometric forms that are reflectively at low cost, though they are faced with challenges of wheel dressing, as a result, there is need to minimize surface roughness which in turn lowers the surface damage, the grinding wheel loading and minimization of the loading capacity. As a result, through this technology, it offers a greater promise in which it can overcome the conventional setback of grinding materials which are hard and brittle. This technique can provide the continuous and uniform dressing for the metal bonded wheels when undergoing the grinding process [Zhang, Ohmori, Li 2000].

According to past research done, results indicate that the electrolytic dressing forms oxide products on the surface of a wheel with a steel or iron bond matrix. The wheel normally goes through two phases of the dressing using the electronic in-process dressing in which the first phase is the pre-dressing whereby it removes the bond matrix for 1/3 to 1/2 of the grit particle size, in which it exposes the grit for use. These phases normally end automatically through the creation of an oxide layer thickness whereby it inhibits the electricity flow. Then the second phase occurs during the grinding. Normally the oxide layer is removed through the grinding action in which the electrical current is restored to the portion of the wheel in use. As a result, it causes a further oxide creation in this zone and a fine truing of any remaining run out from the wheel. Additionally, the

process continues to dress the bond in the portions where the grit is used. Usually, halting the grinding action leads to the creation of a new oxide layer and the dressing is inhibited automatically. This ability results in longer wheel life and a larger grinding ratio. In this technique, the creation of the oxide layer is assisted by the electricity that normally flows through one direction usually on the positive side of the electrode gap. The DC voltage is placed across the gap will cause the oxide to form.

In this stage of pre-dressing the grinding wheel, the abrasive material is in the form of grains and normally protrudes due to the removal of the metallic bonds from the surface of the wheel through the process of the electrolysis. At this moment, a layer of oxides forms on the surface of the wheel. Often, the bore of the grinding disk increase after pre-dressing due to the creation of the oxide layer. For the instance of a cast iron bonded grinding disk, the cast iron bond it is normally ionized into Fe2+.The ionized Fe later reacts with the hydroxide leading to the production of a hydroxide compound, in which it transforms to become an oxide of iron forming a protective layer on the surface of the wheel. This protective layer normally results in a reduced current flow, on the other hand, it increases the voltage in which it is termed as an anodic effect. The rate of growth of the oxide layer reduces with a reduction in the current flow [Zhang, Ohmori, Li 2000].

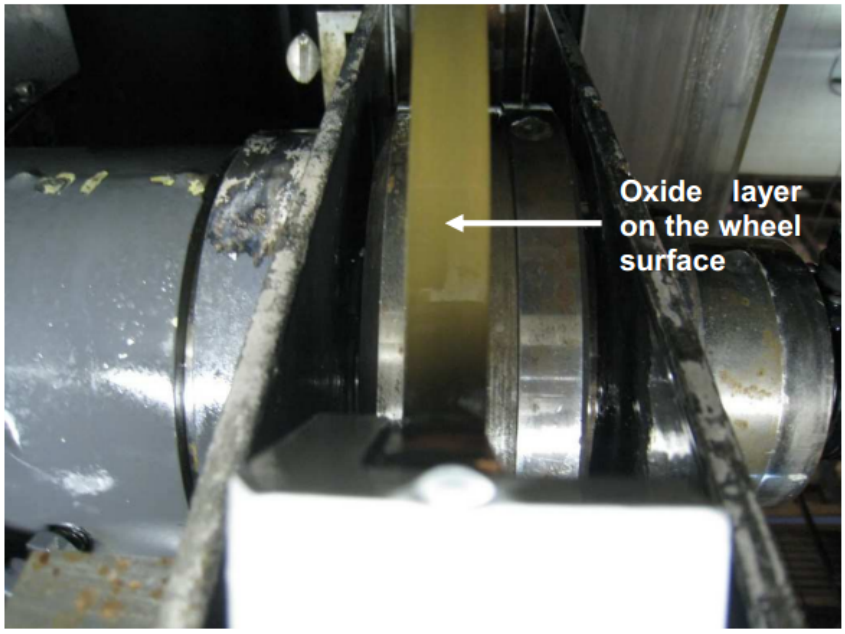

Figure 0 – 1: Shows the yellow-brown oxide layer formed on the cast iron bonded wheel surface [Han 2009].

The sketch above indicates the oxide coating that is produced on this cast iron surface that is bonded to the disk when the TRIM C270 in which it is utilized as the grinding fluid. Usually, the oxide coating plays a critical function in this ELID grinding method though the oxide coating grows so that the depth and the rate of growth are limited [Lim, Fathima, Senthil, Rahman 2002].

1.4 Coolant and Electrolysis

The coolant, the lubricant, and the flushing normally acts as the electrolyte to the ELID system in which these components of an electrolyte comprises of the pH value of the fluid, the electrical conductivity of the fluid and the metal corrosion inhibition. As a result of the grinding, it is recommended that the fluid to be used should of high conductivity and have a high PH value; it is recommendable to consider the metal corrosion inhibition on the electrolysis. As a result of the Ohm's law, the conductivity normally influences the electrolytic dressing and as a result impacting the current flow. The pH usually influences the ELID since the hydroxide participates present during the electrochemical reaction at the anode. As a result, pH of this solution used for grinding can be termed to be in the alkaline pH domain. As a result, most studies indicate that the electrolyte that has a higher pH value is more preferred since it normally elevates the oxidation rate of the electrolyte as shown below:

$$Fe \rightarrow Fe^{2+} + 2e^{-}$$
$$Fe^{2+} \rightarrow Fe^{3+} + e^{-}$$
$$H_2O \rightarrow H^{+} + OH^{-}$$
$$Fe^{2+} + 2OH^{-} \rightarrow Fe(OH)_2$$
$$Fe^{3+} + 3OH^{-} \rightarrow Fe(OH)_3$$
$$Fe(OH)_3 + O_2 \rightarrow Fe_2O_3 + H_2O$$

Equation 1

Normally the grinding fluid properties which may affect the electrochemical reaction resulting in corrosion impacts the dressing process's result and thus it is crucial to

be able to minimize and control any corrosion scenario for one to be able to protect the mechanical components and parts from corrosion. Taking for instance, manufacturer in many cases add corrosion preventers to the grinding fluid to maximize the corrosion prevention in which it is aimed to give protection to the wheel and the work piece. Therefore, a relatively low metal corrosion is recommended for the granulating fluid since it is important to ensure an effective ELID grinding process [Zhang, Ohmori, Li 2000].

Chapter 2

Literature Review

The technique of dressing grinding wheels with electrochemical technology was initially introduced by Murat in year 1985. The first technique to be invented was electrolytic in-process dressing (ELID), which was used for dressing metallic bonded wheels for rough grinding of structural ceramics with high strength. The ELID technology passed through various advancements based on experimental, experience and research. The major advancement took place at 1990s, when the fine grinding silicon wafers and the surfaces produced had a mirror finish. Controlling and optimization systems were also developed by other researchers and this further advanced the ELID technology [Rahman 2009].

An efficient and new method was later brought in play for grinding hard and brittle materials, holding grit size smaller than 1000 micrometers [Murata, Okano, Tsutsumi 1985]. According to Ohmori & Nakgawa, (1997), the experiment showed determine the parameters that affect the fluid and the oxide layer during the process of grinding. They proved throw mathematical calculations based on the results from series

of experiment that additive variety dominated the efficiency and productivity of the ELID.

2.1 ELID Grinding

The hard and brittle nature of structural ceramics implies that grinding them is a difficult operation. Grinding wheel of softer grades has been employed in machining the harder materials but they have diameter limitations due to wear [Doi, Uhlmann, Marinescu 2015]. Thus, harder abrasives with stronger bonds have been the better option. Electrolysis occurs on the new layer formed due to grit wear resulting in bonding removal for improved protrusion of the grits [Rowe 2013]. With in-process grinding, the grinding force is considerably reduced in ELID.

2.2 Types of ELID Grinding

Based on the applications of the grinding process and the materials on the ground, the process of ELID grinding can be categorized into four major classes despite the imminent similarity in the in-process dressing principles [Xu, Spanu, Marinescu 2015]. These four categories include the listed below. Electrolytic In-process Dressing (I), Electrolytic Interval Dressing (II), Electrolytic Electrode-less dressing (III) Electrolytic Electrode-less dressing using alternate current (IIIA).

The first type is Electrolytic in-process dressing (I). The basic components of the ELID system include an electrode, metal bond grinding wheel and a source of power

[Wang, Ren, Chen, Zhang, Deng 2018]. The spacing between the grinding and the electrode may be adjusted to a 0.2 mm with 0.1 mm positive and negative extensions allowed [Xu, Spanu, Marinescu 2015]. This determines the in-process dressing since it allows for ease flow of the coolant used. The grinding wheel parameters dictate the size of the electrode which could be 1/ 4 or 1/6. The electrode material selected in this case could be graphite or copper in normal circumstances. A cup or straight type of wheel is used in these applications with the shape of the electrode normally being an arc.

The second type is electrolytic interval dressing (II). In most fields in industries, hard and brittle materials are required to be machined with some having small-hole machining requirements [Doi, Uhlmann, Marinescu 2015]. Machining in micro holes presents challenges among them difficulties in high quality preparation of small grinding wheels, compensation determination of the wear in the grinding wheel and unsatisfactory machined-hole surface finish and accuracy. The suitability of the existing grinding processes in machining micro-holes is thus not satisfactory due to electrode mounting challenges [Maitra 2013]. Thus the Electrolytic Interval Dressing (II) and the Electric Discharge Truing (EDT) are the suitable approaches for micro-hole machining in combination with small diameter grinding wheels. The EDT method helps in improving the accuracy of the smallest grinding wheel by 0.1 mm. Improved grain protrusions can be achieved by pre-dressing the small grinding wheels by use of electrolysis [Wang, Ren, Chen, Zhang, Deng 2018]. Excessive wear of the grinding wheel can be avoided by careful selection of the dressing parameters. Based on the force of grinding, a definite interval is used for the grinding wheel. Redressing the wheel is required if the threshold of the grinding force is exceeded beyond the set value.

The third type is electrode-less in-process dressing (III). Clogging and wheel loading are among the challenges encountered when ELID grinding is used with materials such as steel [Jackson, Davim 2011]. The wheel effectiveness is reduced by swarf that embeds on the surface of the grinding wheel. The grinding wheel effectiveness is increased with the smaller sizes of the swarf removed. Grinding wheels with metal resin bonding are adopted for conductive materials machining such as hardened steels [Wang, Ren, Chen, Zhang, Deng 2018]. The electrode in this case will be the the conductive work piece with the process of electrolysis occurring between the work piece and the grinding wheel. Bronze and copper are among the bonding materials used in this case. The diamond grit is used for removing the electrolytic layer that forms on the work piece thus allowing Therefore, the electrode-less in-process dressing (III) helps in controlling the swarf production [Xu, Spanu, Marinescu 2015]. The process of electrolytic dressing results in oxidation of the base material with the resins and diamond grits contained in the wheel surface. The electrolysis process is initially intended to remove the metal bonds but results from experimentation indicate that cavity spaces are contained in the surface of the grinding wheel as a result of the discharge in electricity. The election of high electric parameters results in an increase in the amount of discharge causing damage to the ground surface as well as the wheel [Doi, Uhlmann, Marinescu 2015]. The selection of low feed rates, low duty ratios, low currents and low voltages helps in generating a better surface finish.

The last type is electrode-less in-process dressing using alternative current (IIIA). This process is used to eliminate the electrode-less in-process dressing difficulties. The surface of the work piece is coated by a thick oxide layer as a result of the alternative

currents preventing the grinding wheel from coming into direct contact with the work piece [Wang, Ren, Chen, Zhang, Deng 2018]. Thus, the process improves the surface finish by eliminating the electric discharge between the work piece and the grinding wheel.

2.3 ELID Grinding Components

The demand for high precision in machining mechanical components and elements has been on an increase over the recent years. Innovations and inventions of new and better components are made in the engineering sector. Nevertheless, the ELID components have undergone gradual but significant changes over the years since its inventions at about 18th century. The gearing factor for the invention and innovation for the ELID grinding systems is to improve wear resistance, attain lighter components and resist corrosion under extreme conditions by making it harder, brittle and tougher [Gizella, Zoltán 2003].

The self-sharpening effect of the grinding wheel requires the electrolyze cell. A power supply, electrolyte, electrode and a conductive wheel are the cell components which form the ELID system. While establishing contact with the wheel shaft, the brush is smoothly applied to make a positive pole on the metal-bonded grinding wheel. The negative pole thus becomes the electrode [Doi, Uhlmann, Marinescu 2015]. An electric current and the grinding fluid is supplied through the narrow gap between the negative pole and positive pole where electrolysis occurs. The different components are discussed further below.

2.3.1 The ELID-Grinding Wheels

The grinding wheel is made up of a variety of abrasives which vary in size and composition and are normally bonded by different bonding materials and components. As a result of the abrasive grains, the bond material and the pores that are available to the grinding wheel normally influence the electrolytic dressing process. For the case of the kinematic grinding parameters, they involve factors of the speed of the wheel, the rate of feed and the cutting depth. For the pre-dressing phase, the speed of the wheel is the only factor analyzed.

Their benefits of studying the measurement of the cross-section area of the oxide layer in which from most researchers they indicate those grinding exercises with thicker layer normally results in the production of the smooth surfaces compared with wheels having thin oxide layers. From the available experimental data, results indicate clearly that the grit depth can be varied by adjusting the strength of the bond. The thickness of the oxide was obtained through studying the various coordinates on the CNC grinder just prior and after the session of the electrolytic dressing if the grinding disk surface touched the similar work piece cover. In which from the experimental result it shows that the speed of the wheel did not affect the ELID pre dressing and the oxide coating thickness over a range between 200 RPM and 1000 RPM.

Conductive materials are used for making the grinding wheel including bronze, copper and cast iron [Xu, Spanu, Marinescu 2015]. A mixture of the diamond grits and the metal is used for the preparation of the diamond layer with powder metallurgy used

for the preparation of the wheels. The grinding wheels have a variety of shapes and sizes for different applications.

2.3.2 The Electrodes

The grinding wheel determines the shape and size of the electrode dimensions. Attempting to remove any hindrance in the machining process is the sole reason for the choice of the size of the electrode. The effect of electrolysis is reduced by higher grinding wheel spindle speeds [Saleh, Bahar 2017]. Therefore, the electrode size should be carefully selected to ensure it matches the required in-process dressing effect. The width of the grinding wheel provides a basis for which the electrode thickness can made 1 – 2 mm larger.

The electrode materials are commonly chosen from stainless steel, graphite and copper. A thin layer is formed on the surface as the migration of the metal ions occurs from the anode to cathode thereby necessitating the need for galvanization. The selection of the material for the cathode should therefore be carefully analyzed [Xu, Spanu, Marinescu 2015]. The process can use the electrochemical electromotive sequence to investigate the reaction of the material in electrolysis. Anode mud is formed for materials that do not react such as copper. Electrolysis however occurs for materials with a lesser standard potential than copper. The capability of the standard potential is indicated by giving up electrons in regard to hydrogen ions [Doi, Uhlmann, Marinescu 2015]. This implies, oxidation occurs more readily with negative potential elements and more difficult to occur with than hydrogen with positive potential elements. Copper ions precipitate in the cathode during the process of grinding with grinding wheels bonded

with copper thus forming a more pure layer of copper. The anode mud is formed of the impurities in the grinding wheel that do not react during the process of electrolysis [Jackson, Davim, 2011]. Therefore, when using wheels bonded with bronze and copper, a conductive and pure cathode ought to be used.

2.3.3 Electrode Spacing (Gap)

While the gap between the electrodes should allow for ease of flow of the electrolyte, it should not exceed the thickness of the layer of the oxides formed. The gap can be adjusted between 0.1 – 0.3 mm accordingly. Nonetheless, the wear of the wheel makes it difficult maintaining it throughout the process [Wang, Ren, Chen, Zhang, Deng 2018]. Therefore, automated adjustment systems should be used for this process with gap sensors aiding the determination of the separation.

2.3.4 Electrolyte

The in-process dressing process is critically determined by the electrolyte. The electrolytic properties determine the performance of the grinding [Yu, Huang, Xu 2016]. If a soluble oxide layer is formed during the process, the wheel surface will bear no oxide layer. The process however adopts an electrolyte for which the oxide layer will be a non-soluble. This therefore results in metal deposits on the surface of the grinding wheel in this process [Wang, Ren, Chen, Zhang, Deng 2018]. Water is used to dilute the electrolyte which also acts as a coolant for the grinding operation. Chlorine influences the electrolysis due to positive potentials and this should be put to consideration. [Prabhu,

Vinayagam 2013] found that adding carbon nanotubes to conductive coolant could greatly lower the surface roughness and the number of micro cracks.

2.3.5 Power Sources

Normally the ELID power supplied to the negative and the positive electrodes whereby the electric conductivity of the wheel rises, in which it activates the electrolytic dressing. Usually, the consignations that are supplied to the pulse current normally impact the amount of the layer oxidizing from the grinding wheel surface [Lim, Fathima, Senthil, Rahman 2002]. When long pulses are introduced to the system, they increase the wheel wear, while for the short pulses of time they improve the grinding efficiency. Therefore, when changing the electrical parameters, they normally influence the in-process dressing and the layer thickness.

According to studies done, they indicate that the three are just one self-governing parameter that can show how the electrical energy is applied during electrolysis in a specified period [Lim, Fathima, Senthil, Rahman 2002]. A number of the studies indicate that the voltage the ELID system should be between 60 to 90 V which is recommendable to the ELID grinding. Considerate of the DC, pulsed DC and AC power sources, each has its own set of advantages to the process. The dressing currents in recent studies have been found to produce more control with pulsed power than the rest [Xu, Spanu, Marinescu 2015]. An understanding of the basic pulsed DC supply is however essential prior to its use in application. [Yang, Ren, Jin 2010] developed a fuzzy control program using a high-frequency pulse power supply. [Lee, Kim 1997] provided a theoretical analysis and

developed a basic system for optimum ELID grinding by monitoring the change of grinding current.

2.4 Fundamentals of ELID Grinding

The fundamentals of ELID technology, covering many current topics related to control systems, machine development, and the application of ELID technology to various materials was reviewed by Rahman [Saleh, Rahman 2014]. The ELID system uses electrolysis process for electrolytic-dressing. The worn abrasive parts and grains protrude from the wheel surface during the in-process dressing, which bonds with the bonding materials. The protruding grains are made of cast irons: has good electrical conductivity. The fig 2-1 below shows a typical ELID grinding system construction.

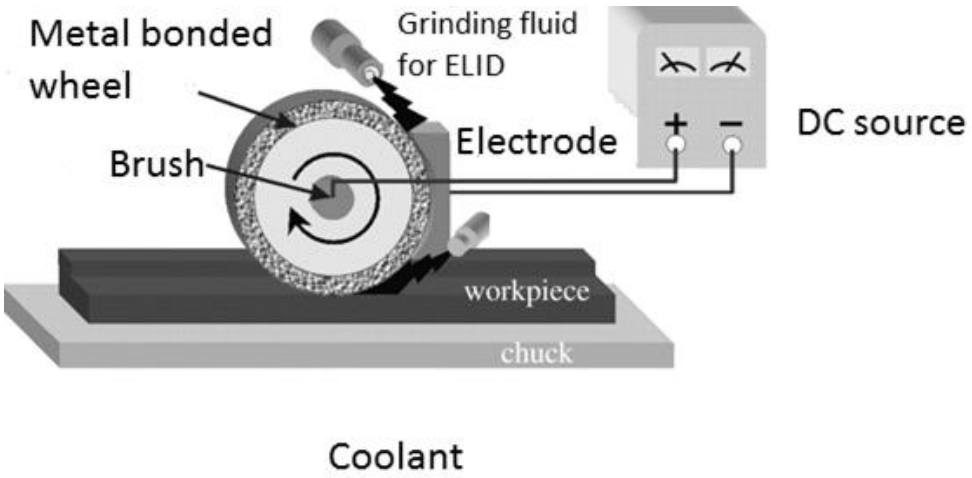

Figure 0 – 1: Shows the basic construction of an ELID system [Ohmori, Marinescu, Katahira 2011]

The metal bond is ionized and removed through the electrolysis process. The bond on the grinding wheel is ionized into Fe^{2+} as shown in then equation below.

$$Fe + 2\ H_2O \text{ -+ } Fe_2(OH) + H_2$$

Fe^{2+} forms hydroxides that further changes into metallic oxides and grow on the wheel surface, hence, lowering the electro-conductivity. Therefore, the current and voltage flow in the system will be adversely affected. The thickness of the formed oxides layers rely on rate of chemical reaction and the stability of the oxides.

The ELID technology is performed by making metallic bonded grinding wheel the anode and providing a conductive cathode. A gap of a range of 100μm to 500μm is established between the grinding wheel and the cathode where the electrolytic action occurs [Saleh 2008]. The electrolytic action is usually initiated by a high DC voltage (usually between 60V and 120V) and the electrolysis doubles when the coolant is flushed into the existing electrode gap, with a pulsating and a high frequency power source. The

electrolysis results is the formation of a soft, friable, brittle and an insulated layer of an anodic oxide. The layer is formed after the electrolysis consumes the metal present in the grinding wheel [Gizella, Zoltán 2003]. The brittle and soft nature of the oxide makes it easy to wear off during the grinding action and hence the grinding wheel will start to expose the sharp abrasives which are usually embedded in most of the metallic bonded matrix. Further the removal of the anodic oxide during grinding helps in the elimination of the grinding chips and abrasives that may be blunt. The electric insulation of the layer of anodic oxides reduces resistance as it wears off and hence it increases the dressing current leading to formation of more anodic oxide layer and as a result the eroded oxide layer is reinstated in the process of grinding [Biswas, Kumar, Rahman 2010].

According to Gizella & Zoltan, (2003), since the protruding grains are responsible for grinding process of the workpiece, as shown in fig 2-2 below, it wears down as well as the oxide layer. The electro-conductivity of the wheels will increase as a results of this wear of oxide layer. The flow of the current in the circuit will subsequently increase and the worn grains fades rapidly as the new grains forms due to weakening of the fixing force of the grains through machining of the bond by continuous and constant electrolytic dressing. This allows to get rid of the worn out grains easily.

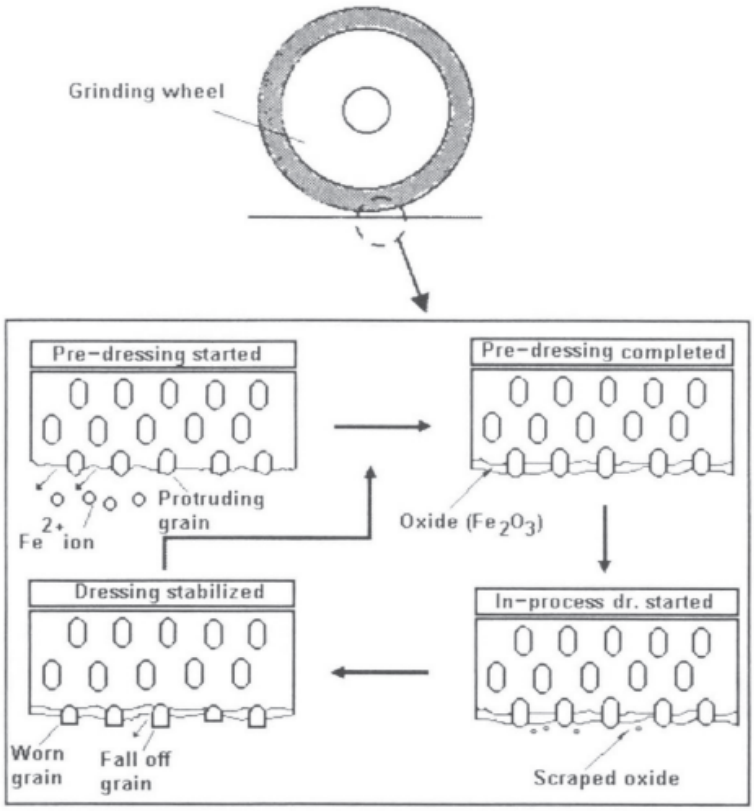

Figure 2 – 2: A schematic showing the mechanism of an in-progress dressing [Lee 2000]

Subsequent grinding will again erode the anodic oxide and then it regenerates again during the grinding process. The cycle repeats itself during any grinding action. This makes it essential for the anodic oxide layer to be available for achievement of an efficient and effective ELID grinding [Saleh 2008]. But usually the layer is not available at the start of the grinding process and therefore it has to be grown before the grinding operation starts, the growing procedure is called the pre-dressing procedure and it is done with only the grinding wheel rotating without performing any grinding operation takes 10

to 90 minutes depending on the user requirements. The basic principles of a typical ELID grinding are well illustrated by the fig 2-3 below.

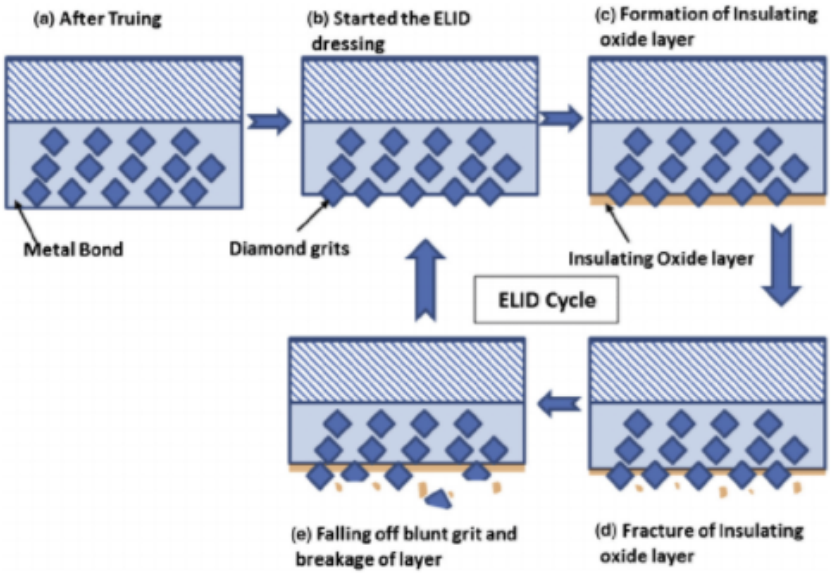

Figure 0– 3: Illustrate the basic principles of ELID grinding (Selah & Rahman, 2014)

2.5 Detailed Mechanism Analysis of ELID Grinding

The ELID grinding operation was initially developed by Murata and it was applied for coarse grinding of only structural ceramics and it used grinding wheels with 400μm abrasive size. And with some advancements of the ELID grinding technology, Ohmori came to prove that the process was also valid for application on fine grinding of brittle and hard materials. Also, the end surface was of mirror finish. Therefore, the technique came to be applied in fine grinding of silicon wafers, BK7 glass and silicon nitride, the fine surface finish was achieved by grinding the materials with grinding

wheels fitted with ultrafine abrasive sizes from different grinding schemes [Rahman 2009].

The ELID technology has also been performed for cast iron bond grinding wheels. According to Ohmori & Nakgawa, (1997), when the wheels were made anodic, the iron metal dissolved into the electrolyte forming ferric and ferrous ions (see equation 1). The electrolyte afterwards dissociated to form hydroxyl and hydrogen ions. The hydroxyl ions moved towards the wheel anode due to their negative charge forming ferric and ferrous hydroxides, which form a layer on the grinding wheel surface. In this research, exploration of possible variations of the wave forms of the input voltage, the electrolyte to use, the bonding materials for the grinding wheels and the magnitudes of the grinding forces to be applied for different electrolytes were conducted. The changes in dressing voltage and current during the pre-dressing process were also investigated and it was established that for a cast iron bond-diamond grinding wheel, the thickest anodic oxide layer was produced when a DC power supply was use. The use of a pulsating DC power source produced a medium anodic oxide layer. Whereas an AC power supply produced the smallest layer of anodic oxide. However pulsating DC power supply became the most preferred choice for ELID because it was characterized by the lowest corrosion of metal bonds [Ohmori, Nakgawa 1997].

Ohmari and Bandyopadhyay, contributed to advancement, understanding and development of the ELID technology by discussing unstable and stable nature of the necessary grinding forces (Xu et al, 2015). Klocke compared the oxide layer thicknesses formed on different bronze-bonded grinding wheels [Klocke, Klink, Henerichs 2009]. According to Wu et al. (2018), a study to compare the results of the variation of the duty

ratios and feed rates and later comparing the values to those from other conventional grinding techniques was conducted. From this research, it was established that the anodic oxide layer grows and build up to a specific thickness where the magnitude grinding force is high enough to break the oxide layer thickness, and hence this force reduces the thickness of the anodic oxide layer. With the anodic oxide layer reduced, the dressing current starts to increase. This investigation proved that the anodic oxide layer enhances finer surface finish and also functions as a damping mechanism. A higher duty ratio results not only in the reduction of the values of roughness of the material surface, but it also increases the wear rate of the grinding wheel. The maximum grinding federate after which the grinding burn may occur is call the threshold feed rate value, the grinding burn occurs due to a very high grinding wheel wear rate which outruns the rate of the anodic oxide formation.

The generation of a mirror surface (fine surface finish) on the brittle and hard materials is usually possible via a technique called the *ductile regime grinding*. Fathima is a researcher who proved that a high critical depth of cut on a material with the use ELID technology can easily lead to the production of a mirror finished surface, unlike in most conventional grinding techniques. The research linked the oxide layer which is an active part of the grinding wheel to the success of ductile regime grinding, it also established that the main cause of wheel wear was macro-fractures which could be limited by employing a shorter pulse time, the ductile regime grinding technique was fully dependent on the electrolysis process. Damages on the material surfaces was linked to current duty ratio and Kumar reported that cracks and other brittle modes of material

removal was caused by low duty ratios and higher duty ratios produced better surface finish characteristics.

2.6 Parameters for a Hybrid ELID Grinding System

There are various parameters which are involved in the electrolysis process, and these parameters further complicate the mechanism in which the grinding is based on. Hence, it makes this technique very different from conventional grinding methods [Rahman 2009]. The advancement of the ELID technology modification and development of the main components of the electrolysis process, power supply, machine tools to use, grinding wheel type, electrolytes and electrodes aid in the achievement of an hybrid ELID technology. This modification has enabled the achievement of better and easier grinding technique.

2.7 Applications of ELID Grinding

The description in this stage involves the difficult to grind materials in the numerous applications. The ELID process have been applied in material removal operations in brittle and hard ceramic materials when utilizing a very low grinding force compared to the forces used in the conventional grinding techniques. ELID has also been successfully applied in fine grinding of almost every kind of hard and brittle material, these materials usually range from, BK7 glass, mono-crystalline silicon, hardened steel, silicon carbide, silicon nitride, aluminum nitride and many more other materials. The fine grinding usually provides a high quality surface finish which is characterized by a very

limited sub-surface damage [Saleh 2004] [Biswas, Kumar, Rahman 2010]. Rahman et al. had summarized some of the main areas of application of ELID grinding as discussed below [Rahman, Kumar, Lim, Fatima 2003].

The structural ceramic components: The high resistance to degradation, thermal resistance and wear resistance are among the considerations for the selection of structural ceramics in varied applications despite the difficulties in grind [Wang, Ren, Chen, Zhang, Deng 2018]. The low material removal rates of ceramic materials imply that grinding them to the required finish is a costlier and difficult process. The process of ELID grinding seeks to maintain grain protrusion as a constant with the cast iron–bonded diamond grinding wheels [Rowe 2013]. An increase in the material removal rate has shown the possible decline in the grinding force required under this operation. Previous studies have examined various components of ELID systems and found that varying the experimental parameters can greatly improve the material removal rate and surface quality of the workpiece. Bafakeeh studied the effects of grinding parameters (force, grinding wheel and spindle speed) on resultant material removal rate and surface roughness; he also found that trajectory of the workpiece had a significant effect on surface roughness [Bafakeeh, Khoshaim, Marinescu 2016].

Bearing steel: The manufacturing industries have gone to great lengths to implement the cylindrical surfaces. The rolling surface performance is majorly affected by the waviness and the surface roughness due to the vibrations and noise induced in the component being machined [Doi, Uhlmann, Marinescu 2015]. The sample roundness, waviness, surface finish and the ELID are used to carry out the steel precision grinding of bearing in comparison to other techniques used. The CBN and the cast iron-bonded

diamond wheels can be used for the process with the average finish compared between the results

Chemical vapor deposited silicon carbide (CVD- SiC): The excellent optical and physical properties depicted by the application of CVD-SiC have resulted in its widespread use in the recent past. The material hardness and brittleness have resulted in the imminent difficulties in machining despite the ideal advantage of the material in making reflections [Xu, Spanu, Marinescu 2015]. The ductile mode is the only process that will allow material to be removed with a Nano-surface finish. The thickness of the insulating layer in ELID has been found to be a major contributor of a better surface finish of the grind. This last damps the vibrations during the process, producing better finish.

Precision internal grinding: Manufacturing industries have been known to use the cylinder surfaces often for precision. The tolerance and the accuracy of the surface finish for hard and brittle materials are difficult to achieve since the grinding wheel profile greatly influences it [Yu, Huang, Xu 2016]. Good tolerances can only result when a perfect profile of the wheel is used. Internal grinding of the cast iron-fiber-bonded grinding wheels thus suits ELID-II process. EDT is then used to further the process improvements.

Mirror surface finish on optical mirrors: The conventional process of grinding is a difficult process for finishing of larger X-Ray mirrors [Saleh, Bahar 2017]. Higher machining accuracies are possible to achieve due to process of roughing and finishing of the ELID grinding.

Micro lens: Portable information devices, optical storage systems and fiber optics are among the applications of micro optical components. Smaller grinding wheels are required for micro component fabrication in addition to sufficient stiffness of the work pieces and low speeds of grinding [Doi, Uhlmann, Marinescu 2015]. The implementation of the one-pass grinding allowed lower feed rate and deep cuts to be made during the process. ELID grinding resulted in high accuracy and good profile on the micro lens produced.

Form grinding: The micro machining process greatly relies on the production of micro threads. The tolerance and the accuracy of the produced threads should be of top form [Yu, Huang, Xu 2016]. The process of machining micro threads is highly effective when the grinding wheels are small and hard with diamond bonding. A high profile grinding accuracy is produced with the help of cast iron-bonded diamond wheels [Hitchiner, Marinescu, Uhlmann, Rowe, Inasaki 2016]. Based on shape requirements, a special wheel form can be prepared.

Die Materials: The manufacturing industries are coped with the challenge of accuracy and high surface finish when machining hard die materials [Saleh, Bahar 2017]. The wear of the wheel is significantly increased with a lower grinding ratio. Such harder conductive materials can only be successfully ground with ELID–IIIA methods. The positive pole connects to the work piece while the negative pole connects with the grinding wheel with a bonded metal-resin [Xu, Spanu, Marinescu 2015]. An oxide layer is formed on the surface of the work piece as the process of electrolysis occurs between the grinding wheel and the work piece. This oxide layer improves the grinding wheel shape accuracy and surface finish while reducing the effective cut depth.

Precision grinding of Ni-Cr-B-Si composite coating: Material prevention from corrosion and wear is highly achievable through surface coating. A ground surface can be coated with the use of CBN grinding wheels [Wu, Ren, Zhang 2018]. Primary and secondary carbides indicate minimal damage with ELID surface finish. Localized fractures and carbide pullout are among the forms of damage present on the ground surface when the process is carried out without ELID as large particles are removed from the work piece [Doi, Uhlmann, Marinescu 2015]. The carbide pullouts are however eliminated in the ELID grinding giving a smooth grit projection.

Micro-hole machining: The manufacturing industries are often challenged with micro-hole machining in brittle and hard materials. Ceramics can be used with micro-holes of 0.25 mm diameters in some applications [Xu, Spanu, Marinescu 2015]. The cast-iron and cobalt-iron grinding wheels are among the commonly used for micro-hole production. The efficiency of the grinding process can be compared with a variety of grinding fluid. The grinding force is strongly influenced by the selection of the coolant. The application of the grinding fluid determines the thickness of the etched and the oxide layers [Yu, Huang, Xu 2016]. On the basis of the grinding application, the tube and arc electrode types have been used often for interval dressing.

ELID-lap grinding: The basic requirements in most industries are increased components flatness and a mirrored surface finish. With a very fine grinding wheel with metal bonding, the ELID-lap grinding process applies a constant pressure for the operation [Saleh, Bahar 2017]. For materials depicting varied levels of harness simultaneously, this process has been proven effective on such surfaces [Rowe 2013].

The surface finish improves considerably when the process is used to grind surfaces that may consist of two or more different materials.

Grinding of silicon wafers: The semiconductor industry is in great demand of mirror finish of component surface with Nano accuracy for silicon wafers [Wang, Ren, Chen, Zhang, Deng 2018]. A good choice on the silicon wafers surface finish improvement is the selection of ELID grinding wheels with metal bonding.

2.8 ELID Grinding with or without ELID Processes: A Comparison

Material removal processes from metals are completely different from those for hard and brittle materials [Doi, Uhlmann, Marinescu 2015]. Thus for brittle materials, specific methods are used to perform the process namely:

a. Brittle mode,
b. Semi-ductile mode and
c. Ductile mode

The achievement of the required surface finishes in any brittle machining processes almost uses these three methods. An understanding of the different modes of grinding is essential to determine their effectiveness. Comparing the results of the data between the ELID grinding and without ELID is the core function in this section [Wang, Ren, Chen, Zhang, Deng 2018]. Thus, the surface finish of the ground component without ELID from measurements gave a surface roughness with almost double the value

when compared to that of ELID. This indicated the efficiency of the ELID process in improving the surface finish of the brittle and hard materials when the grinding modes have been fully implemented for both categories. The investigation of the surface finish between the two methods can be clearly evident when viewed under the Normarski microscopes for a semi-ductile material [Doi, Uhlmann, Marinescu 2015]. In this case the conventional grinding method compared to the performance of ELID process indicates that the latter has better results. Less crashed parts can be evidently seen for the process with ELID than for that without.

2.9 Wear Mechanisms of ELID-Grinding Wheels

The culmination of a variety of wear processes between the work piece and the grit results in an extremely complicated wheel wear process. Expressed as the volumetric material losses from the wheel, this conventional way presents an approach to wear quantification and the mechanism of wear [Xu, Spanu, Marinescu 2015]. The three wear mechanisms imminent in the grinding wheels include the bond fractures, grain fractures, and attritious wear. The growth of wear flats and dull abrasive grains is attributed to attritious wear as the work piece rubs against the wheel. The fracture of grains and the removal of materials by abrasive fragments occur by the process of grain wear. The abrasive is dislodged from the binder in bond fracture. The grain dislodging and reduced bond strength causes binder erosions [Yu, Huang, Xu 2016]. The decrease in wear volume is least for the attritious wear and only this process determines the wheel life. The process causes decreased grit projected heights and sharpness causing to glazing of the wheel and the eventual end of life.

Basically, increased grinding forces dictate the end of wheel life leading to work piece size losses, the form and finish. Special sensors can be adopted for determination of the end of wheel life but in their absence, skilled operators can deduce [Xu, Spanu, Marinescu 2015]. The grinding operation requires that the wheel is redresses during the grinding with ELID. To result in high tolerances and accuracies, compensation of the wheel wear must be accounted for. The rate of wear decreases considerably with prior dressing of the wheel before end life and may significantly affect the work piece surface if it occurrence id delayed. To ensure that the wear is contained within reasonable limits and better grinding is achieved, a balance is the dressing interval is carefully chosen. The process of wear in this operation occurs by two stages. Initially, it is limited to pre-dressing but eventually progresses to in-process level [Doi, Uhlmann, Marinescu 2015]. To enhance the precision of the grinding operation, it is important to have good knowledge of the two stage wear.

2.10 Wear during Pre-Dressing

The process of grinding is facilitated by the provision of adequate grit protrusions which results from pre-dressing of the grinding wheel. The electrolysis process may at times result in three electrons or two electrons from the bind metal transition. Voltage increases as the current drops due to the resistance to current flow created by the self-protected oxide layer [Saleh, Bahar 2017]. An optical microscope is then used to inspect the wheel from which the oxide layer is observed to have covered the entire bond surface. The grinding process however removes the oxide layer totally if it had been formed as a result of metal oxide deposition. The oxide formed is not soluble in the electrolyte and

thus may result in diameter increase of the electrode. The oxide that initially forms on the grinding surface prevents further oxidation on the wheel [Maitra 2013]. Thus, the electrolyte used and the bond material in the pre-dressing operation influences the wear of grinding wheels. Pavel provided a theoretical analysis and experimental verification of pre-dressing time, the period during which oxidation occurs [Pavel, Pavel, Marinescu 2004]. The effects of grinding wheel wear, which are closely related to the formation of the oxide layer have been discussed both by theoretical modeling [Chen, Li 2000] and experimental observation [Biswas, Kumar, Rahman 2010].

Pre-dressing a grinding wheel that has been cast iron-bonded has resulted in differed conclusions on wear mechanism [Wang, Ren, Chen, Zhang, Deng 2018]. As the oxide layer continues to accumulate on the wheel surface, the flow of current drastically drops. The grinding force exerted by each grit and the bond strength produced by the maximum holding force of the grits are the major forces that are present in the diamond grits during the wear process. As the grit wears, the grinding force increases gradually with the operation. The worn out grits dominate the surface of the wheel at this stage, causing the development of cracks and the propagation of macro fractures which causes extensive wear of the wheel surface [Wu, Ren, Zhang 2018]. The macro fractures may induce the separation of the oxide layer insulating the ELID grinding wheel enhancing the in-process electrolysis.

2.11 ELID Pre-Dressing and Oxide Layer

Pre-dressing of the grinding wheel is th first stage required before starting the ELID grinding. At this stage, the removal of metal bond from the wheel surface by electrolysis

is done to protrude the abrassive grains. At the same time, an oxidation layer is formed on the weheel suface. Pre-dressing increases the diameter of the grinding wheel becauee of this oxide layer. For the case of iron, like in this project, it is important to note the formation of iron ions which reacts in a dseries to form iron oxides compound. The researchers focused on the growth of oxide layer and how it can affect the pre-dressing conditions. Also, they investigated the role played by the oxide layer on the ferrous corrosion inhibition. An abbrassive grain experiment was conducted by Ning, Loan and Michael focused on determination on the effect of adapting additive in the ELID proces on the oxide layer [Hasegawa, Itoh, Nemoto, Ohmori, Kato, Igawa 2007].

2.12 The Effects of Parameters on Oxide Layer Formation

According to Han dressing voltage and current influences the oxide layer that is formed during ELID pre-dressing [Han 2009]. This implies that when the power is changed, the layer formed is affected. From the experimental investigation, increasing the dressing power increases the oxide film production rate and hence the thickness of the grinding wheel will increase. In addition, the process is stongly influenced by the coolant/grinding fluid properties, particularly for ferrous corrsion inhibition [Han 2009].

To achieve high quality surface finish, the wheel speed is increased, feed rate is decreased, and the depth of the cut is decreased. According to Han, the better surface finish was obtained when the speed of the wheel was increased from 9.8m/s to 16m/s, feed rate decreased from 2m/min to 0.5m/min or reducing the depth from 5micrometers to 1mincrometers during an experiment on sapphire materials [Han 2009]. When the

depth of cut is increased, the oxide layer breaks which causes a rapid increase in AE_{RMS}. This indicates the grinding mechanism transition [Murata, Okano, Tsutsumi 1985].

2.13 Chapter Summary

A comprehensive research has been conducted on the application and advancement of ELID grinding technique since its discovery. Demands for precise and high quality dimensions, surface finish, and form of accuracy which are required for many applications like optical appliances have led to many researches. It is difficult to achieve such desired surfaces by using conventional grinding procedures. To make the finish surface feasible, the grinding wheel is dressed simultaneously during grinding procedure through the use of ELID method.

Research have pointed that ELID, a new technique, has high efficiency and accuracy that can achieve mirror surface finish, particularly on hard, brittle and tough materials such as diamond [Lim, Fathima, Senthil, Rahman 2002]. Murata et al. discovered the ELID in about 1985 and applied on ceramic materials using a wheel made of metal bonded diamond, having grit size less than 400 micrometers. An efficient and new method was later brought in play for grinding hard and brittle materials, holding grit size smaller than 1000 micrometers [Murata, Okano, Tsutsumi 1985]. According to Ohmori & Nakgawa, (1997), the experiment showed determine the parameters that affect the fluid and the oxide layer during the process of grinding. They proved throw mathematical calculations based on the results from series of experiment that additive variety dominated the efficiency and productivity of the ELID.

According to Saleh, theoretical investigations on basic principles of ELID performed by Bifano based on Faraday's Laws of Electrolysis to find the wheel corrosion rate and oxide film/layer growth rate while comparing with theoretical results showed that it is difficult to predict and control efficiency of ELID grinding [Saleh 2004]. The shortcomings were based on the material inhomogeneity, and effects of film formation in microscopic scales. Also, an investigation on the process of electrolysis was conducted in relation to Farady's Law [Wang, Ren, Chen, Zhang, Deng 2018]. According to Xu the design and development of a suitable electrode for the electrolytic dressing of high-speed ELID grinding requires high precision and accuracy that cannot be attain using conventional methods [Xu, Spanu, Marinescu 2015]. Furthermore, Lim and the rest proposed a model for ELID grinding based on the fact that contact between wheel and workpiece, in ultra-precision grinding, was not through abrasives but through asperities on the surfaces of the wheel and work material. Several tests and measurement of the wheel were carried out to find parametric values of the model and the simulated grinding forces for different parameters could be explained with experimentally obtained forces [Lim, Fathima, Senthil, Rahman 2002].

From the research on the discussion above, among others, it is clear that the focus has been on finding the best method to imprive effiecincy of ELID system: by advancing the princples of operations, changing the parameters, corrosion rate and wear rates and other factors. However, the materials used for the metal bonded-wheel is generally diamond. In addition, experiments have been conducted to measure the diameter of the oxide layer, but effeciecny for high precision has never been attained as from the experiments performed by Hasegwa and the rest [Hasegawa, Itoh, Nemoto, Ohmori,

Kato, Igawa 2007]. The authors conducted the research using metal-resin as the bonded wheel. The smoothening of micro-functional parts effieciency in ELID lap. It was realized that the ground can be done smoothly using a different material like metal-resin. There is a correlation between the parameters used in grinding: a better ELID grinding can be achieved by changing variables such as changing the material used to make grinding wheel, and changing the direction of measurements of the oxide layer. Also, from the discussion above, voltage, current and fluid used as coolant during grinding has a significant influence on the efficiency of the process. the aim for any designer is to attain high effeiciency, use cheap and light materials and most of all, maintain high top quality. Experimetal measurement are done at a cross sectional direction of the oxide layer. In addition, other measured parameters include voltage, velocity of electrolyte, and gap between two electrodes where the anode is the wheel made of cast iron and cathode is stainless steel. An SEM Microscope is used to measure the thickness of the oxide layer.

Chapter 3

Methodology

A standard 3^3 full-factorial study was designed to study the effects of voltage, electrode-grinding wheel gap, and coolant flow rate on the oxide layer growth. Metallic samples were prepared, after which the cross-sectional area of the sample was examined with SEM to determine the oxide layer thickness and to observe the structure of the oxide layer and oxidation distribution.

3.1 Parameter Selection

This study aims to study the effects of both electrical parameters and grinding parameters on the formation of the oxide layer. Since it is an implementation of a previous study, the same type of parameters was used; however, for each parameters, their levels used were different. Voltage was chosen based on industry practices, using DC between 60 and 90 volts. The gap was also chosen based on actual industrial settings, falling in a range of 0.1 to 0.3 mm. Past studies that included this parameter have used a range of 0.3 mm to 0.7 mm, probably due to constraints of their techniques[Marinescu,

Ohmori, Katahira 2011] [Wang, Ren, Chen, Zhang, Deng 2018]. The coolant flow rate was used to indicate the relative motion between electrode and the grinding wheel, since no relative motion occurred in this experiment. The flow rate was chosen based on the capability of the pumps.

Table 3.1 : Settings for parameters affecting oxide layer formation

Parameter	**Voltage**	**Gap**	**Flow rate**
Low level	60 V DC	0.1 mm	100 mL/min
Middle level	80 V DC	0.2 mm	250 mL/min
High level	90 V DC	0.3 mm	500 mL/min

3.2 Sample Preparation and Post Experiment Processing

Before starting the experiment, the cast iron samples were first cut across the middle and glued to reform their original shape, such that cross-sections could be easily exposed without disturbing the oxidation sites. Then, all glued samples were polished to the same level of surface finish (Fig 3-1).

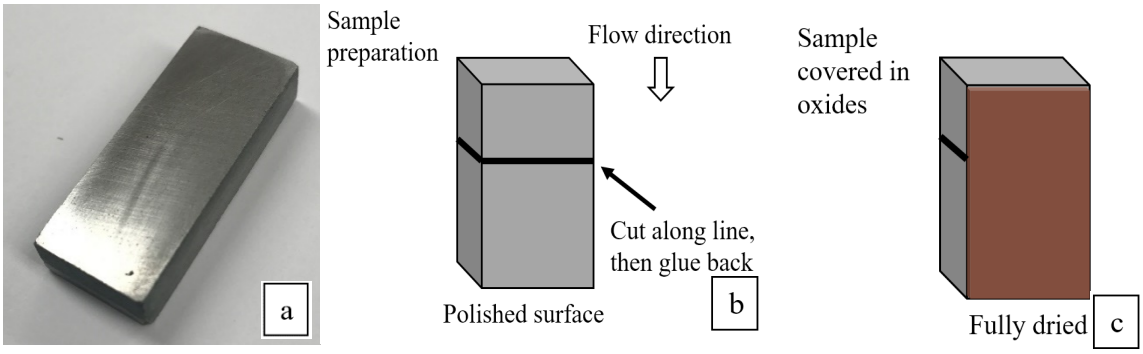

Figure 3 – 1: Schematic of sample preparation for SEM imaging. (a) A metallic sample before preparation; (b) Sample preparation process; (c) Pre-dressed sample.

After the experiment, all samples were left to completely dry in an enclosed space so the oxide layer would not be disturbed. In this way, the oxide layer thicknesses between the samples were kept comparable, even though some shrinkage could occur between the fresh, wet layer and the dried layer. After drying, the top of all the samples were carefully removed along the cut line and put into holder for SEM machines. For each sample, at least five points, spaced evenly from side to side, were examined, and the thickness measured using SEM (Fig 3-2).

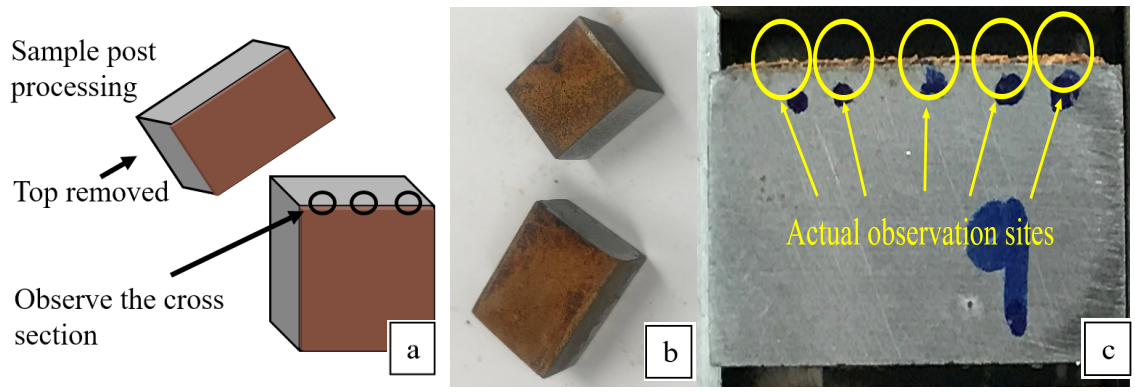

Figure 3 – 2: Sample set prepared for SEM following ELID. (a) The cross section of a sample was exposed and ready to be examined; (b) Actual sample after processing, the oxide layer appeared as a red film; (c) A sample cross section, ready for examination by SEM.

3.3 Experimental Setup

The experimental setup is illustrated in the following images (Fig 3-4). A prepared metallic-bonded sample made of cast iron was secured in an acrylic holder and connected to the negative terminal of the power source, while a stainless-steel electrode was aligned with the sample and connected to the positive terminal of the power source. The electrode-grinding wheel gap was adjusted to a known value using a certified plastic shim and maintained, then the shim was removed. Coolant was dispensed from the top of the sample holder through the gap to enable electrolysis, followed by cycling using pumps.

Table 0.2: Detailed specifications for the experimental setup

Tools used	Specification
Electrode	25 mm (L) x 12 mm (W) x 8 mm (T), stainless steel 316L
Bonded sample	25 mm (L) x 12 mm (W) x 8 mm (T),G2 cast iron
Coolant	Master Chemical Trim ® C270
Power supply	NX-ED911 NEXSYS®
Pump	HV-77521-40 Masterflex L/S variable speed drive
Film	ABQ Industrial CPS Certified Plastic Shims, 100, 200, and 300 μm
SEM	JEOL JSM-7500F with EDS Detector attachment

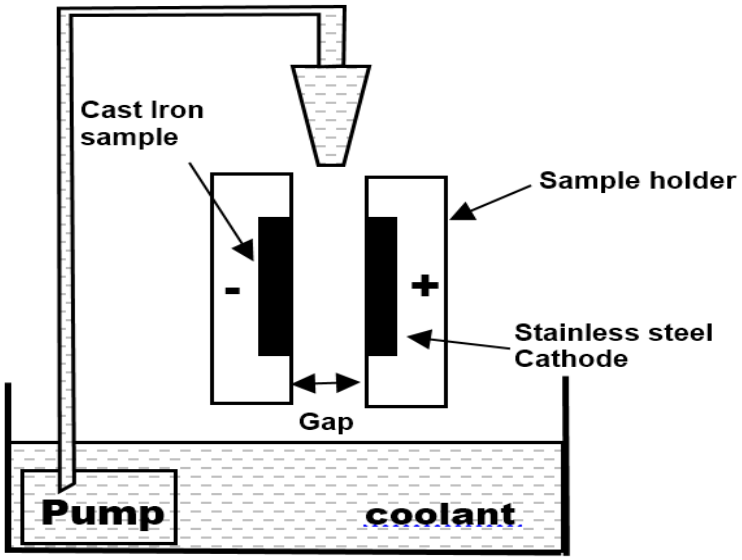

Figure 0 – 3: Schematic illustration of the basic experimental setup

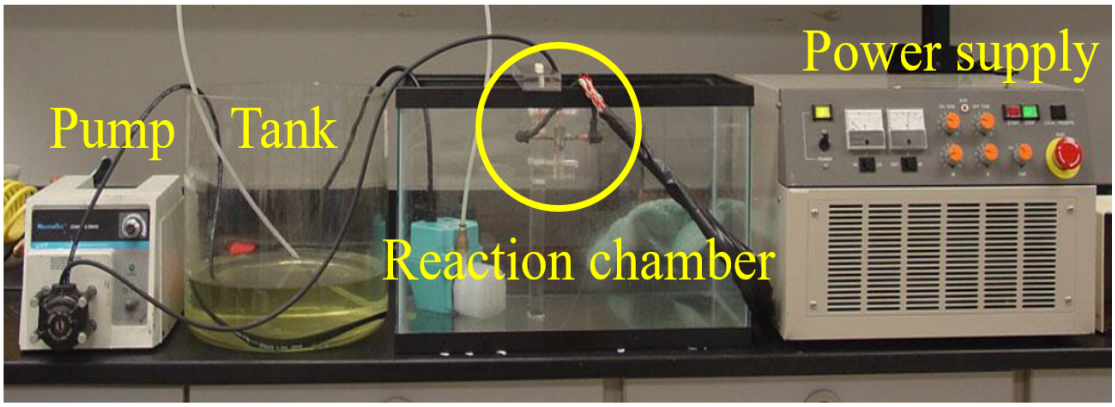

Figure 0 – 4: Actual experimental setup

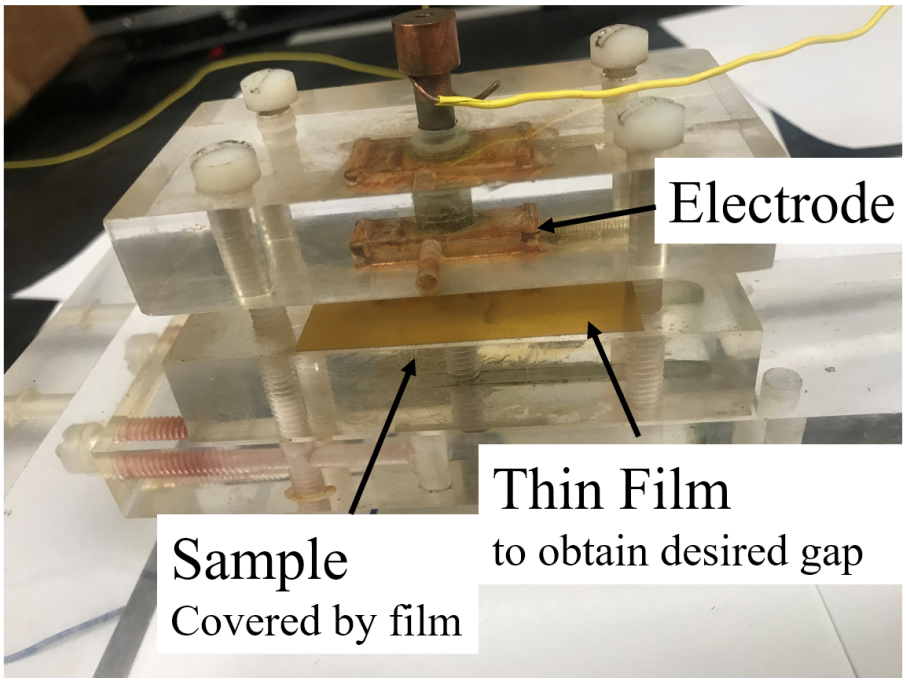

Figure 0– 5: Enlarged, assembled reaction chamber

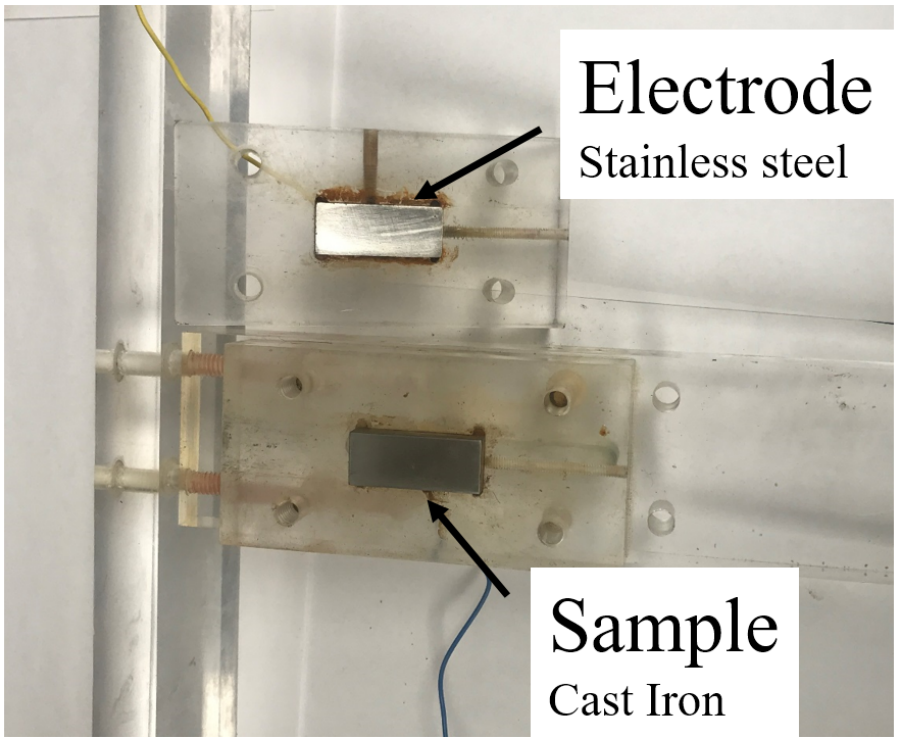

Figure 0– 6: Inside the reaction chamber.

3.4 Experimental Procedure

All experiments were conducted at the Precision Micro Machining Center (PMMC) at the University of Toledo.

The prepared cast iron sample and stainless-steel electrode were secured in the holder. A thin film (certified plastic shims) with a thickness equal to that of the gap was sandwiched between the surfaces as a guide to adjust the gap, after which the film was removed.

The parameters were adjusted, and the power was turned on for 5 min. The sample was removed and left to dry. The experiment was repeated for 10, 15, and 20 min with the same parameters. The data collected for these four repetitions for each sample

was considered one dataset; each included four runs, and data were collected for a total of four samples. The previous step was then repeated using different sets of parameters. Twenty-seven data sets were obtained from a total of 108 runs.

All samples were post processed and the oxide layer thickness was measured using SEM.

Chapter 4

Results and Discussion

In this chapter, the electric behaviors of ELID grinding, the cross-sectional examinations, and measurements of oxide layer thickness were presented. Additionally, a model predicting the oxide layer thickness was proposed using a linear regression model, and validation of the model was carried out.

4.1 Electrical Behavior:

During ELID grinding, the current and voltage undergo passivating behavior because of the ELID cycle, during which the non-conductive oxide layer is removed and formed [Lee, Kim 1997]. However, in this study, only the pre-dressing electrical behaviors were captured.

The voltage and current data were collected from the power source and recorded for four runs for each set of parameters. Immediately after being removed from the workpiece holder, samples were fully covered by an oxide layer with no visible signs of burning (Fig 4-12). It was to note that the power supply was held constant during each run and all the change was introduced by the oxide layer growth.

Since the electrical behavior was not observed frequently during the experiment, the exact time when the oxide layer became fully developed was difficult to determine or estimate. The oxide layer was still developing at the 5-min mark, and in most cases, growth occurred between 5 and 10 min. By 10 min, all oxide layer was fully formed. There were slight variations in electrical behaviors for the same set of parameters, likely introduced by human error when installing the sample at the beginning of the four runs. Table showed one set of data obtained in the experiment. To serve as an example. The data set used is form 60 V, 0.1 mm gap and flow rate of 100 mL/min, which turned out to have the thinnest oxide layer. The data was also plotted on Fig 4-1 to visualize the trend.

Table 0.1: Electrical behavior Voltage: 60V; Gap: 0.1mm; Velocity: 100 mL/min

Time (min)	0	5	10	15	20
Voltage (V)	18.1	50.1	53.8	54.4	55.6
Current (A)	1.47	0.11	0.05	0.04	0.03

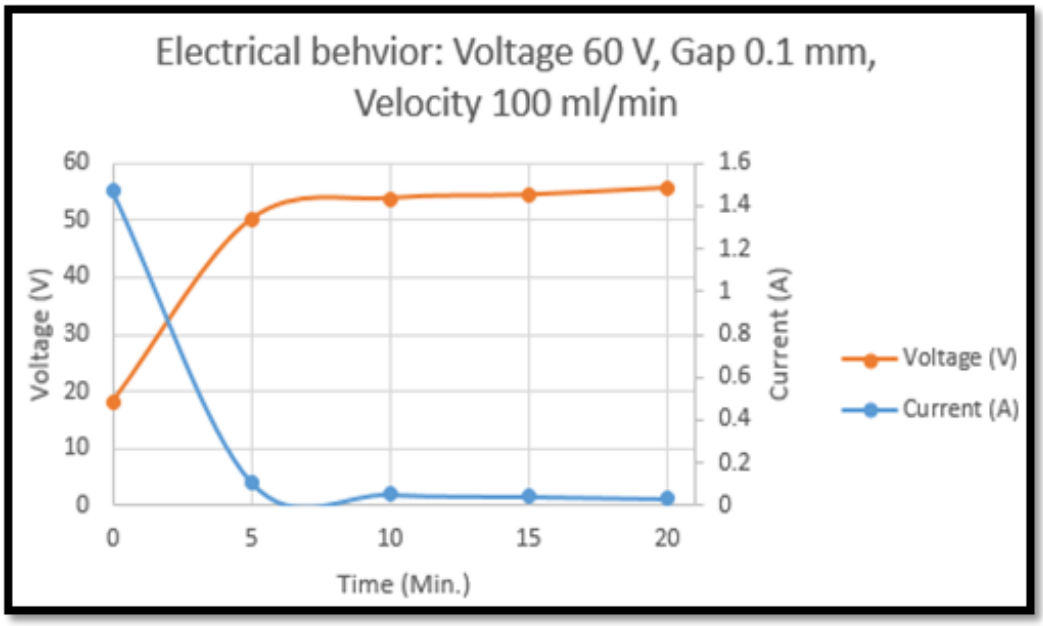

Figure 0– 1: Voltage and Current of data set: 60 V, 0.1 mm and 100 mL/min

As shown in Fig 4 - 1, at the initial stage of the electrolytic process, since there is no oxide layer on the surface of the sample, its conductivity is high. The potential between two electrodes is low while the current is high. The rate of generation of oxide layer is the highest during this stage, so the rate of change of voltage and current is the highest. As the oxide layer is generated on the sample surface continuously, the resistance of the sample increases and the conductivity decreases. From Ohm's law, R=U/I, the potential between two electrodes increases as the resistance increases. The current decreases because of the increasing resistance. This causes the speed of oxide layer generation to decrease, so the rate of change of voltage and current decrease gradually become stable, and no additional oxide layer can be generated.

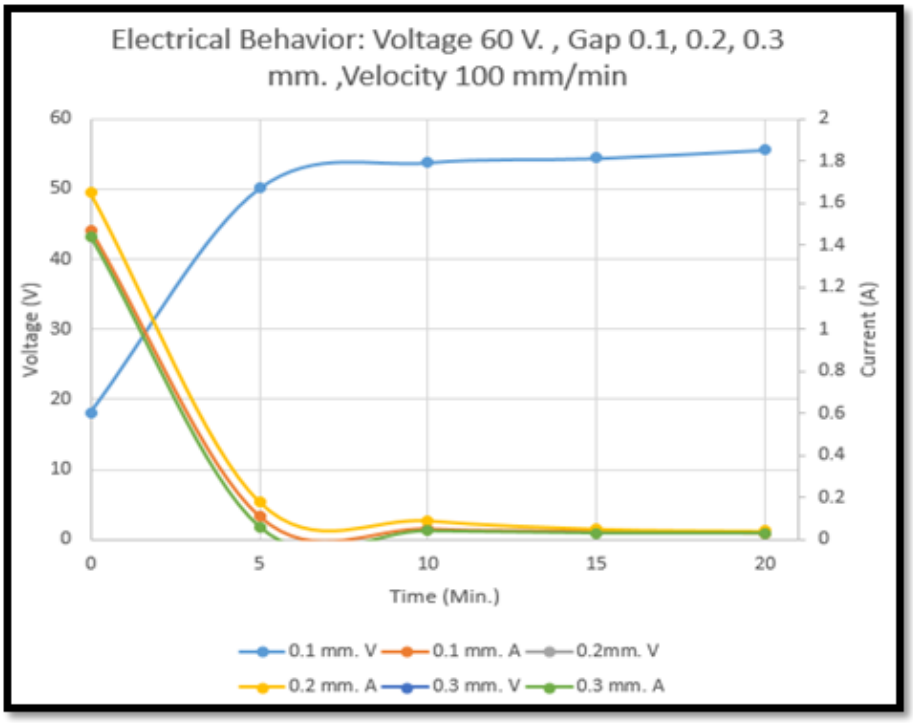

Figure 4 – 2: Electrical behavior, 60 V, Gap 0.2 mm, flow rate 100 mL/min

Combining the data of gaps 0.1, 0.2, 0.3 mm. as shown in Fig 4-2, the data shows that the gap between two electrodes influences the electrical behaviors of voltage and current. But generally, the current becomes stable at the 10-minute. Since the electrical behaviors from all successful run share very similar trend, only a typical data set for 60 and a problematic set at 80 V is analyzed in this section.

As introduced previously, the 80 V data set is problematic and the samples from this data set were discarded. However, these data can serve as an indication as to what caused the problem. The current becomes stable at around the 10 minute-mark at velocity of coolant flow 100 and 250 ml/min, which takes longer than at velocity of coolant flow

500 ml/min. At the end of the experiment, the final current values for velocities 100, 250, 500 ml/min were 0.15, 0.9 & 3.5 A respectively, it means the experiment at coolant velocity of 100 ml/min needs longer time to achieve the oxide generation level obtained with coolant velocity of 500 ml/min. From the graphs of electrical behavior, it can be speculated that the higher voltage, smaller gap and higher velocity of coolant flow would influence the current density change rate more dramatically. According to the experiment, higher current levels would increase the oxide layer generation, so the oxide layer growth rate can be associated with the impacts of voltage, gap and velocity of coolant flow.

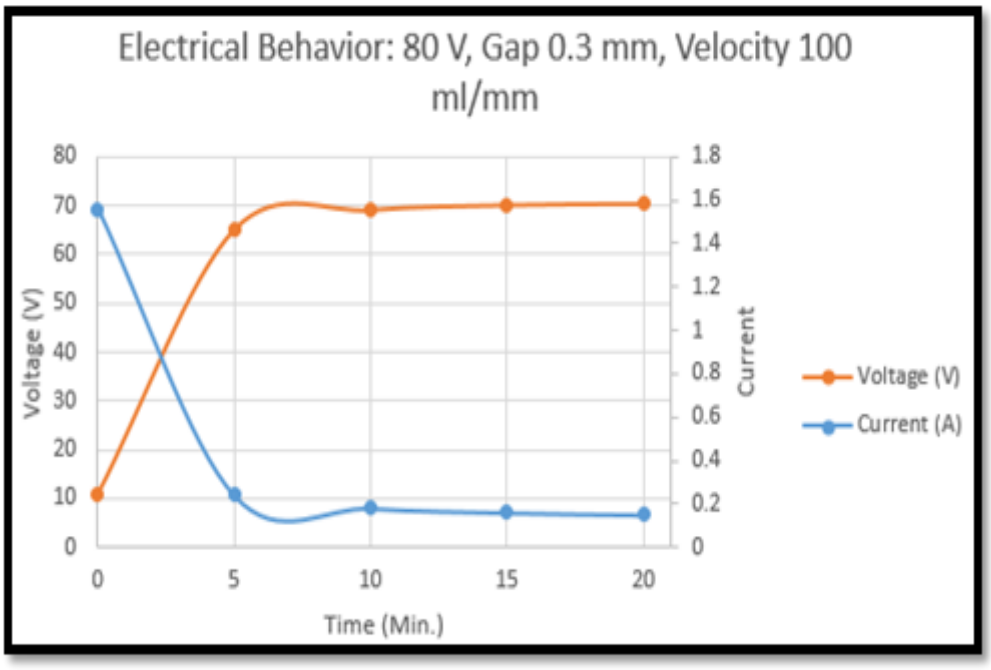

Figure 0– 3: Electrical behavior, 80 V, gap 0.3 mm, velocity 100 mL/min

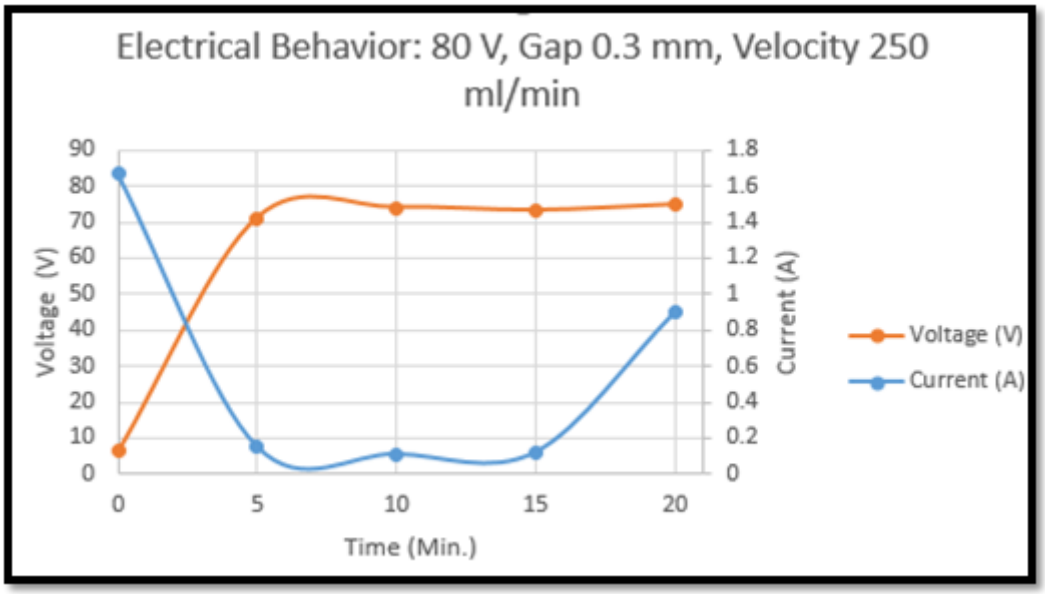

Figure 0– 4: Electrical behavior, 80 V, gap 0.3 mm, velocity 250 mL/min

When the voltage is high, it is possible that the oxides absorbed conductive coolant and become conductive again, causing an electric short at 5 min as shown in Fig 4-5. In this case, it is called “burning”, and the burning phenomenon is analyzed in later section.

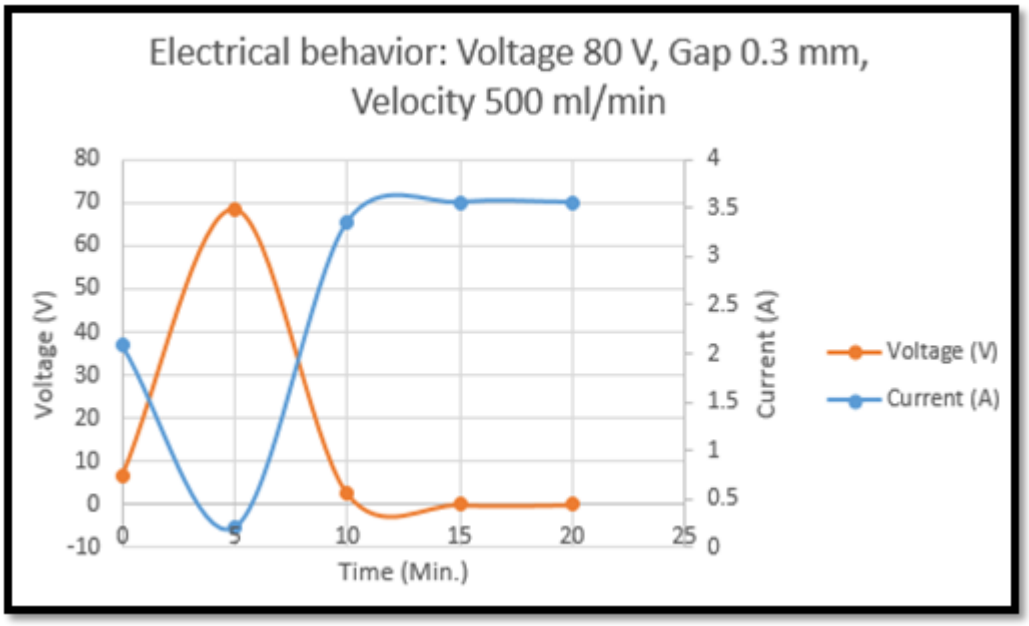

Figure 0– 5: Electrical behavior, 80 V, gap 0.3 mm, velocity 500 mL/min

As a conclusion, the electrical behavior of ELID pre-dressing observed in this study matches the expectations from all previous reported studies.

4.2 SEM Results

SEM imaging of the pre-dressed samples that represented grinding surface revealed previously unknown information and provided explanations and justifications for further experiments that were conducted on the workpiece. The results are discussed in more detail in the following sections. An original image from the SEM machine is presented here to explain how the measurements were obtained Fig 4-6. When the sample cross section was displayed by the SEM imaging system, the oxide layer could be easily

distinguished from the metallic sample surface, since the difference in particle density between the two was great. A grey line was added to the image as a baseline for measurement. Then, the researcher added a parallel line at the thickest part of the oxide layer. The SEM machine would read the difference between the two lines and output the value as the oxide layer thickness. The magnification of all SEM images was 200x.

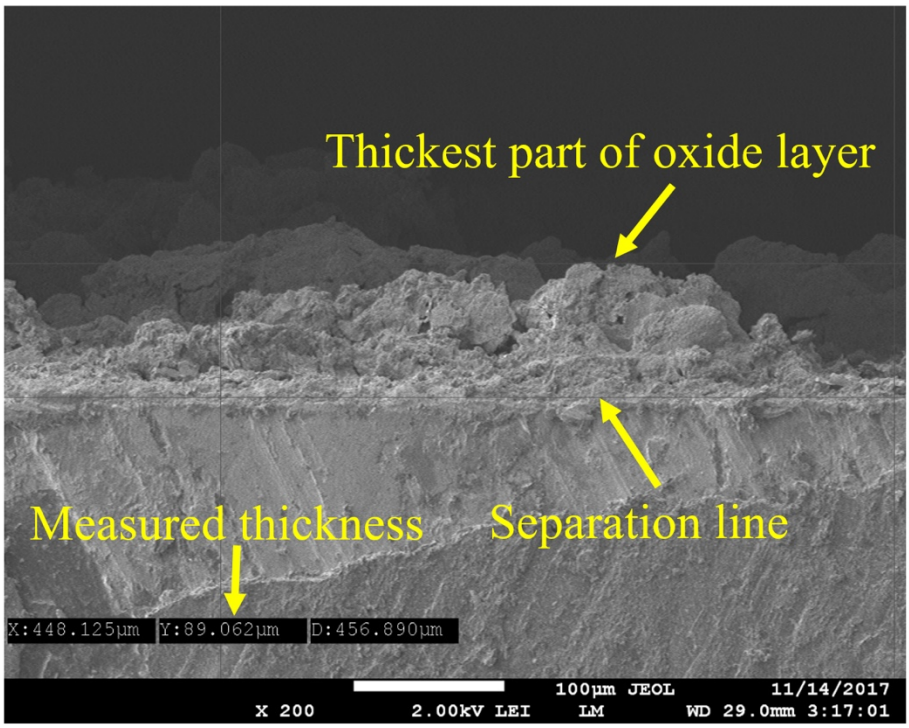

Figure 0– 6: Original image of a sample at observation spot

SEM imaging revealed the structure and distribution of the iron oxide layer. Since the voltage change and fluid type were consistent at the sample surface, the distribution pattern can only be attributed to the coolant flow pattern and possibly the slight gap

inconsistency. In the following figures, each tested area was ~500 μm wide, as marked by the horizontal line, and the layer thickness is marked by the vertical line. Three main oxide morphologies were observed in all SEM images collected: oxide clusters, shells, and mountains.

4.2.1 Underdeveloped Oxide Clusters

The growing oxide formed clusters that could be observed at the sides of the samples before the oxide layer is fully developed. The measured thicknesses were generally large (89 μm and 101 μm, as shown in Fig 4-7, though relatively small amounts of oxide were present judging by the large amount of void in frame. Images from Fig 4-7 show an intermediate state of the oxide layer during pre-dressing.

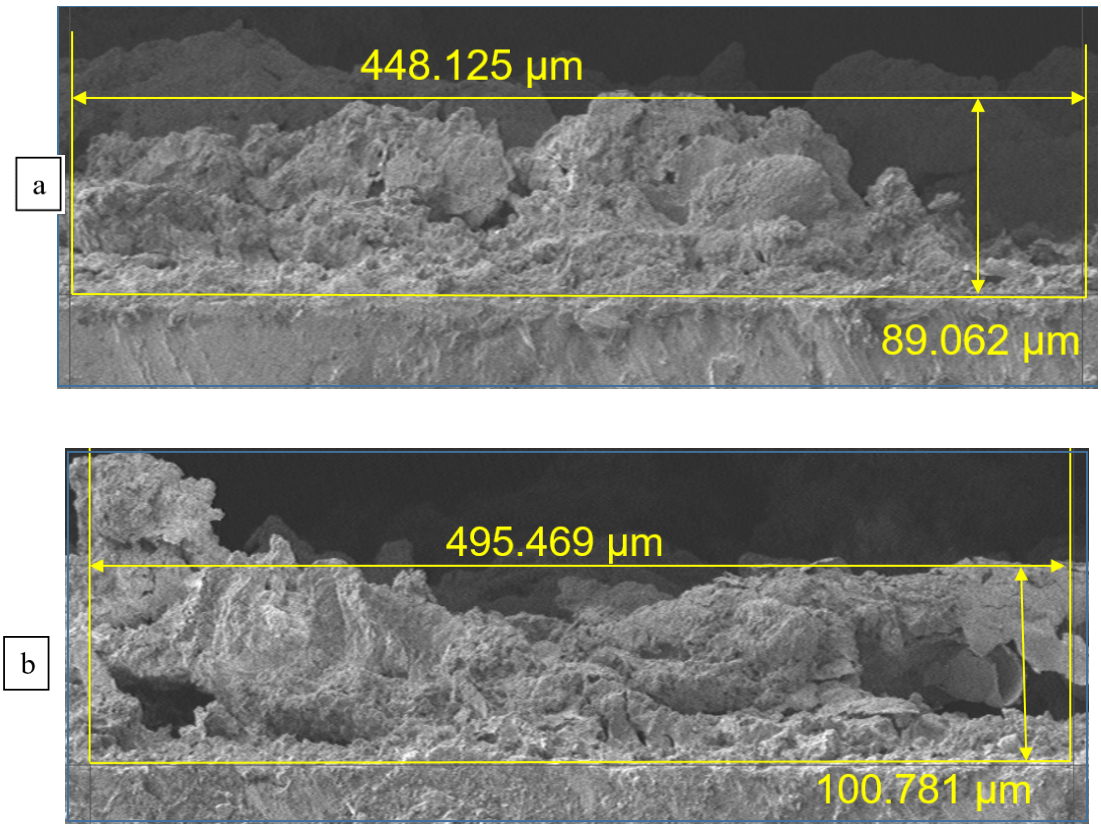

Figure 0– 7: Underdeveloped oxide layer example (a) large oxide cluster with little interconnection. (b) high porosity below the underdeveloped oxide layer.

4.2.2 Developed Oxide Layer in Shell

The oxide layer in the middle section, where the fluid flow is usually the fastest, has similar thickness across the area. However, large porosity exists beneath the outer "shell" and the oxides adhere less to the sample surface; thus, they can be removed easily. This phenomenon directly indicates that during the ELID cycle, the oxide layer and abrasives break off easily from this section of the grinding surface to accelerate the

formation of a new oxide layer. The thickness of the oxide layer shown here were 89 and 58 µm, as shown in Fig. 4-8.

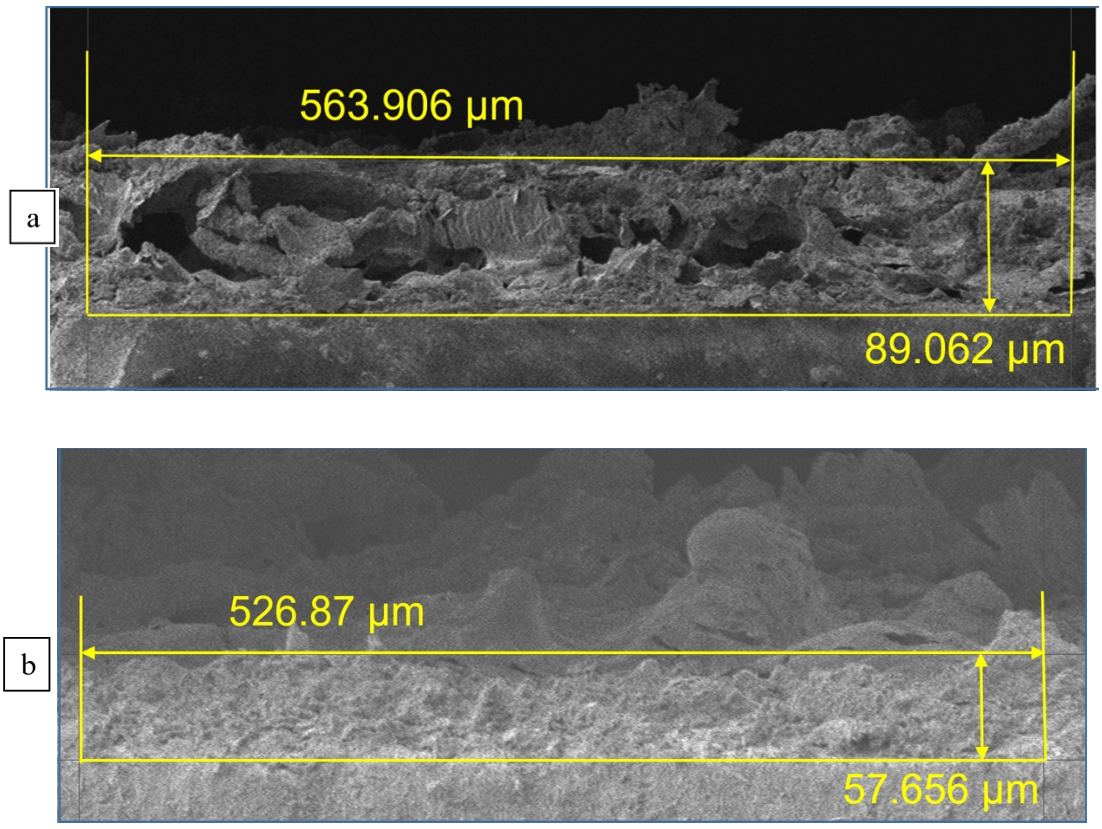

Figure 0– 8: Oxide layer where coolant flow is the fastest across the metallic sample surface (a) Oxide layer in the "shell" formation. (b) a significant amount of oxide was removed by the coolant.

4.2.3 Developed Oxide Layer In Mountains

At high voltage and high electrode-grinding wheel gap, the oxide layer grew quickly and formed more clusters. Since the flow is usually slower on the sides of the sample, these clusters have time to form a thick and denser “mountainous” layer at the sides of the sample. The measurements taken were 191 and 178 µm, respectively as shown in Fig. 4-9. The oxide clusters were tightly inter-connected, leading to lower porosity.

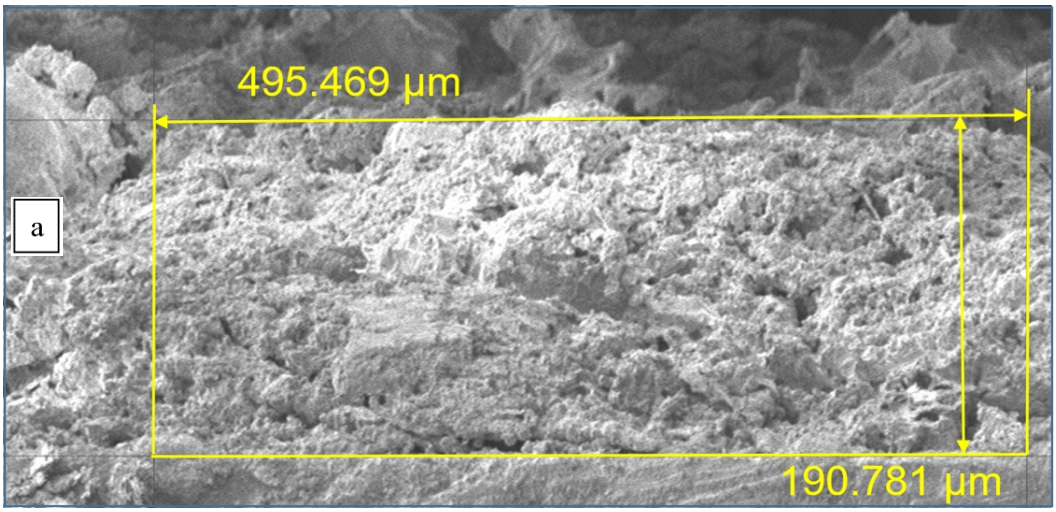

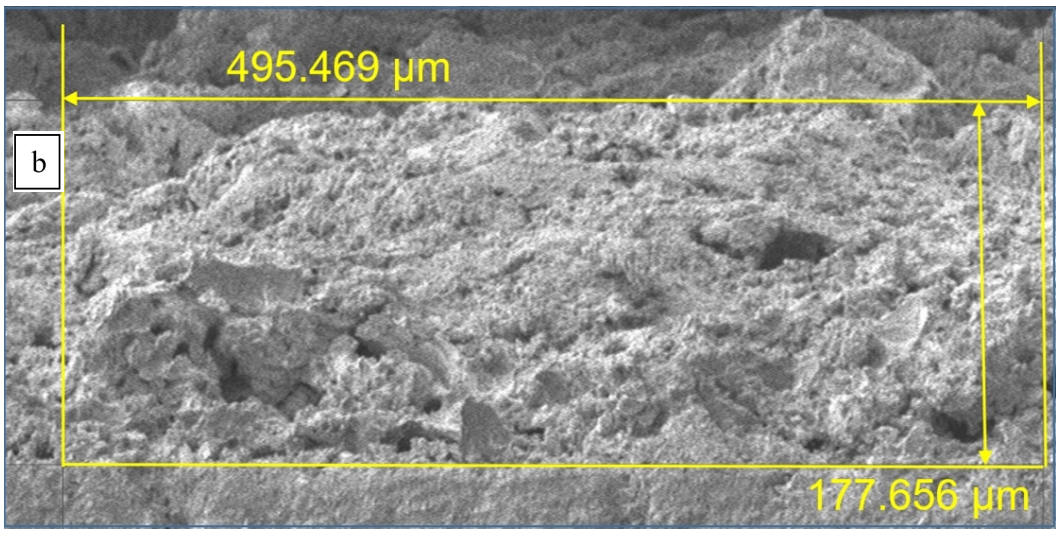

Figure 0– 9: Fully developed oxide layer in a mountainous formation (a) Oxide clusters are highly inter-connected (b) very little porosity can be observed.

4.3 Oxidation Distribution

Oxidation did not occur evenly along the cutline of the sample; instead, for most samples, the sides of the sample usually exhibited higher thicknesses than the middle section. As explained in the previous section, the voltage change and fluid type were consistent at the sample surface, so the distribution pattern can only be attributed to the coolant flow pattern and possibly to a slight inconsistency in gap width. There could be two explanations for the "dip" in oxide layer distribution: 1) the oxidation in the middle section had the "shell" microstructure, and large porosities existed under the top surface, so there was better electric insulation with the small amount of oxide; and 2) the thin outer surface did not support a large amount of oxide deposits, and the oxides were constantly washed away by the faster fluid flow, while at the sides of the sample, the dense structure could allow more oxide to build up.

The graph presented in Fig. 4-10 shows the oxide layer thickness distribution on the pre-dressed metallic-bonded sample at the cross section. The tinted area indicated oxide layer. Data are presented for parameters of 60 V, 0.3 mm gap, 100 mL/min at 10 min.

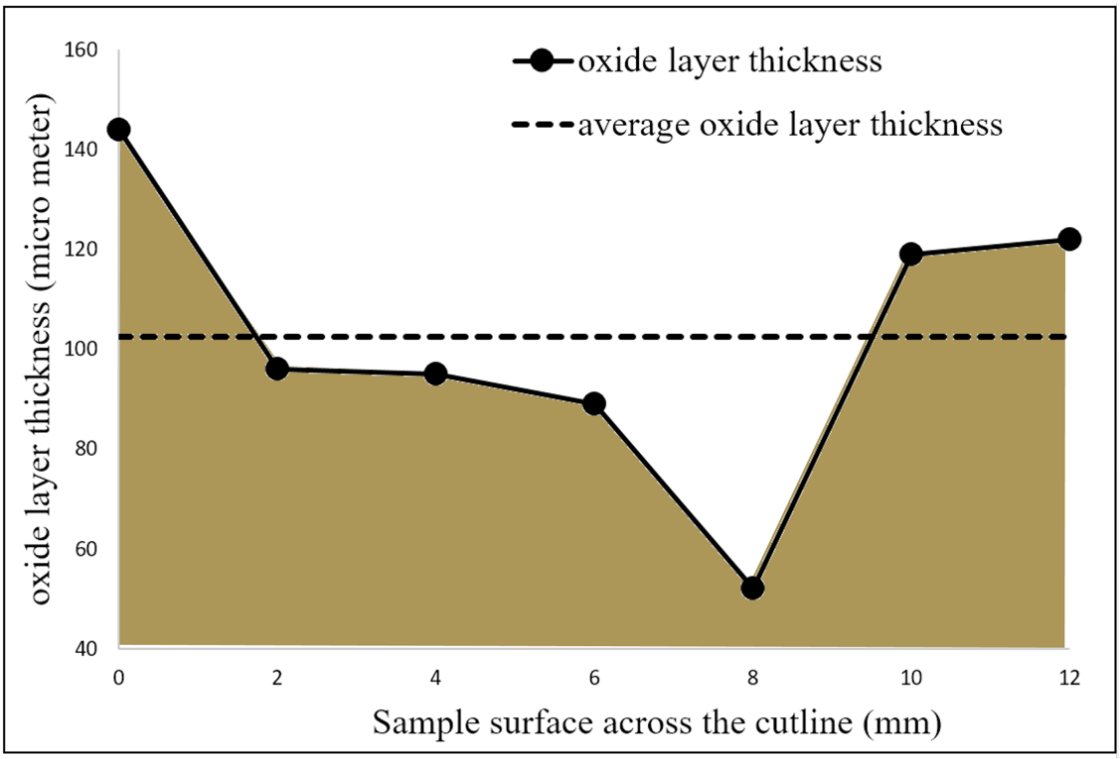

Figure 0– 10: Thickness distribution of the oxide layer as a function (μm) of location across the cutline (mm).

This oxide distribution explains why eccentricity, which indicated the workpiece trajectory on the grinding surface, has been shown to exert significant influence on the material removal rate and surface roughness [Bafakeeh, Khoshaim, Marinescu 2016]. The oxide layer has varying thickness because of the grinding fluid flow pattern, so a

workpiece trajectory that spends longer in the middle can offer a different depth of cut than one that spends more time on the inner or outer section of the grinding wheel.

4.4 Oxide Layer Growth and Burning

A graph of the electrical behavior during pre-dressing is provided in Fig. 4-11. The voltage and current data were collected from the power source and recorded for four runs for each set of parameters. Immediately after being removed from the workpiece holder, samples were fully covered by an oxide layer with no visible signs of burning (Fig. 4-12). The power supply was held constant during each run and all changes in voltage and current were induced by oxide layer growth. Data are presented for parameters of 60 V, 0.1 mm gap and 100 mL/min at 20 min.

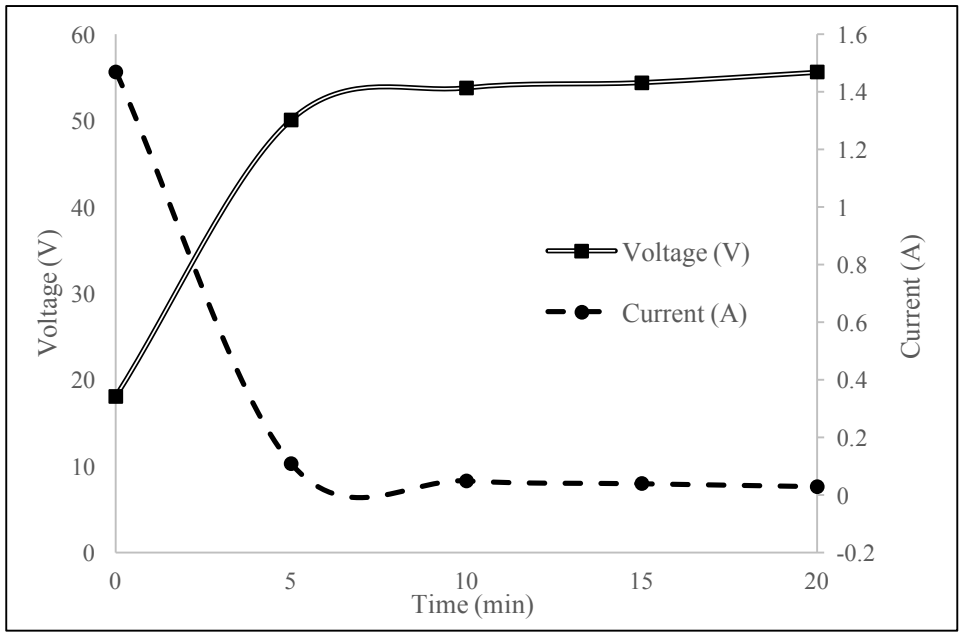

Figure 0– 11: Electrical behavior (voltage and current) during a representative pre-dressing process.

Figure 0– 12: A sample immediately after being removed from the workpiece holder following processing

Since the electrical behavior was not observed frequently during the experiment, the exact time when the oxide layer became fully developed was difficult to determine or estimate. The oxide layer was still developing at the 5-min mark, and in most cases, growth occurred between 5 and 10 min. By 10 min, all oxide layer was fully formed. There were slight variations in electrical behaviors for the same set of parameters, likely introduced by human error when installing the sample at the beginning of the four runs.

4.5 Surface Burning

For cases with high voltage (90 V), the oxide layer was fully developed before 5 min. However, as the oxide layer filled the entire gap and some conductive chemicals from the coolant were absorbed in the spaces between the oxide clusters, the oxide layer became conductive. Therefore, the circuit was shorted and the sample surface was burned. Beside the clear visual indication of black area on the sample itself (Fig. 4-13), the electrical behavior also demonstrated the short (Fig. 4-14). The burnt sample was discarded and no measurements was taken from this sample. Data are presented for the parameters of 90 V, 0.3 mm gap and 250 mL/min at 20 min.

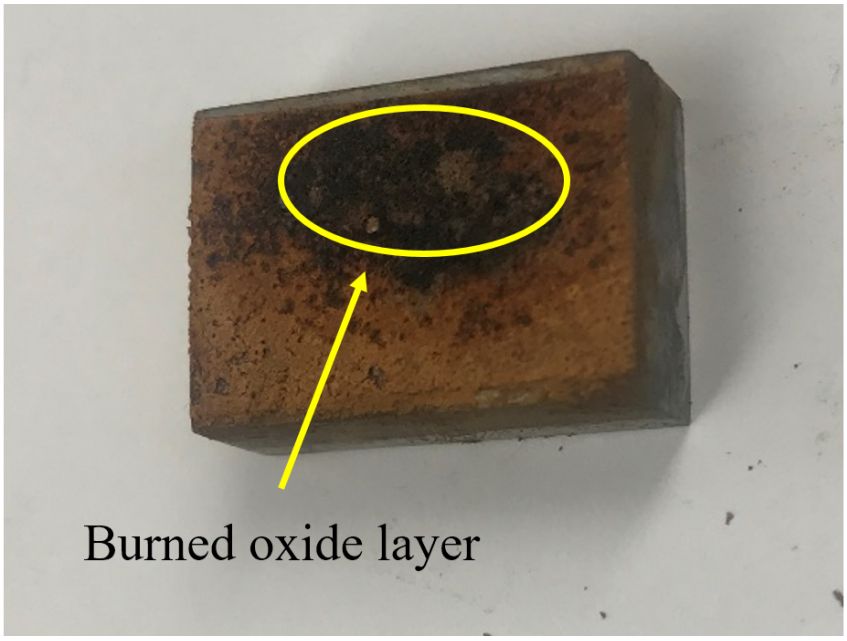

Figure 0– 13: A sample with a visibly burned oxide layer (dark area) following application of high voltage (90 V).

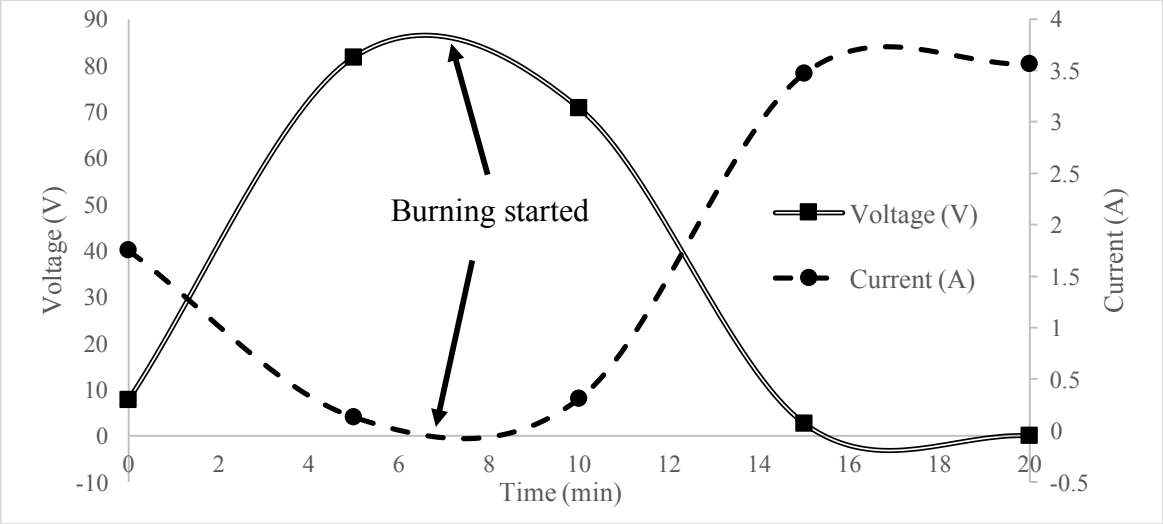

Figure 4 - 14: Electrical behavior of the surface burning process under high applied voltage.

4.6 Modeling Oxide Layer Thickness

A standard ANOVA analysis was conducted using Minitab 18 to model the final oxide layer thickness. The oxide layer was not evenly distributed across the entire sample surface; therefore, it was difficult to define the oxide layer thickness for the sample. To simplify the modeling process, a gross average was taken from all the thickness measurements in each run. All three factors gap, voltage, and coolant flow rate have a positive influence on the model, as does the interaction between the factors. An analysis on main effects and interactions of the three factors is shown in the Figures; plots of residuals that validates the linear regression model are provided.

4.6.1 Thickness Measurement after 5 Minutes

Table 4.2: Analysis of variance for 5 min runs

Source	DF	Adj SS	Adj MS	F-Value	P-Value
Regression	6	0.101562	0.016927	12.12	0.000
V	1	0.008363	0.008363	5.99	0.024
G	1	0.002381	0.002381	1.70	0.207
S	1	0.010025	0.010025	7.18	0.014
V*G	1	0.005334	0.005334	3.82	0.065
V*S	1	0.010324	0.010324	7.39	0.013
G*S	1	0.004593	0.004593	3.29	0.085
Error	20	0.027942	0.001397		
Total	26	0.129504			

P-Values are less than 0.0500 indicate the estimated coefficients are significant. The Analysis of Variance shows that the regression model, Voltage, and Coolant flow are very significant. However, the Gap is not significant because oxide layers are still developing and need more time.

Model Summary:

S	R-sq	R-sq(adj)	R-sq(pred)
0.0373779	78.42%	71.95%	53.75%

The obtained R-sq value is 78.42%, which we consider a good fit for abrasive manufacturing processes.

Regression Equation:

$$T(5) = 0.354 - 0.00445\,\mathrm{V} - 0.743\,\mathrm{G} - 0.000782\,\mathrm{S} + 0.01380\,\mathrm{V}\cdot\mathrm{G} + 0.000010\,\mathrm{V}\cdot\mathrm{S} + 0.000968\,\mathrm{G}\cdot\mathrm{S}$$

Equation (2)

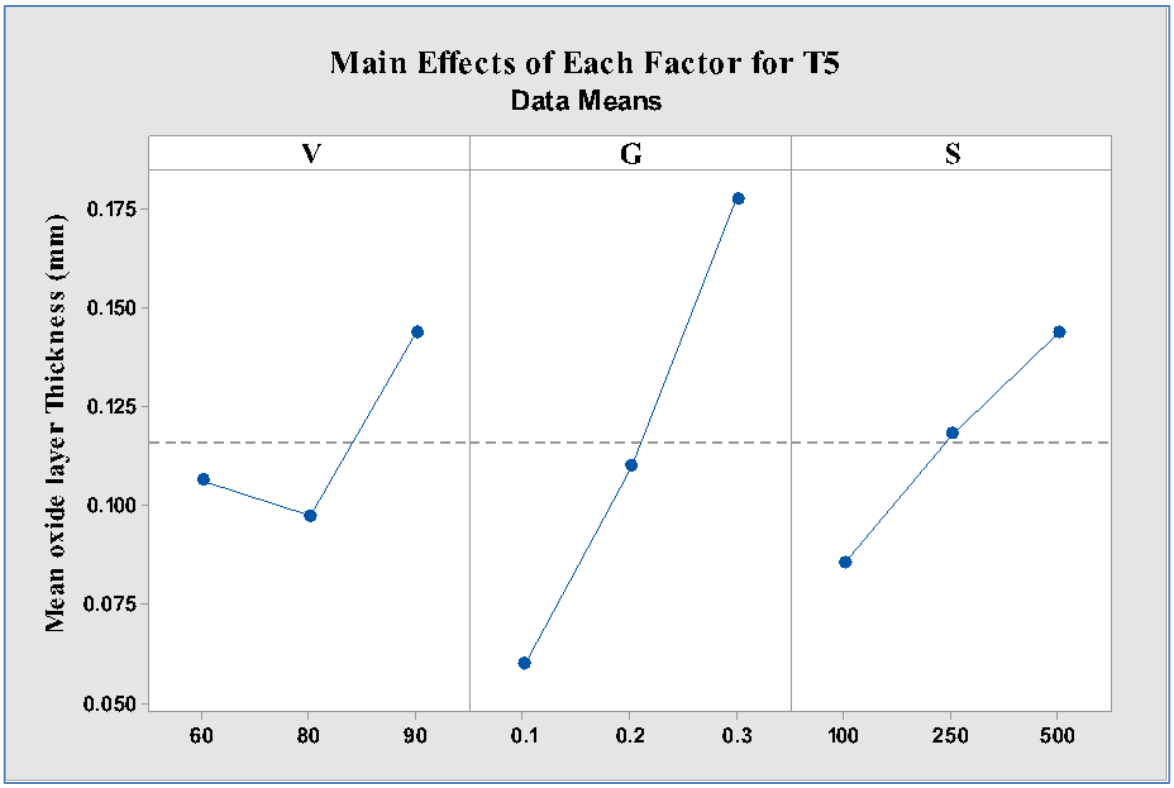

Figure 0– 15: Main Effects of Each Factor for Thickness after 5 min.

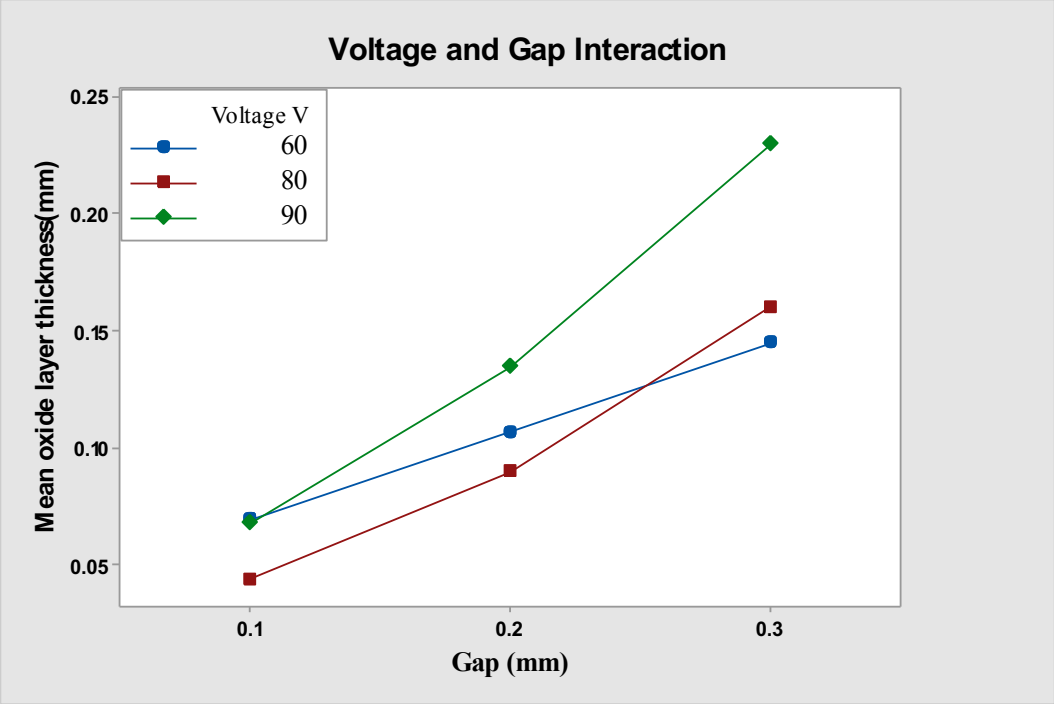

Figure 0– 16: Interaction between Voltage (V) and Gap (mm)

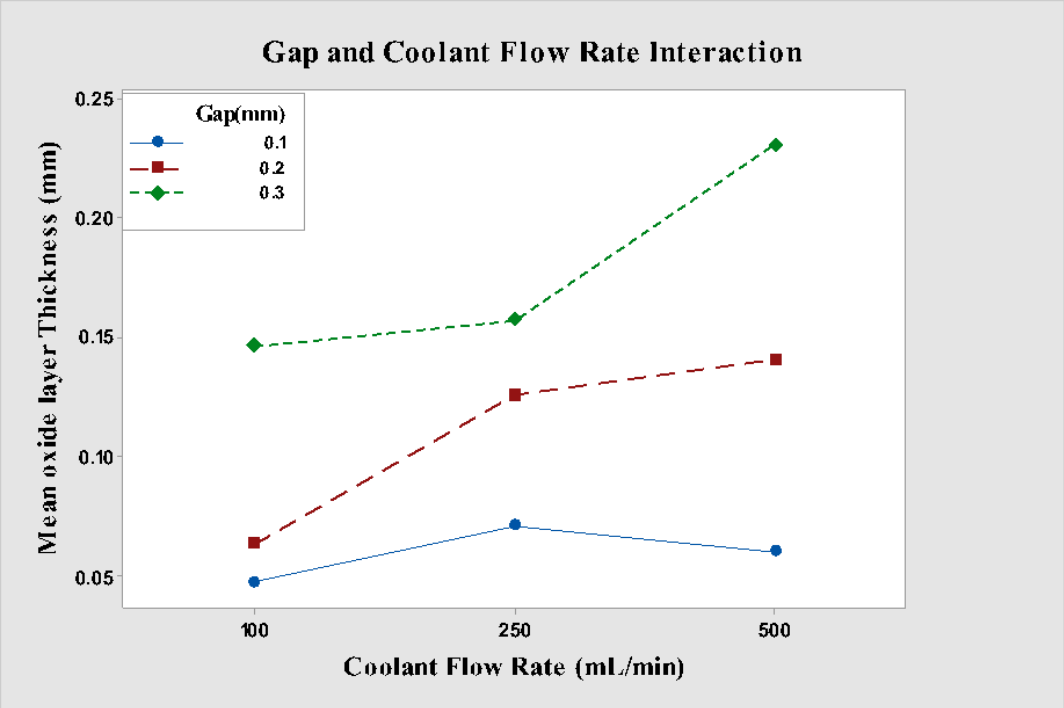

Figure 0– 17: Interaction between Gap (mm) and Coolant Flow (mL/min)

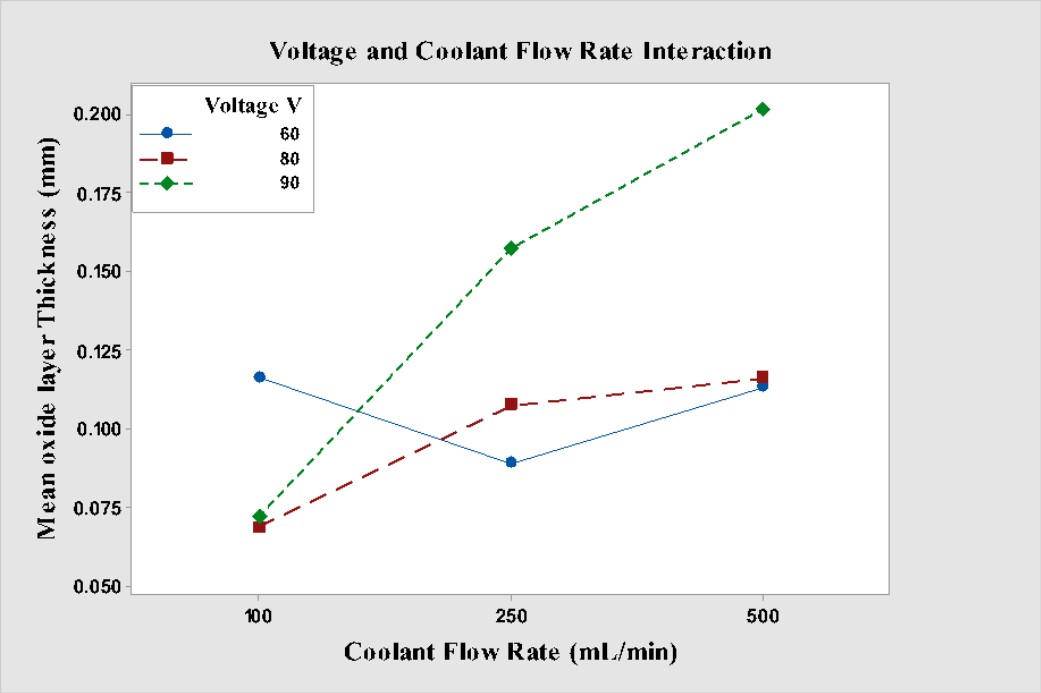

Figure 0– 18: Interaction between Voltage (V) and Coolant Flow (mL/min)

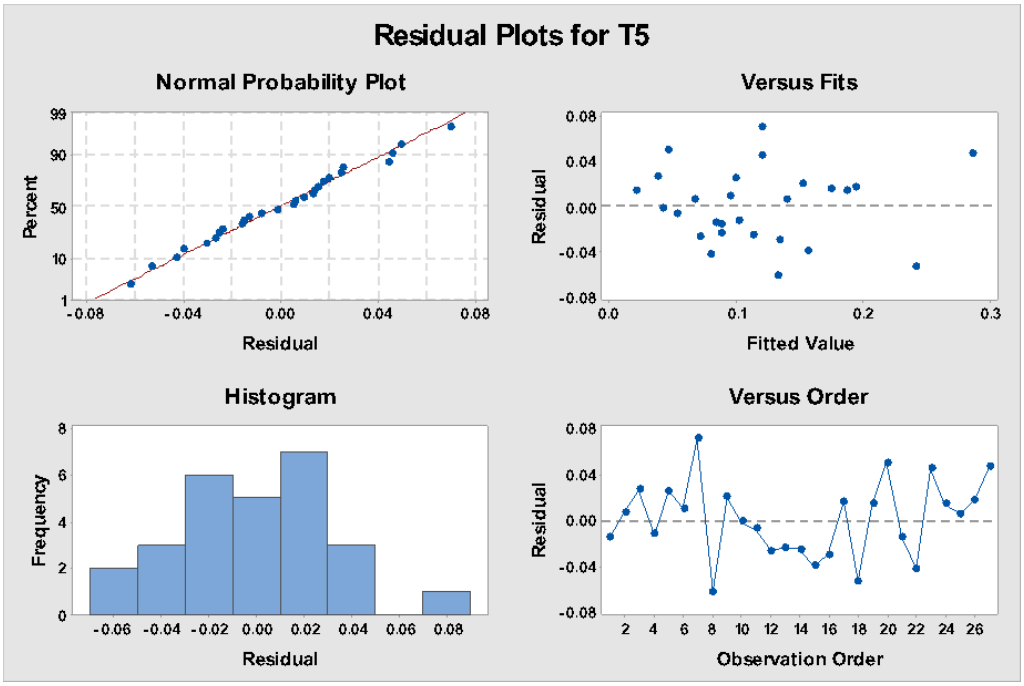

Figure 0– 19: Plots of the residuals for model validation

The residuals plots are normally distributed. No indication of skewed or outlier data. Residuals have a constant variance and presents a good fit. Residuals in the versus plots are randomly distributed and no signs of correlation.

4.6.2 Thickness Measurement after 10 Minutes

Table 4.3: Analysis of variance for 10 min runs

Source	DF	Adj SS	Adj MS	F-Value	P-Value
Regression	6	0.086911	0.014485	8.81	0.000
V	1	0.009482	0.009482	5.76	0.026
G	1	0.009717	0.009717	5.91	0.025
S	1	0.002623	0.002623	1.59	0.221
V*G	1	0.016870	0.016870	10.25	0.004
V*S	1	0.003707	0.003707	2.25	0.149
G*S	1	0.000706	0.000706	0.43	0.520
Error	20	0.032902	0.001645		
Total	26	0.119812			

P-Values are less than 0.0500 indicate the estimated coefficients are significant. The Analysis of Variance shows that the regression model, Voltage, and Gap are very significant. However, the Coolant flow is not significant.

Model Summary

S	R-sq	R-sq(adj)	R-sq(pred)
0.0405597	72.54%	64.30%	54.01%

The obtained R-sq value is 72.54%, which we consider a good fit for abrasive manufacturing processes.

Regression Equation:

$$T(10) = 0.385 - 0.00474\,V - 1.501\,G - 0.000400\,S + 0.02455\,V \cdot G + 0.000006\,V \cdot S + 0.000380\,G \cdot S$$

Equation (3)

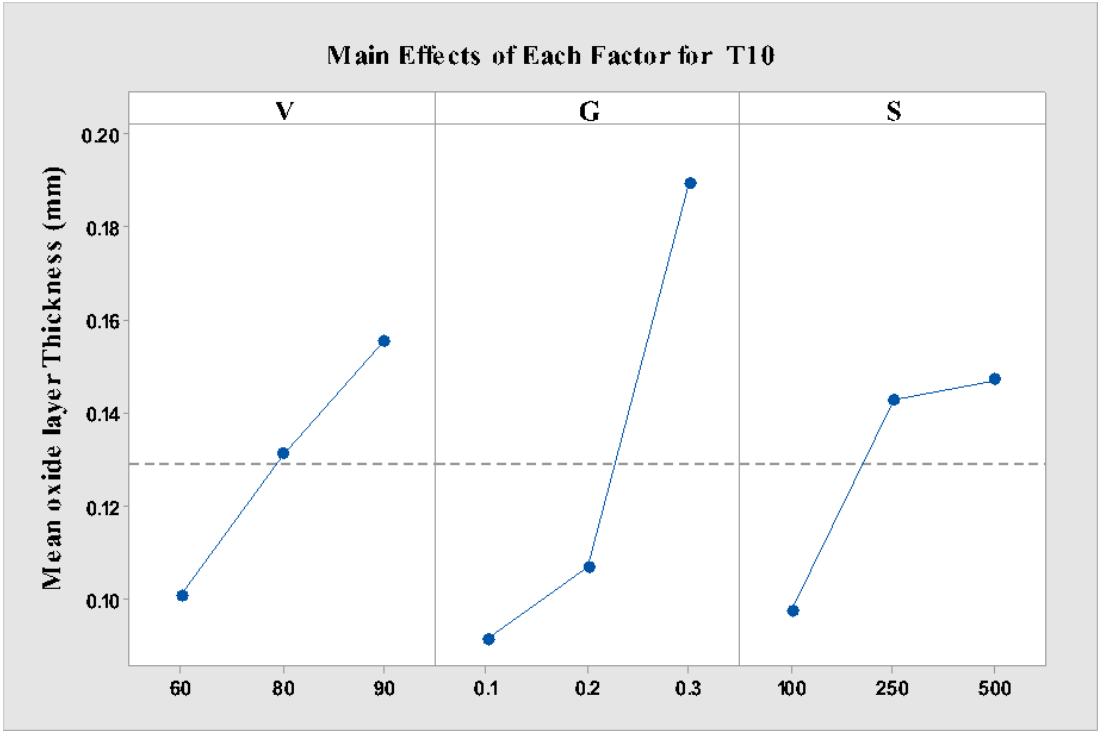

Figure 0– 20: Main Effects of Each Factor for Thickness after 10 min.

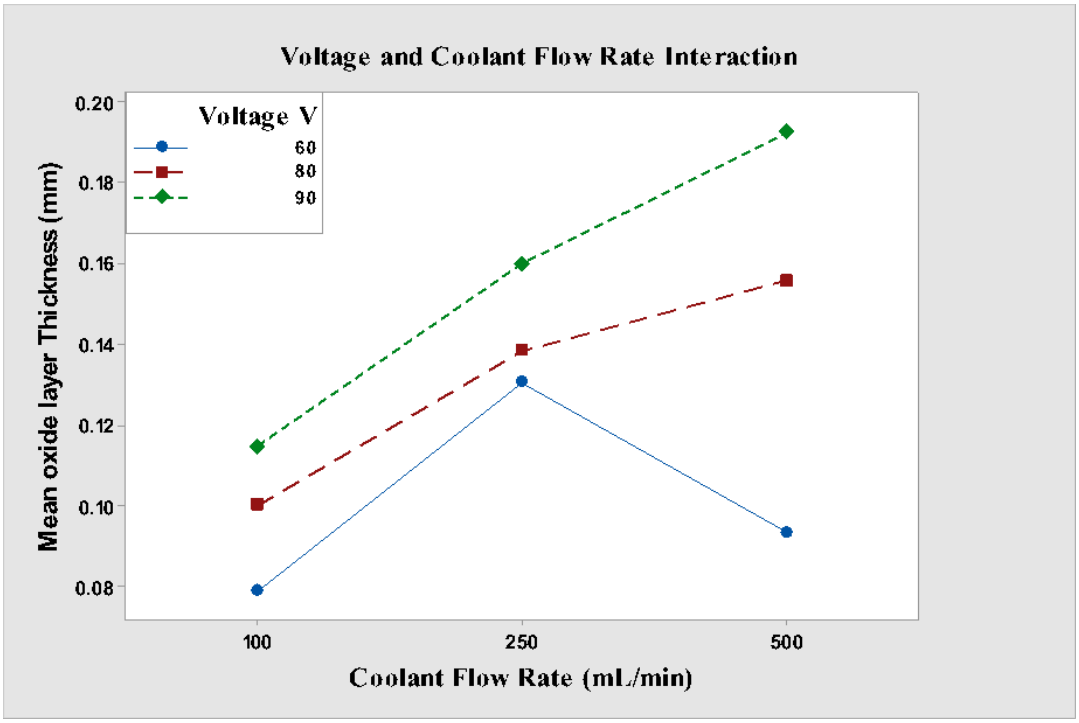

Figure 0– 21: Interaction between Voltage (V) and Coolant Flow (mL/min)

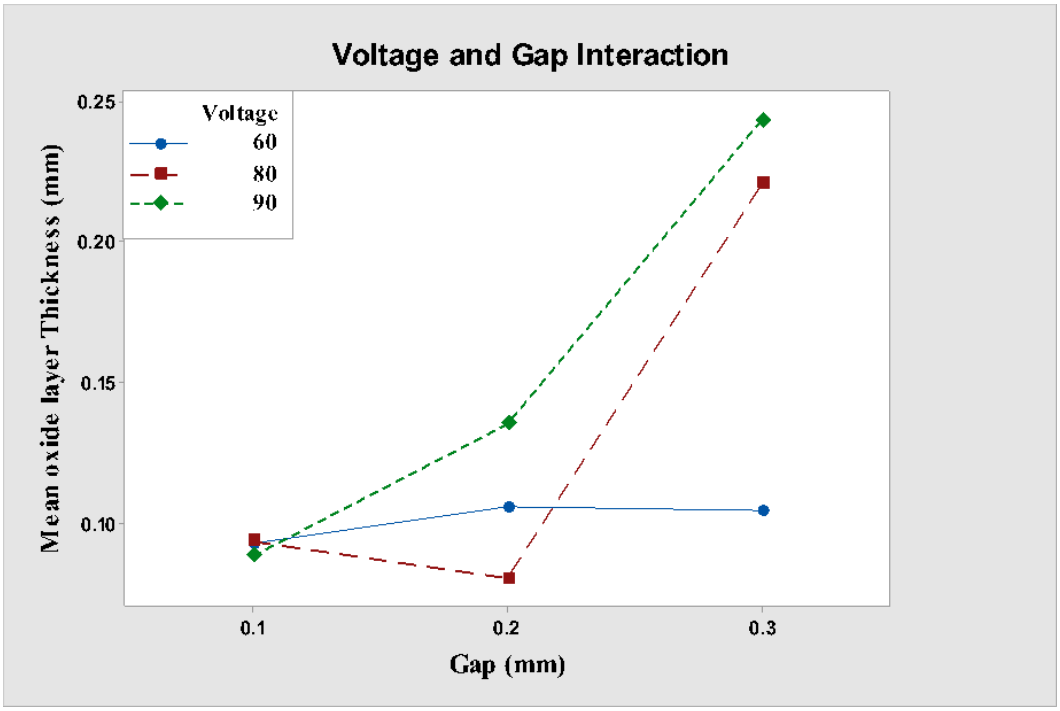

Figure 0– 22: Interaction between Voltage (V) and Gap (mm)

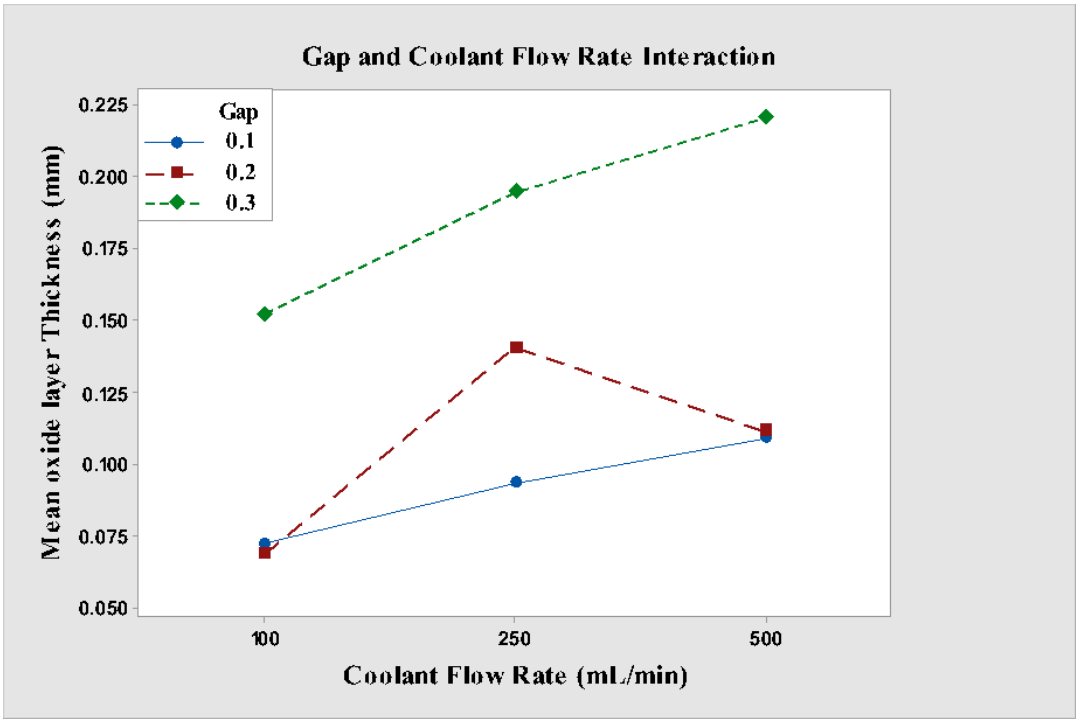

Figure 0– 23: Interaction between gap (mm) and Coolant Flow (mL/min)

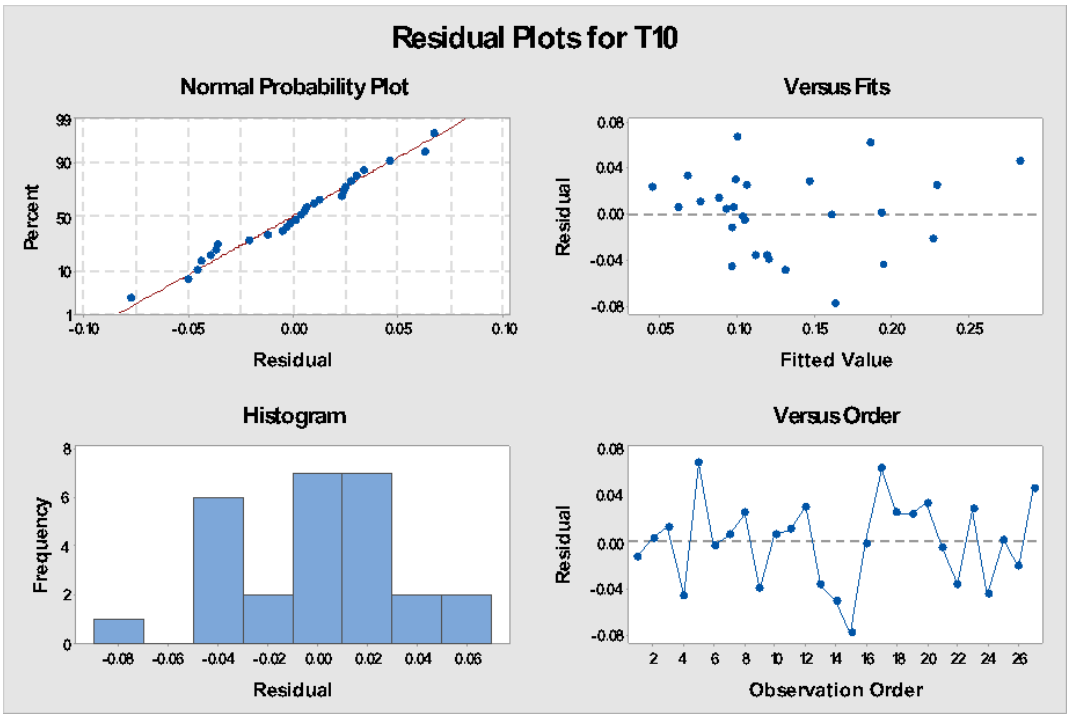

Figure 0– 24: Plots of the residuals for model validation

The residuals plots are normally distributed. No indication of skewed or outlier data. Residuals have a constant variance and presents a good fit. Residuals in the versus plots are randomly distributed and no signs of correlation.

4.6.3 Thickness Measurement after 15 Minutes

Table 4.4: Analysis of variance for 10 min runs

Source	DF	Adj SS	Adj MS	F-Value	P-Value
Regression	6	0.154909	0.025818	11.03	0.000
V	1	0.011459	0.011459	4.90	0.039
G	1	0.019545	0.019545	8.35	0.009
S	1	0.003298	0.003298	1.41	0.249
V*G	1	0.030991	0.030991	13.24	0.002
V*S	1	0.002818	0.002818	1.20	0.285
G*S	1	0.003280	0.003280	1.40	0.250
Error	20	0.046801	0.002340		
Total	26	0.201710			

P-Values are less than 0.0500 indicate the estimated coefficients are significant. The Analysis of Variance shows that the regression model, Voltage, and Gap are very significant. However, the Coolant flow is not significant.

Model Summary

S	R-sq	R-sq(adj)	R-sq(pred)
0.0483743	76.80%	69.84%	52.66%

The obtained R-sq value is 76.80%, which we consider a good fit for abrasive manufacturing processes.

Regression Equation

$$T(15) = 0.438 - 0.00521\,V - 2.129\,G - 0.000448\,S + 0.03327\,V * G + 0.000005\,V * S + 0.000818\,G * S$$

Equation (4)

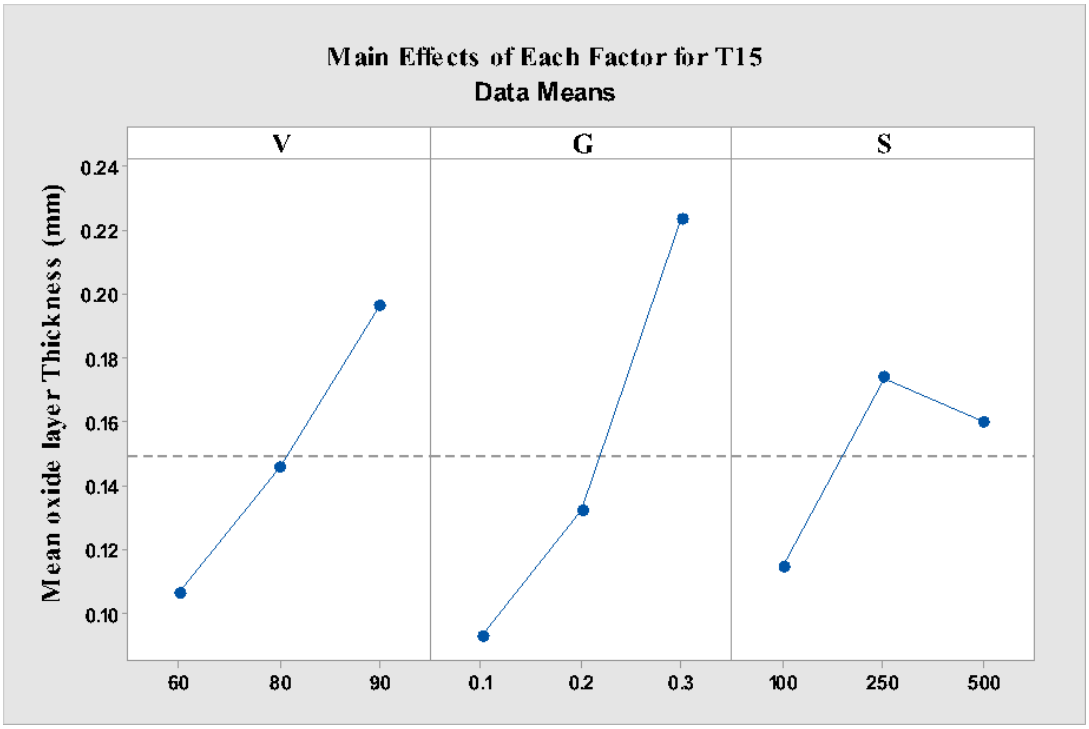

Figure 0– 25: Main Effects of Each Factor for Thickness after 15 min.

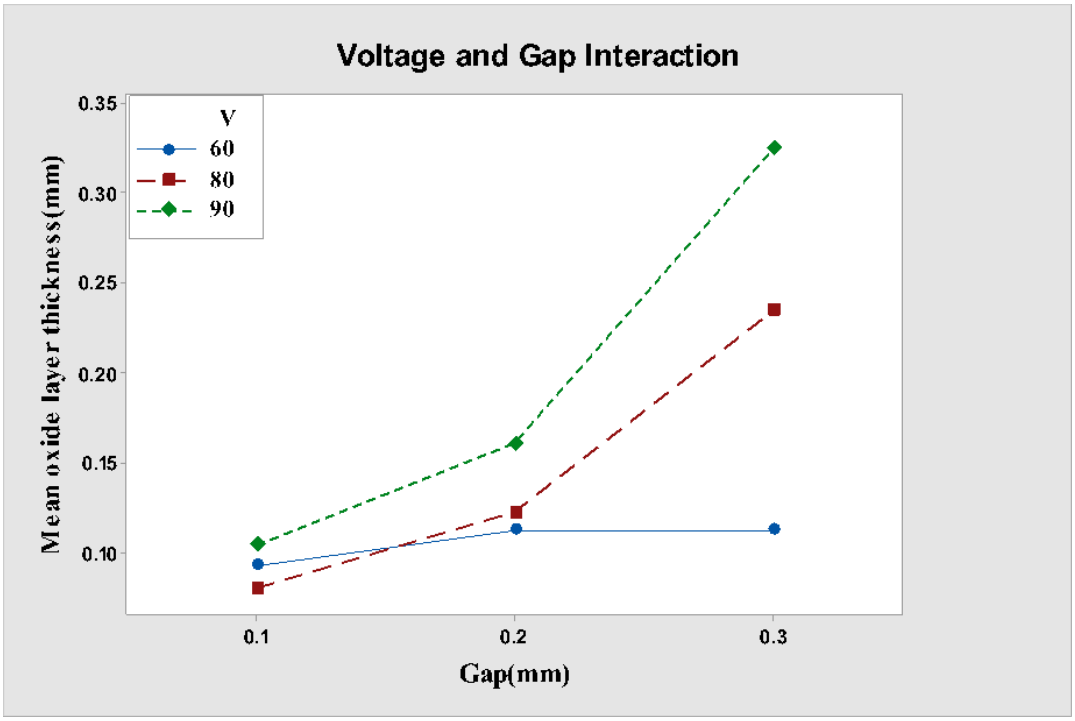

Figure 0– 26: Interaction between Voltage (V) and Gap (mm)

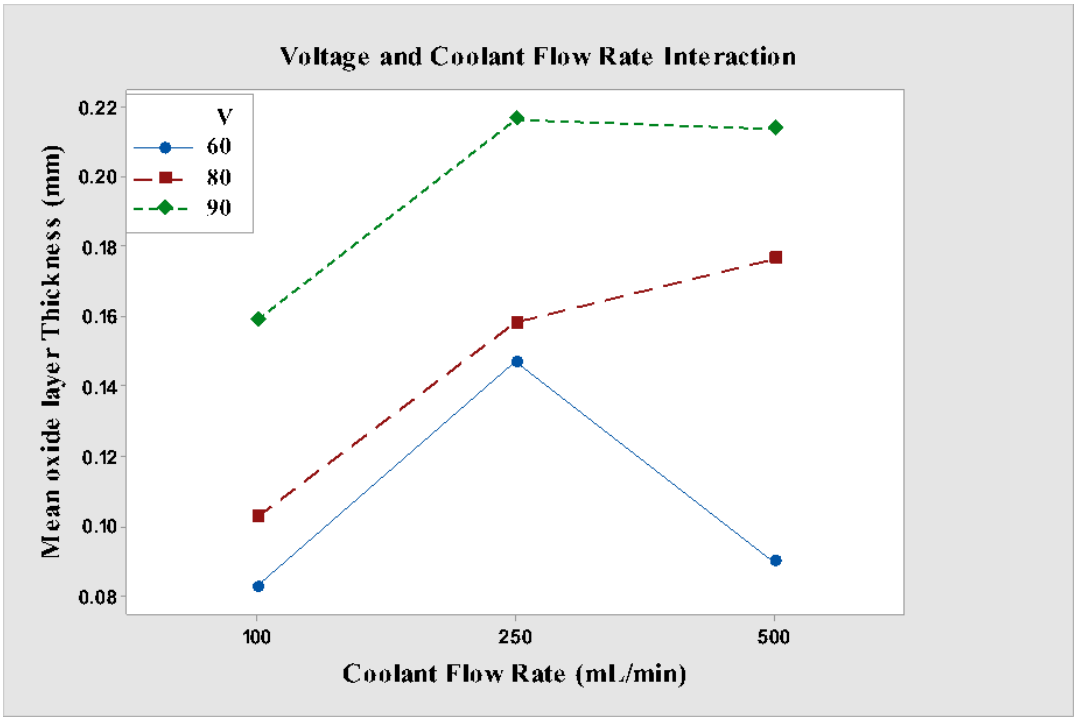

Figure 0– 27: Interaction between Voltage (V) and Coolant Flow (mL/min)

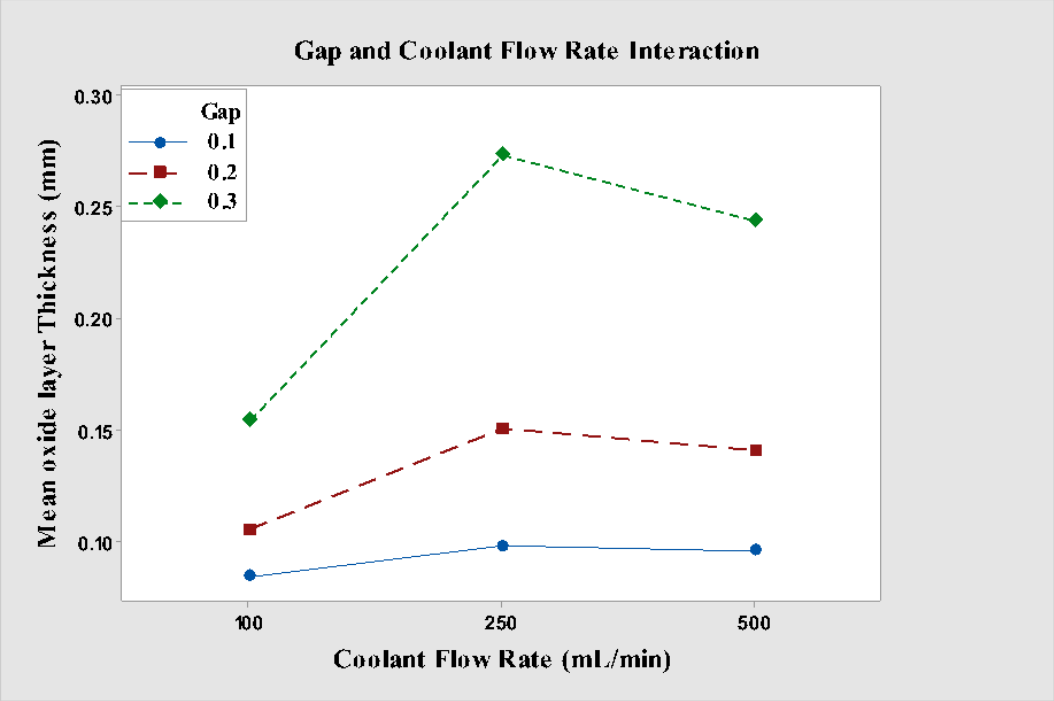

Figure 0– 28: Interaction between Gap(mm) and Coolant Flow (mL/min)

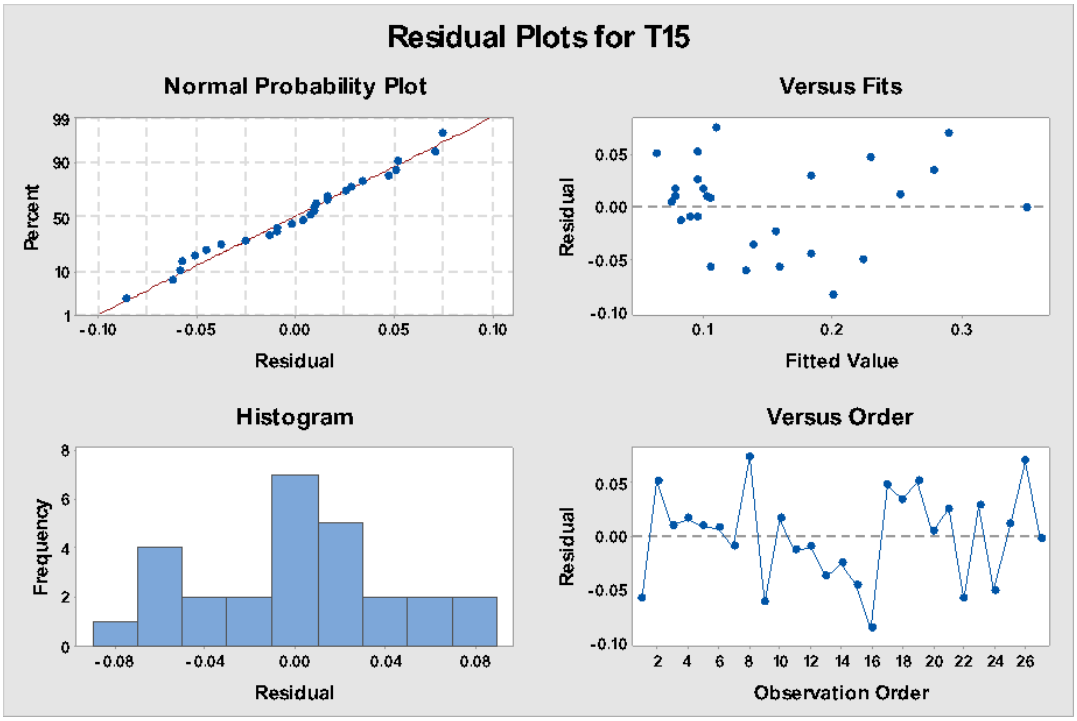

Figure 0– 29: Plots of the residuals for model validation

The residuals plots are normally distributed. No indication of skewed or outlier data. Residuals have a constant variance and presents a good fit. Residuals in the versus plots are randomly distributed and no signs of correlation.

4.6.4 Thickness Measurement after 20 Minutes

Table 4.5: Analysis of variance for 10 min runs

Source	DF	Adj SS	Adj MS	F-Value	P-Value
Regression	6	0.134200	0.022367	11.56	0.000
V	1	0.010395	0.010395	5.37	0.031
G	1	0.014973	0.014973	7.74	0.012
S	1	0.000934	0.000934	0.48	0.495
V*G	1	0.029582	0.029582	15.29	0.001
V*S	1	0.002033	0.002033	1.05	0.318
G*S	1	0.000018	0.000018	0.01	0.924
Error	20	0.038704	0.001935		
Total	26	0.172903			

P-Values are less than 0.0500 indicate the estimated coefficients are significant. The Analysis of Variance shows that the regression model, Voltage, and Gap are very significant. However, the Coolant flow is not significant.

Model Summary

S	R-sq	R-sq(adj)	R-sq(pred)
0.0439908	77.62%	70.90%	58.14%

The obtained R-sq value is 77.62%, which we consider a good fit for abrasive manufacturing processes.

Regression Equation

$$T(20) = 0.400 - 0.00496\,V - 1.863\,G - 0.000239\,S + 0.03250\,V \cdot G + 0.000004\,V \cdot S - 0.000061\,G \cdot S$$

Equation (5)

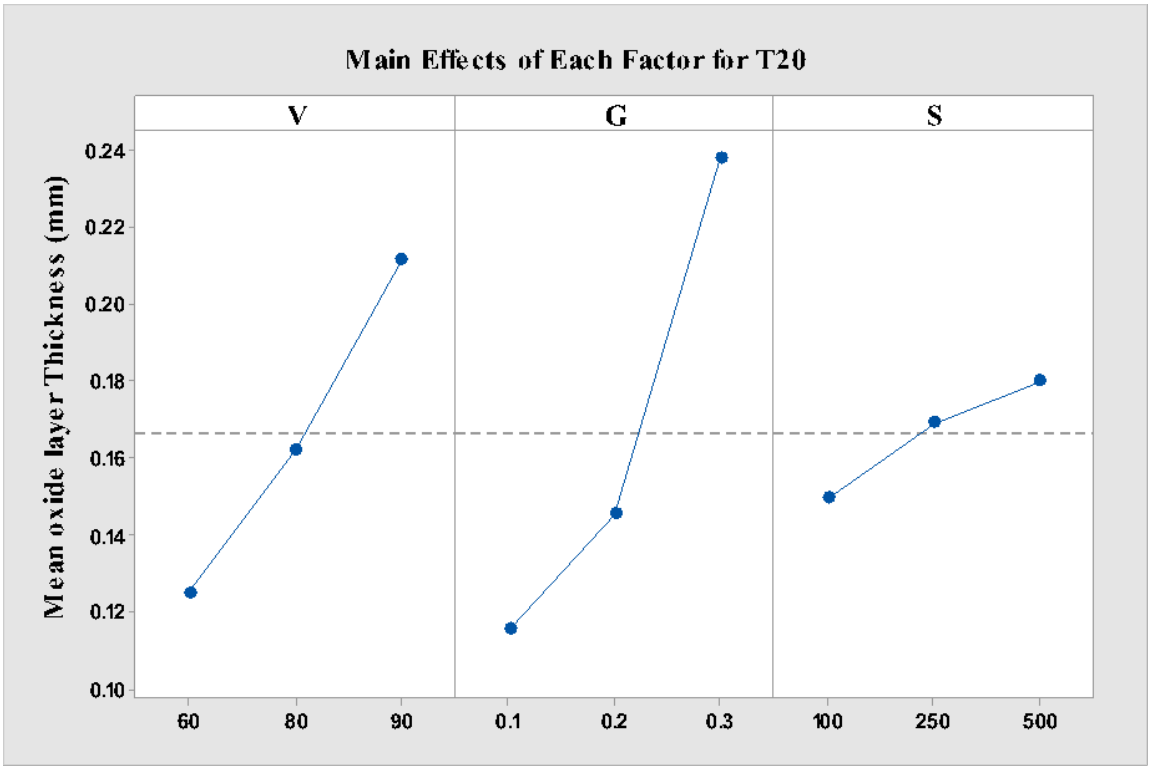

Figure 0– 30: Main Effects of Each Factor for Thickness after 20 min.

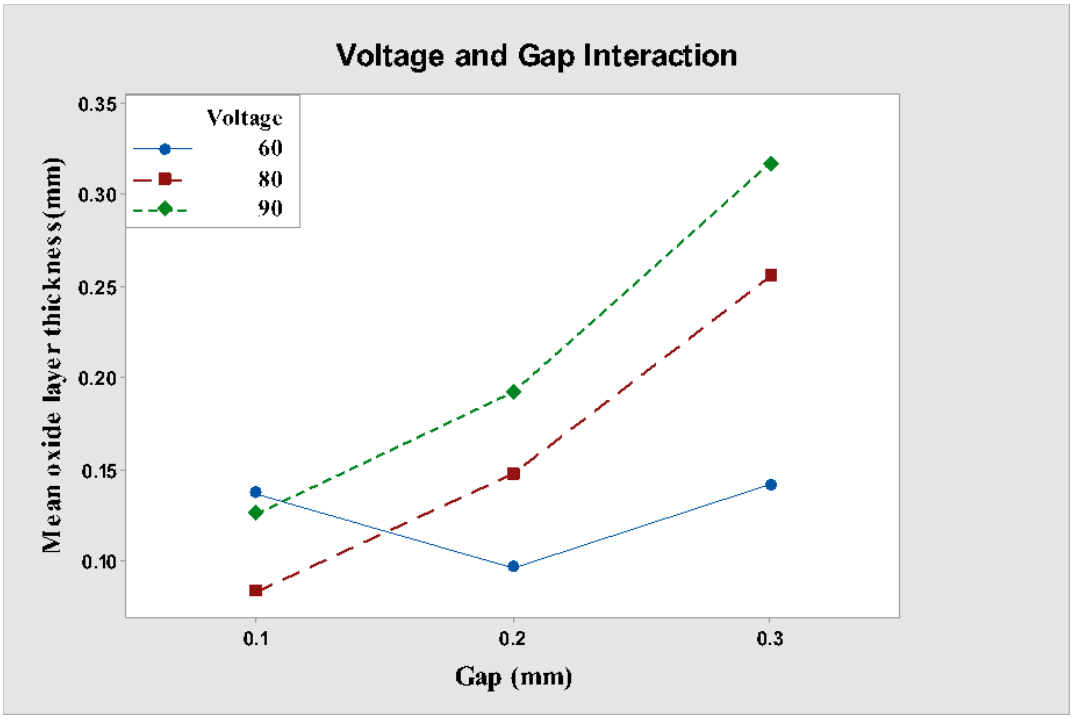

Figure 0– 31: Interaction between Voltage (V) and Gap (mm)

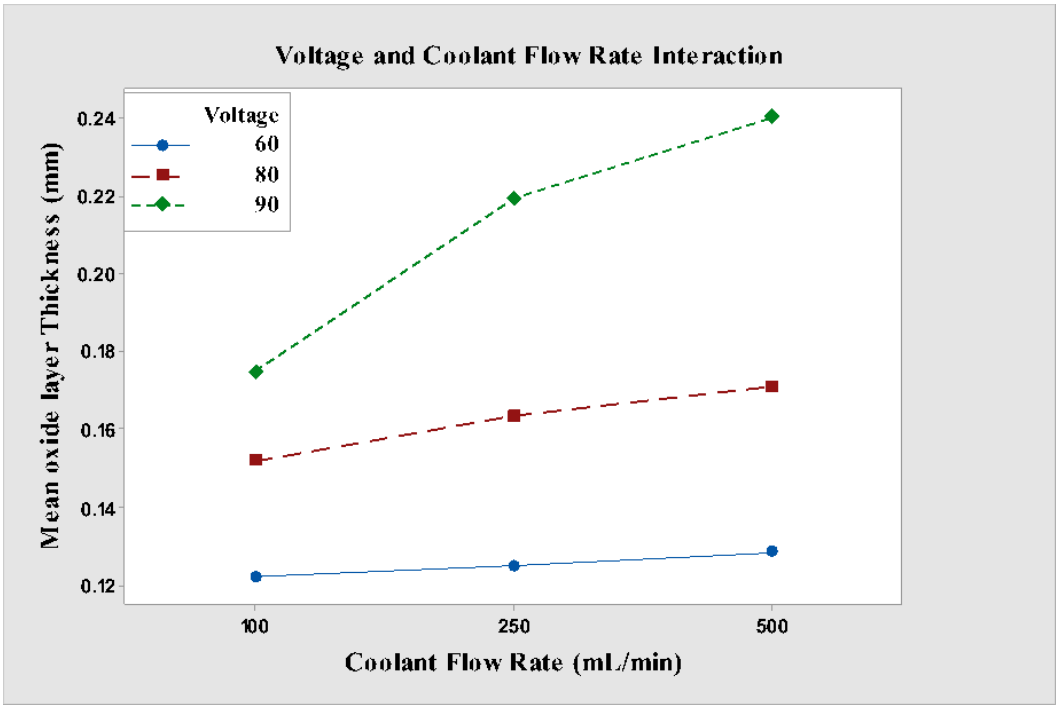

Figure 0– 32: Interaction between Voltage (V) and Coolant Flow (mL/min)

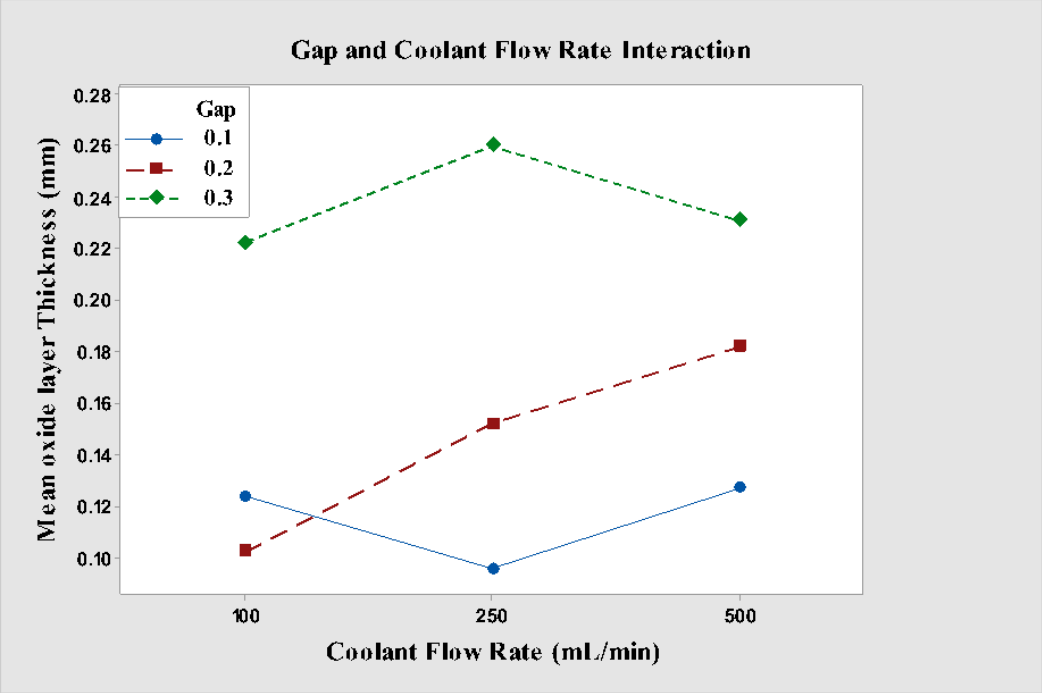

Figure 0– 33: Interaction between Gap(mm) and Coolant Flow (mL/min)

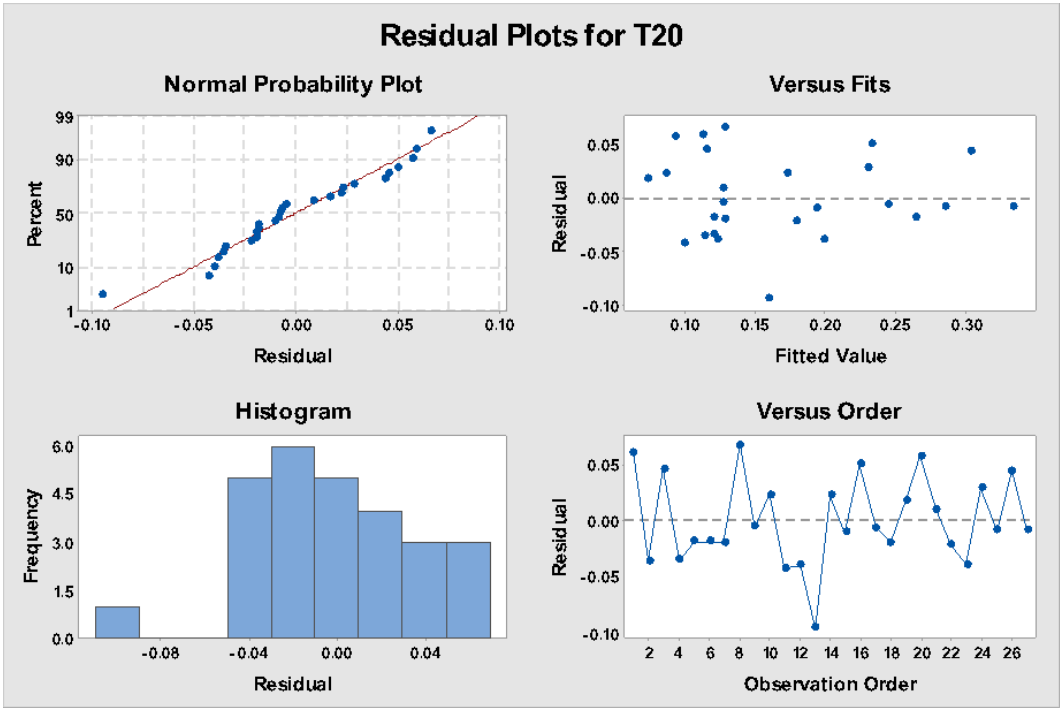

Figure 0– 34: Plots of the residuals for model validation

The residuals plots are normally distributed. No indication of skewed or outlier data. Residuals have a constant variance and presents a good fit. Residuals in the versus plots are randomly distributed and no signs of correlation.

To simplify the final modeling process and putting into consideration that by 10 min all oxide layer was fully formed and after 10 min surface burn might occur, only the thicknesses measured in the 10-min runs were used to model the final oxide layer thickness, since that time point was considered the point at which the initial growth of oxide layer would have finished.

For several sets of experiments, the oxide layer thickness on the sides of the sample was very close to the electrode-grinding wheel gap, indicating that the only limiting factor for the oxide layer thickness at high voltages was the gap. Therefore, when the predicted thickness exceeded the electrode-grinding wheel gap, the gap value is used as the predicted oxide layer thickness.

All three factors gap, voltage, and coolant flow rate have a positive influence on the model, as does the interaction between voltage and gap. An analysis on main effects and interactions of the three factors is shown in Fig 4-35 ~38; plots of residuals that validates the linear regression model are provided in Fig 4-39.

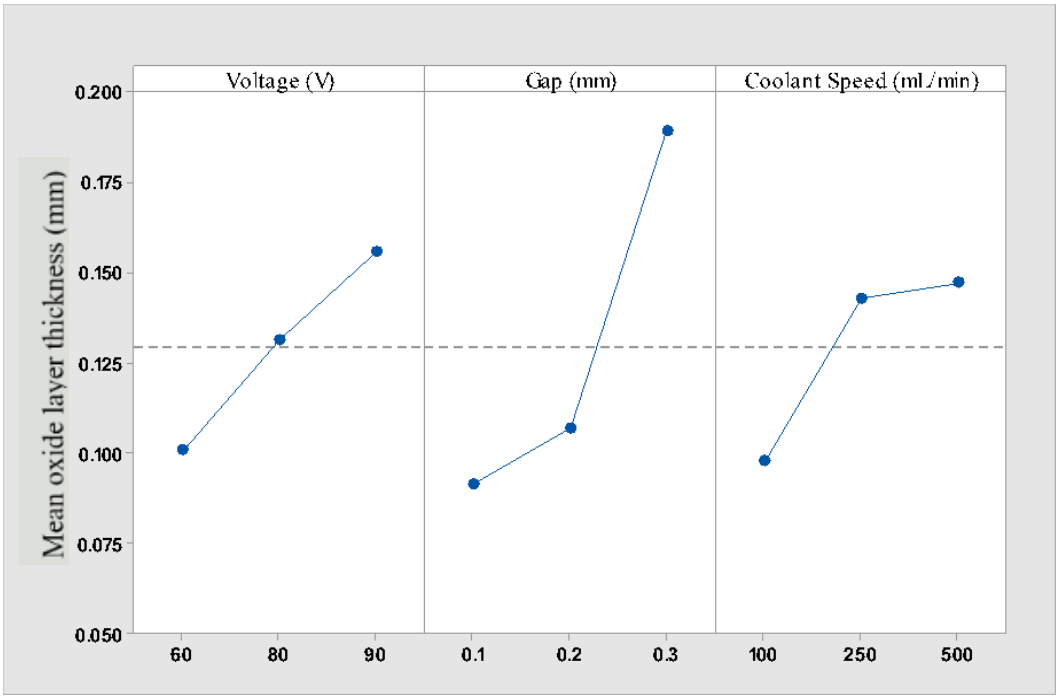

Figure 0– 35: Main Effects of Each Factor for Thickness after 10 min.

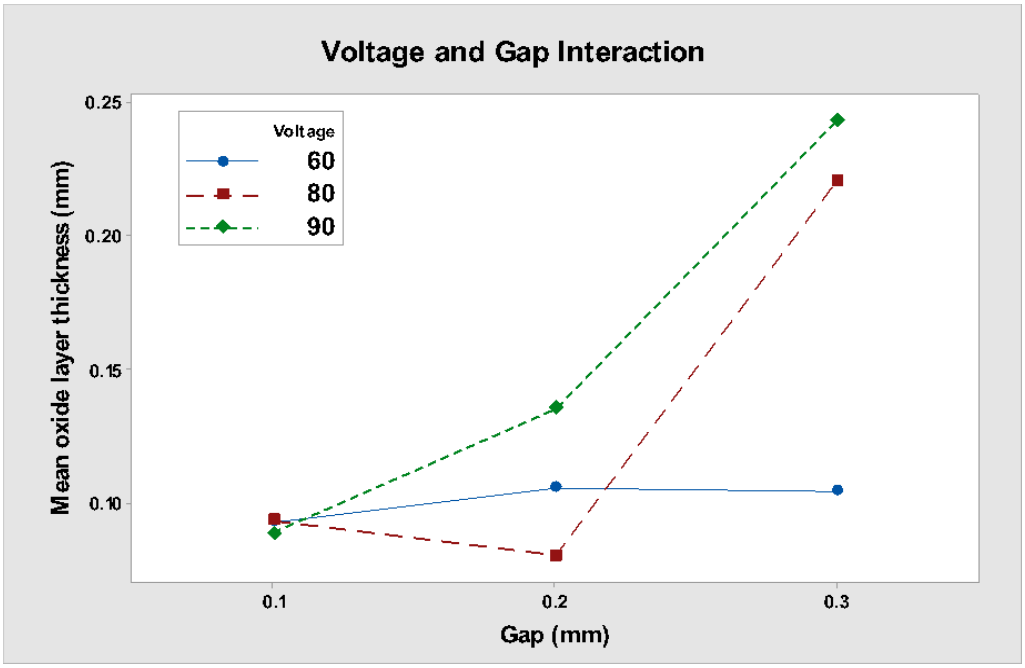

Figure 0– 36: Interaction between Voltage (V) and Gap (mm)

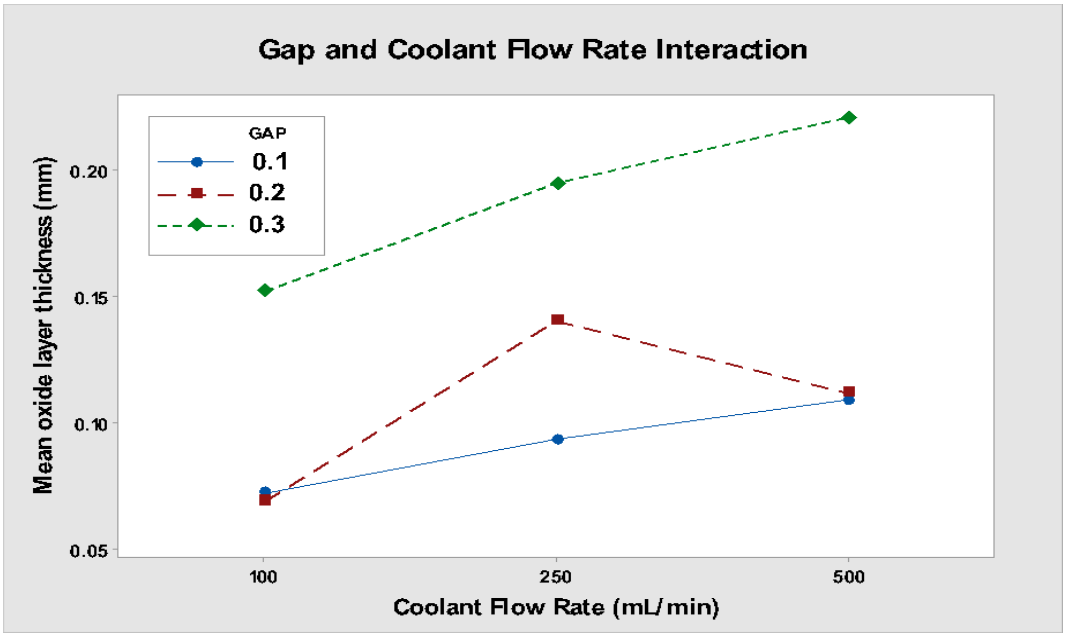

Figure 0– 37: Interaction between Gap (mm) and Coolant Flow (mL/min)

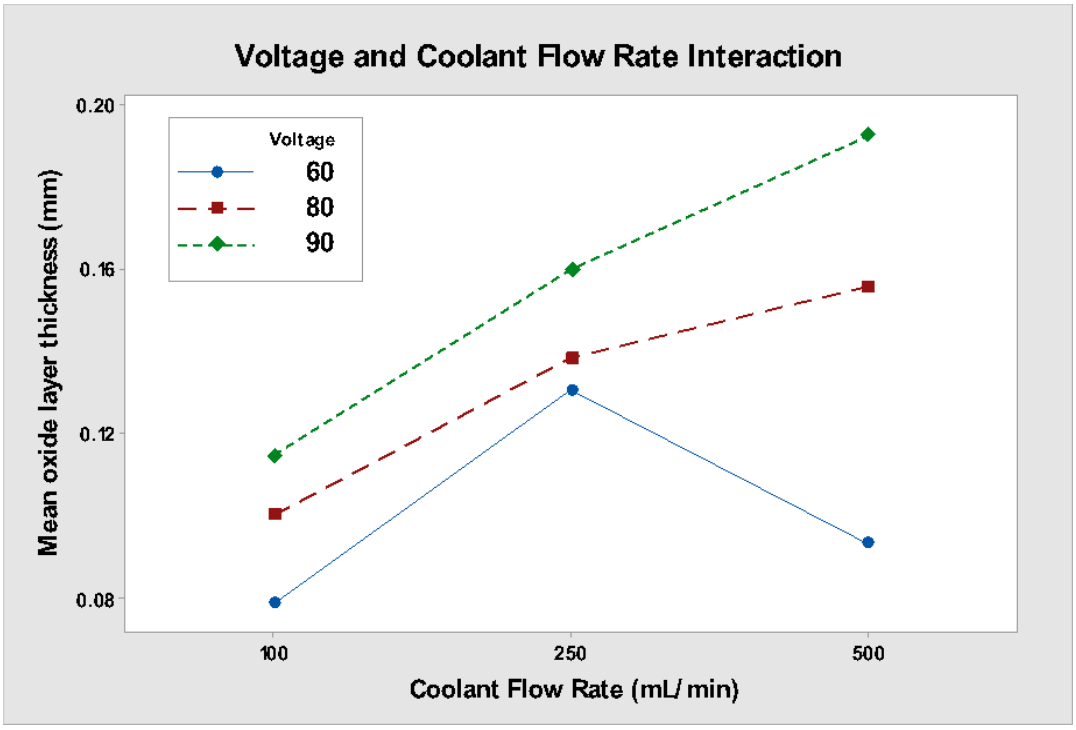

Figure 0– 38: Interaction between Voltage (V) and Coolant Flow (mL/min)

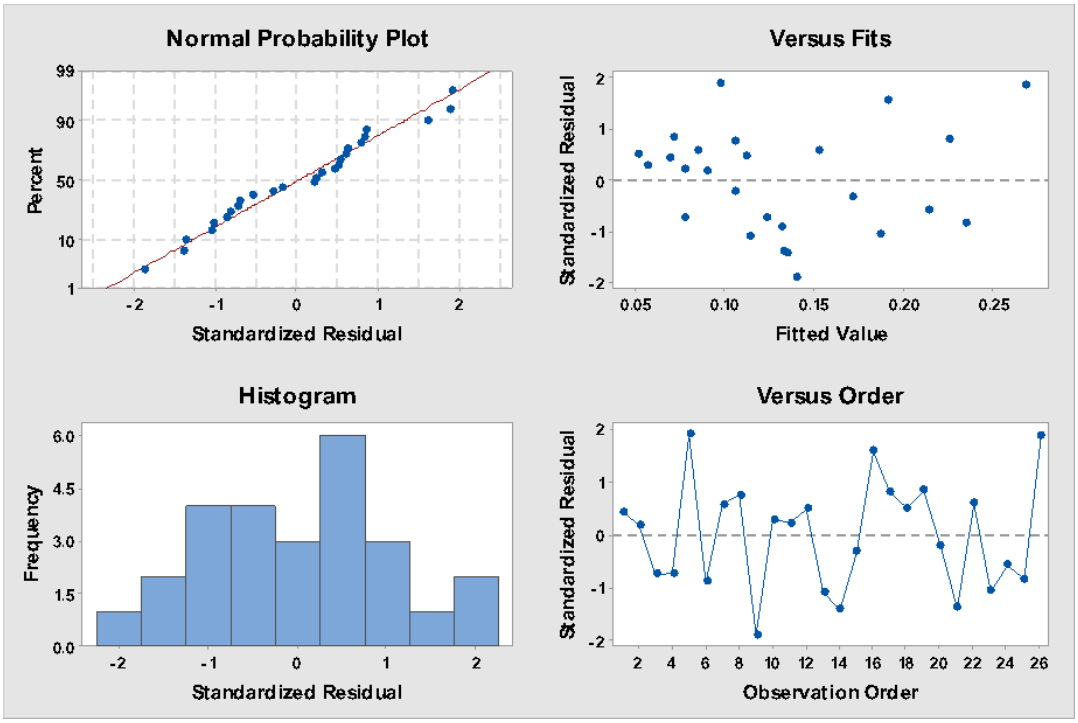

Figure 0– 39: Plots of the residuals for model validation

A linear regression model was fitted using Minitab 18 as follows: When the oxide layer thickness (T_{OL}) was greater than the gap, the gap (G) was predicted as the final oxide layer thickness, as the oxide layer cannot grow more than the gap allows; the unit used in this model is in mm. A graph was generated comparing the original data and the values predicted from this model (Fig 4-40). The obtained R-sq value is 0.7351, which we consider a good fit for abrasive manufacturing processes.

$$T_{ol} = 0.23 - 0.00306V - 1.393G + 0.000137S + 0.02455VG(if T_{ol} < G)$$

or

$$T_{ol} = G\ (if T_{ol} \geq G) \qquad \text{(Equation 6)}$$

Several attempts were made to fit the model with polynomial and logistic regressions; however, these models yielded smaller R-sq values. Linear regression was found to be a better fit than higher-order models.

Two past studies which focused on oxide layer thickness both agreed that higher voltage increased the oxide layer thickness and the size of the gap had no significant effect [Marinescu, Ohmori, Katahira 2011] [Klocke, Klink, Henerichs 2009]. This study confirmed that the voltage had a positive effect on the thickness; however, the electrode-wheel gap also had a large effect. Most likely, the high range of gaps in past studies contributed to the observed difference. Considering the range of gap used here was chosen from industrial practices, this study produced more meaningful results to the industry.

The model presented here was only applicable to this specific study, because the parameter “coolant flow rate” was only used to indicate the relative speed between the grinding wheel and the electrode. Once a direct relationship between them can be established, since the range of voltage and gap were all within industry requirements, this model can be adjusted to be generally applicable.

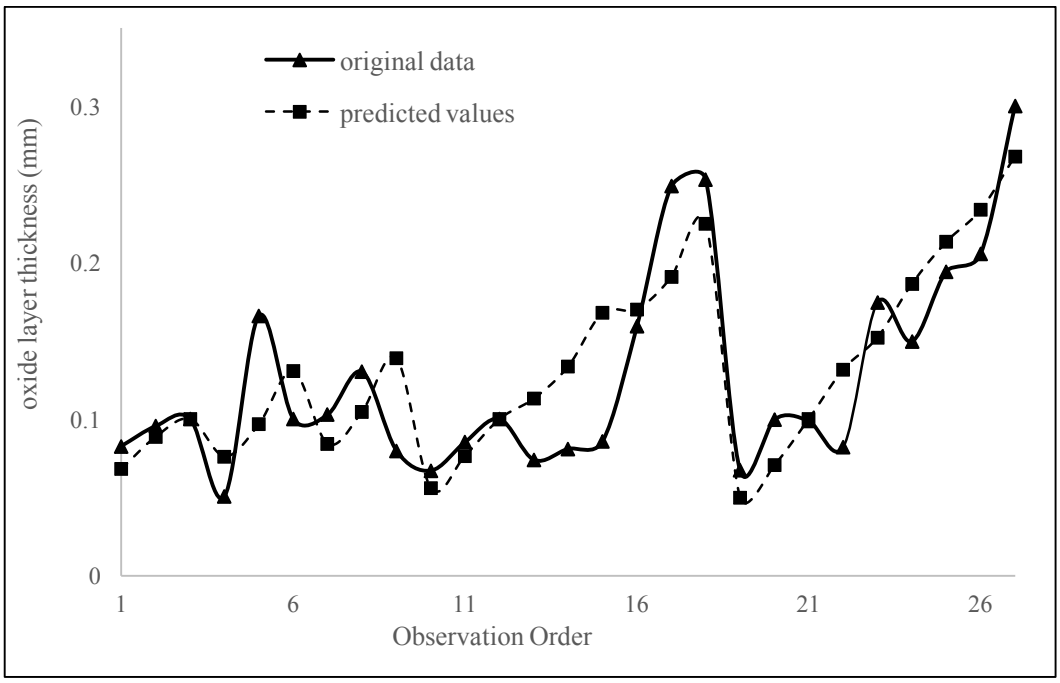

Figure 0– 40: Comparison between original oxide layer thickness data obtained at 10 min and oxide layer thickness predicted by the proposed model for the same parameters.

4.7 Model Validation

A series of experiments is carried out to validate the validity of the model. Two different cases were selected for the test. In case 1, three parameter sets that have previously been experimented on were selected to test how well the model explained itself; and in case 2, three parameter set that was randomly selected to be in the parameter range covered by the model to see if the model is effective within the parameter range.

The parameter sets used in two cases is shown in table 4.6 and 4.7.

Table 0.6: Case 1 parameter from previous experiment

Case 1	**Voltage (V)**	**Gap (mm)**	**Flow rate (mL/min)**
1a	60	0.1	250
1b	60	0.3	500
1c	80	0.2	100

Table 0.7: Case 2 randomly selected parameter

Case 2	**Voltage (V)**	**Gap (mm)**	**Flow Rate (mL/min)**
2a	65	0.1	200
2b	70	0.3	350
2c	75	0.2	150

The SEM images of sides and middle of the samples is shown in Fig 4-41.

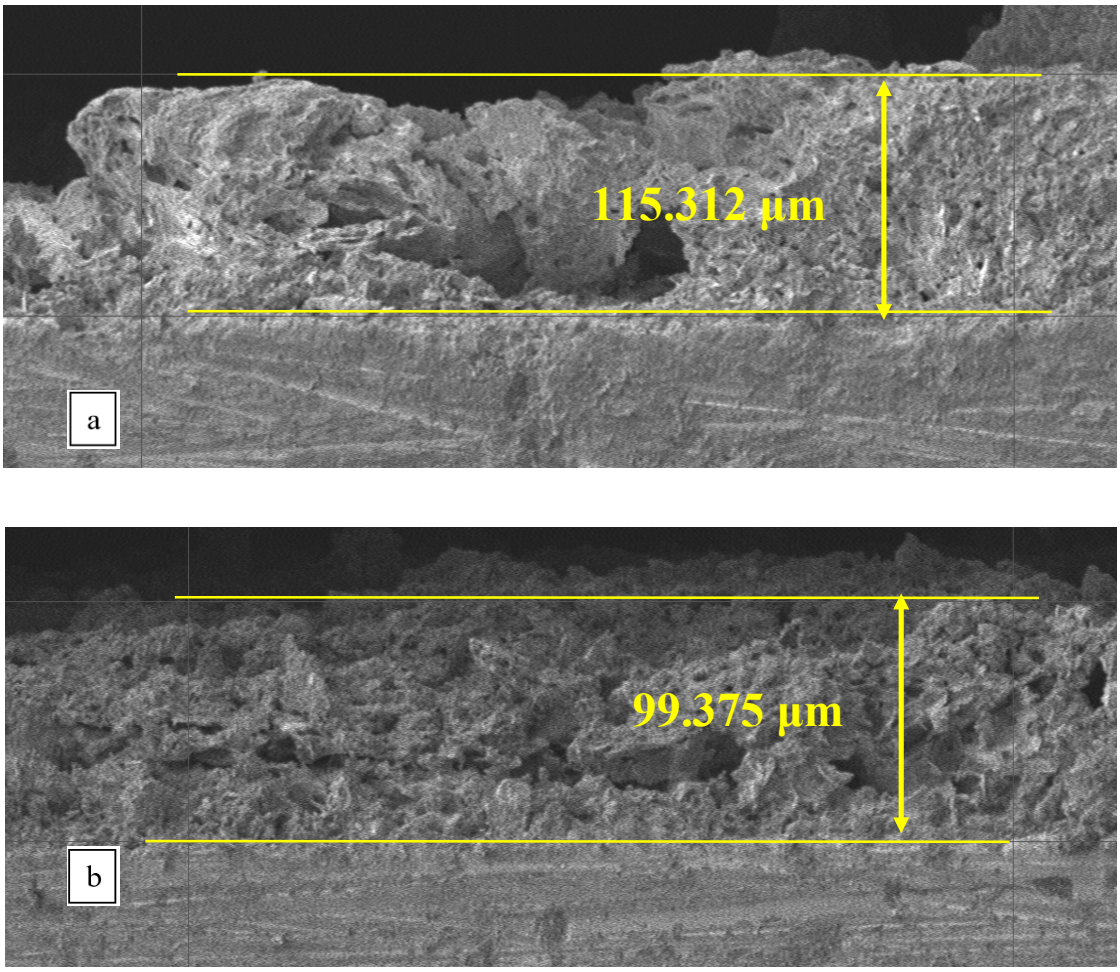

Figure 0– 41: Fully developed oxide layer in a mountainous formation (a) Oxide clusters are highly inter-connected (b) very little porosity can be observed.

SEM images of sides is shown in fig 4-42.

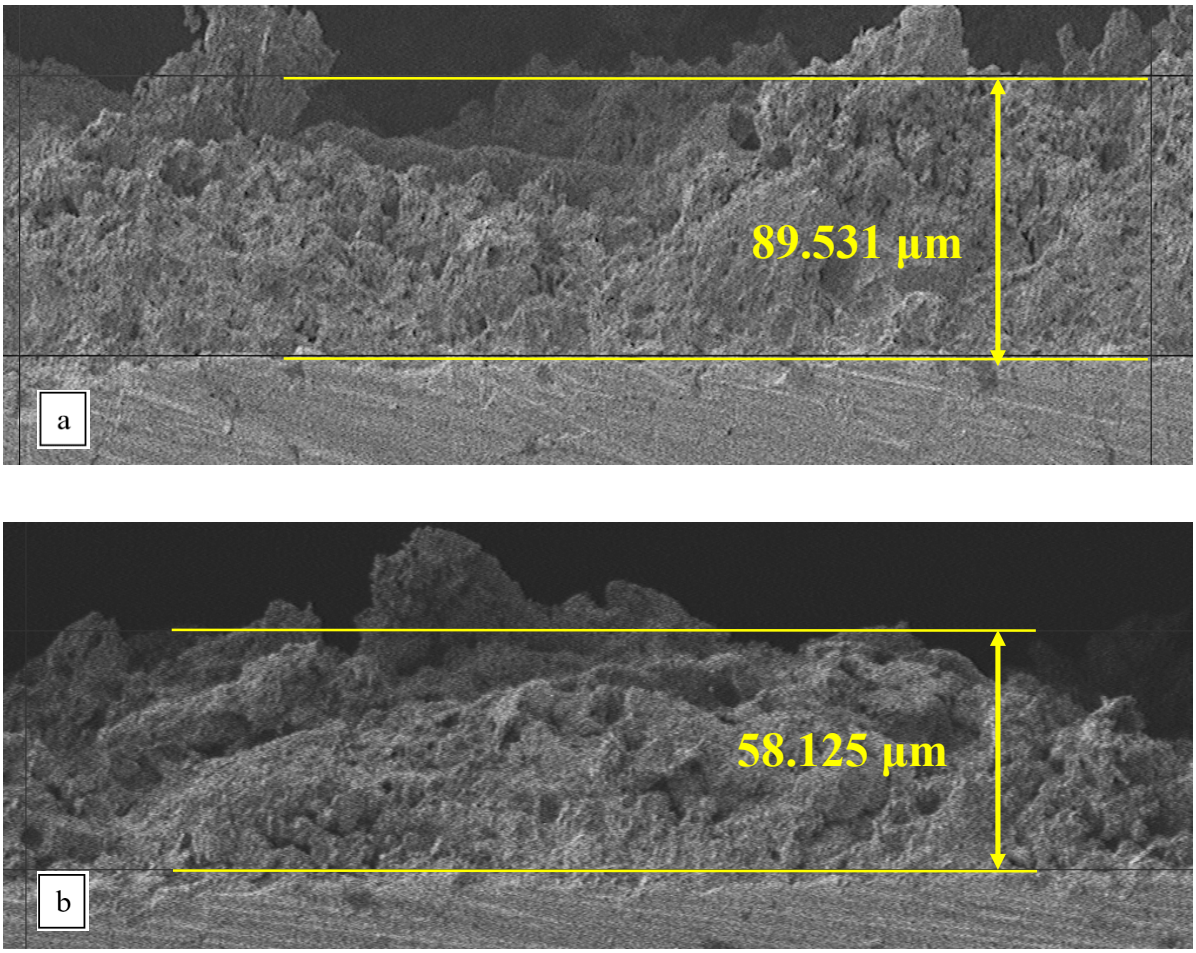

Figure 0– 42: Oxide layer where coolant flow is the fastest across the metallic sample surface (a) Oxide layer in the "shell" formation. (b) a significant amount of oxide was removed by the coolant.

The oxide layer distribution was shown in fig 4-43.

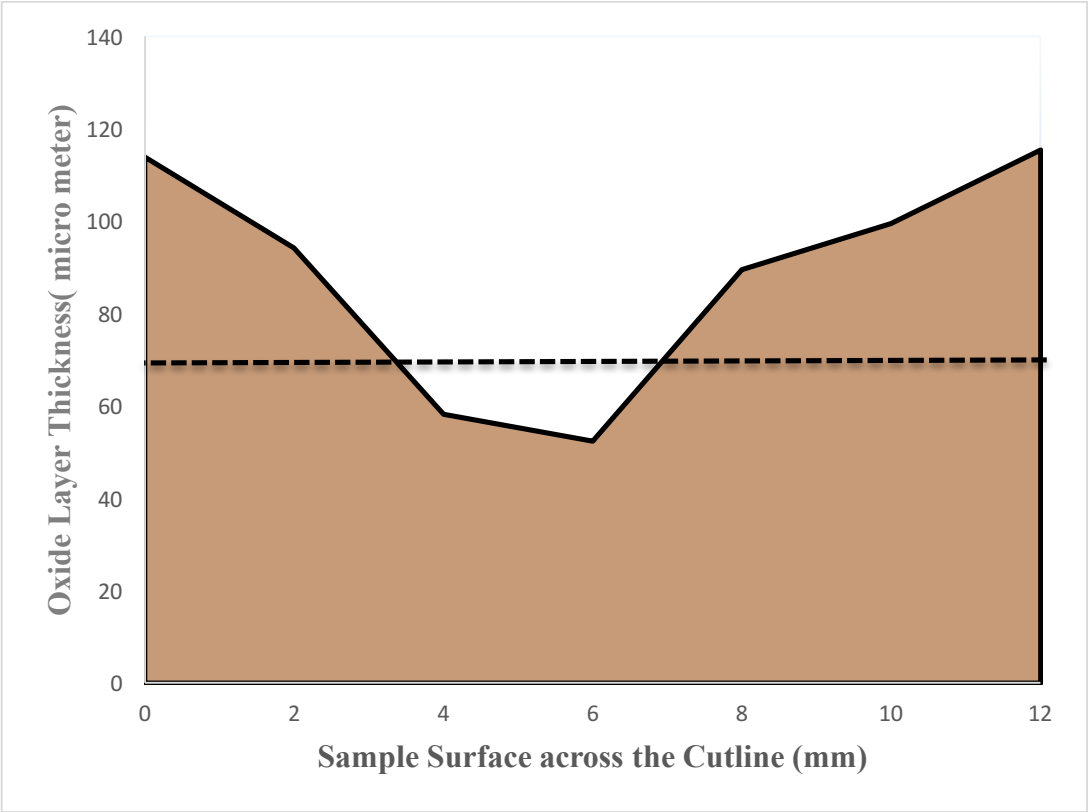

Figure 0– 43: Thickness distribution of the oxide layer as a function (μm) of location across the cutline (mm). The tinted area indicated oxide layer.

Oxide layer thicknesses of the samples was measured and averaged using the same principles as the original study and presented in table 4.7.

Table 0.7: Percentage error between Predicted and Observed results

Case	Voltage (V)	Gap (mm)	Flow Rate (mL/min)	Predicted (mm)	Observed (mm)	Error %
1a	60	0.1	250	0.08865	0.09239	4.22
1b	60	0.3	500	0.1389	0.12037	13.34
1c	80	0.2	100	0.1131	0.09544	15.61
2a	65	0.1	200	0.078775	0.087323	10.85
2b	70	0.3	350	0.1614	0.1803	11.71
2c	75	0.2	150	0.1107	0.09167	17.19

The percentage error presented in table 4.7 is acceptable since the obtained R-sq value is 73.51%, which we consider a good fit for abrasive manufacturing processes.

Chapter 5

Conclusion

5.1 objective original contributions:

The objective of this study is to observe how the oxide layer forms on the grinding surface during pre-dressing, and how the voltage, the gap between electrode and grinding wheel, and coolant flow rate affect the oxide layer thickness. The experiment described here implemented the observations from previously reported studies on the thickness of the oxide layer [Marinescu, Ohmori, Katahira 2011] [Biswas, Kumar, Rahman 2010], which used metallic-bonded prism samples without abrasives instead of a full grinding machine system. The implementation of the system used in this study included the use of electrode-grinding wheel gaps that match the actual grinding parameters and the use of scanning electron microscopy (SEM) to observe the state and measure the thickness of the oxide layer. The major contribution of this study is the extensive comparison of the morphology of the cross-section of oxide layers.

5.2 Summary

By examining the ELID oxidation sites using SEM imaging on a pre-dressed metal sample, this research provides valuable information on the oxidation layer for ELID grinding and helps researchers better understand the effects of fluid flow and workpiece trajectory for ELID grinding:

- The microstructure of the oxidation sites varied greatly between each observation site, most likely due to the different coolant flow patterns across the sample surface.
- The oxide layer was found to be unevenly distributed at the sample surface. It was thicker at the sides of the sample, and thinner at the middle of the sample.
- All three factors studied, voltage, electro-wheel gap and coolant flow rate, are all statistically significant, and all positively affected the oxide layer thickness. There was also noticeable interaction between voltage and gap.
- A model predicting oxide layer thickness for different parameters has been developed and provided. The model was specific to this study now but has the potential to be expanded to be generally applicable.
- The pre-dressing process generally takes less than 10 minutes, and it can be shortened by increasing voltage.
- Pre-dressing at high voltages is likely to cause burning on the grinding surface.

References

Alqahtani, B., Zhang, M., Marinescu, I., Bafakeeh, O. T., & Al Sofyani, S. (2019). Microscopic characterization and modeling of oxide layer for electrolytic in-process dressing (ELID) grinding with focus on voltage, electrode-wheel gap, and coolant flow. *The International Journal of Advanced Manufacturing Technology*, 1-10.

Zhang, C., Ohmori, H., & Li, W. (2000). Small-hole machining of ceramic material with electrolytic interval-dressing (ELID-II) grinding. *Journal of Materials Processing Technology*, *105*(3), 284-293.

Doi, T., Uhlmann, E., & Marinescu, I. D. (Eds.). (2015). *Handbook of ceramics grinding and polishing*. William Andrew.

Gizella, K., & Zoltán, L. (2003). The Development of an Expert System when ELID Grinding Hard Materials. *IFAC Proceedings Volumes*, 36(3), 193-197. doi: 10.1016/s1474-6670(17)37756-x

Han, P. (2009). A study on electrolytic in-process dressing (ELID) Grinding of Sapphire with Acoustic Emmission Monitoering . The University of Toledo.

Hasegawa, Y., Itoh, N., Nemoto, A., Ohmori, H., Kato, T., & Igawa, Y. (2007). 208 ELID Lap Grinding using a Lapping Wheel with Anodic Oxidation. *The*

Proceedings Of Yamanashi District Conference, 2007(0), 58-59. doi: 10.1299/jsmeyamanashi.2007.58

Jackson, M. J., & Davim, J. P. (2011). *Machining with abrasives* (pp. 4-5). New York: Springer.

Hitchiner, M. P., Marinescu, I. D., Uhlmann, E., Rowe, W. B., & Inasaki, I. (2016). *Handbook of machining with grinding wheels*. CRC Press.

Lim, H. S., Fathima, K., Senthil, K., & Rahman, M. (2002). A Fundamental Study on the Mechanism of Electrolye In-Process Dressing (ELID) Grinding. *International Journal of Machine Tools & Manufactur*e(42), 935-933. Retrieved from https://www.researchgate.net/publication/223749913_A_fundamental_study_on_the_mechanism_of_electrolytic_in-process_dressing_ELID_grinding

Maitra, S. (2013). A Brief Description of the Processing of Ceramics. Published by: *Indian Institute Of Ceramics*, 22(1), 16.

Murata, R., Okano, K., & Tsutsumi, C. (1985). Grinding of Structural Ceramics. *A journal on Grinding Symposium* PED, 16.

Ohmori, H., & Nakgawa, T. (1997). Utilization of Nonlinear Conditions in Precision Grinding with ELID (Electrolytic In-Process Dressing) for Fabrication of Hard Material Component . Tokyo, Japan: *The Institute of Physical and Chemical Research*.

Rahman, M., Kumar, A. S., Lim, H. S., & Fatima, K. (2003). Nano finish grinding of brittle materials using electrolytic in-process dressing (ELID) technique. *Sadhana*, *28*(5), 957-974.

Rahman, M. S. (2009). A Review of Electrolytic In-Process Dressing (ELID) Grinding; Key Engineering Material. *Progress in Abrasive and Grinding technology*, Vol 4.

Rahman, T & Selah, T. (2014). Electrolytic In-Process Dressing (ELID) Grinding for Nano-Surface Generation. Amsterdam, Netherlands: Elsevier Ltd. Retrieved from https://www.researchgate.net/publication/277006398_Electrolytic_In-Process_Dressing_ELID_Grinding_for_Nano-Surface_Generation

Rowe, W. B. (2013). *Principles of modern grinding technology*. William Andrew.

Saleh, T. B. (2004). Efficient dressing of the wheel in ELID grinding by controllable voltage with force feed baack. Vol 2.

Saleh, T., & Bahar, R. (2017). ELID Grinding and EDM for Finish Machining. *Comprehensive materials finishing*, 1, 364-407.

Saleh, T. B. (2008). In-process Truing of Metalbonded Diamond Wheels for Electrolytic In-process Dressing (ELID) Grinding. *International Journal of Precision Engineering and Manufacturing*, Vol 2.

Wang, Z., Ren, C., Chen, G., Zhang, L., & Deng, X. (2018). A comparative study on state of oxide layer in ELID grinding with tool-cathode and workpiece-cathode. *The International Journal of Advanced Manufacturing Technology*, 94(1-4), 1299-1307.

Wu, M. L., Ren, C. Z., & Zhang, K. F. (2018). Wear life characterization of the grinding wheel for electrolytic in-process dressing (ELID) grinding of ball bearing raceways: a new perspective based on a moving normal distribution curve of

the grit state variation. *The International Journal of Advanced Manufacturing Technology*, 1-10.

Xu, Z., Spanu, C., & Marinescu, I. D. (2015). ELID Grinding and Polishing. In *Handbook of Ceramics Grinding and Polishing* (pp. 326-359).

Yu, X., Huang, S., & Xu, L. (2016). ELID grinding characteristics of SiCp/Al composites. *The International Journal of Advanced Manufacturing Technology*, 86(5-8), doi: 101165-1171. 148.

Ohmori, H., & Nakagawa, T. (1990). Mirror surface grinding of silicon wafers with electrolytic in-process dressing. *CIRP annals*, 39(1), 329-332.

Ohmori, H., & Nakagawa, T. (1995). Analysis of mirror surface generation of hard and brittle materials by ELID (electronic in-process dressing) grinding with superfine grain metallic bond wheels. *CIRP annals*, 44(1), 287-290.

Marinescu, I. D., Ohmori, H., & Katahira, K. (2011). Electrolytic in-process dressing (ELID) technologies: fundamentals and applications. CRC Press.

Bafakeeh, O. T., Khoshaim, A. B., & Marinescu, I. D. (2016). ELID fine grinding of sapphire rollers with emphasis on roughness and material removal rate. *Procedia Manufacturing*, 5, 1249-1264.

Prabhu, S., & Vinayagam, B. K. (2013). Analysis of surface characteristics by electrolytic in-process dressing (ELID) technique for grinding process using single wall carbon nano tube-based nanofluids. *Arabian Journal for Science and Engineering*, 38(5), 1169-1178.

Lee, E. S., & Kim, J. D. (1997). A study on the analysis of grinding mechanism and development of dressing system by using optimum in-process electrolytic

dressing. *International Journal of Machine Tools and Manufacture*, 37(12), 1673-1689.

Lee, E. S. (2000). A study of the development of an ultraprecision grinding system for mirror-like grinding. *The International Journal of Advanced Manufacturing Technology*, *16*(1), 1-9.

Yang, L., Ren, C., & Jin, X. (2010). Experimental study of ELID grinding based on the active control of oxide layer. *Journal of materials processing technology*, 210(13), 1748-1753.

Klocke, F., Klink, A., & Henerichs, M. (2009). ELID dressing behavior of fine grained bronze bonded diamond grinding wheels. *International Journal of Abrasive Technology*, 2(4), 358-367.

Pavel, R., Pavel, M., & Marinescu, I. (2004). Investigation of pre-dressing time for ELID grinding technique. *Journal of materials processing technology*, 149(1-3), 591-596.

Chen, H., & Li, J. C. (2000). Anodic metal matrix removal rate in electrolytic in-process dressing I: Two-dimensional modeling. *Journal of Applied Physics*, 87(6), 3151-3158.

Biswas, I., Kumar, A. S., & Rahman, M. (2010). Experimental study of wheel wear in electrolytic in-process dressing and grinding. *The International Journal of Advanced Manufacturing Technology*, 50(9-12), 931-940.

Klocke, F., Klink, A., & Schneider, U. (2007). Electrochemical oxidation analysis for dressing bronze-bonded diamond grinding wheels. *Production Engineering,* 1(2), 141-148.

Appendix A

SEM Images

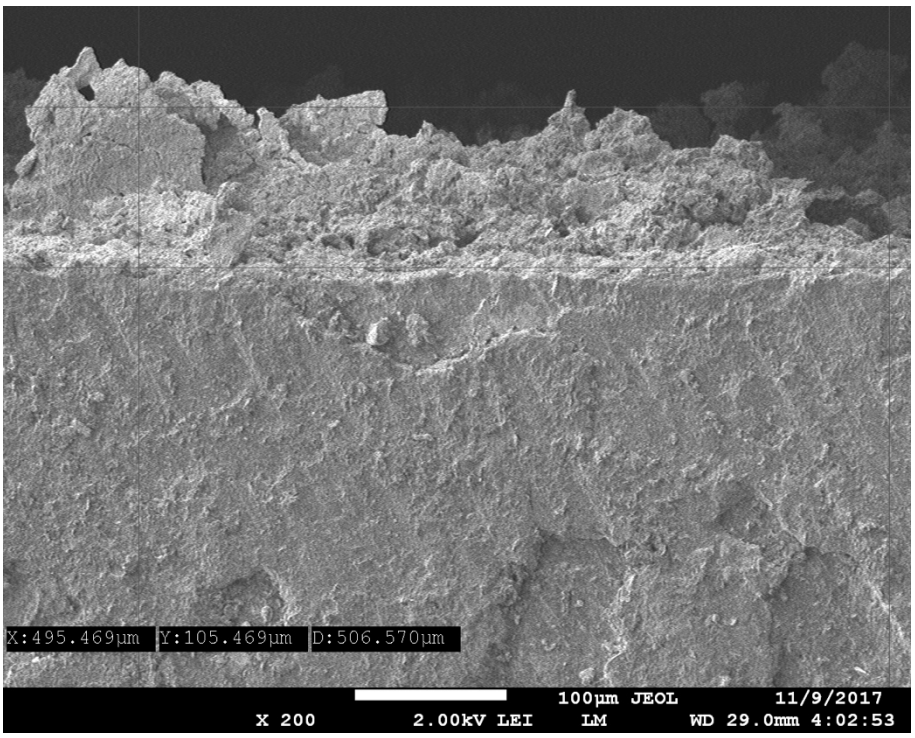
X:495.469µm Y:105.469µm D:506.570µm
100µm JEOL 11/9/2017
X 200 2.00kV LEI LM WD 29.0mm 4:02:53

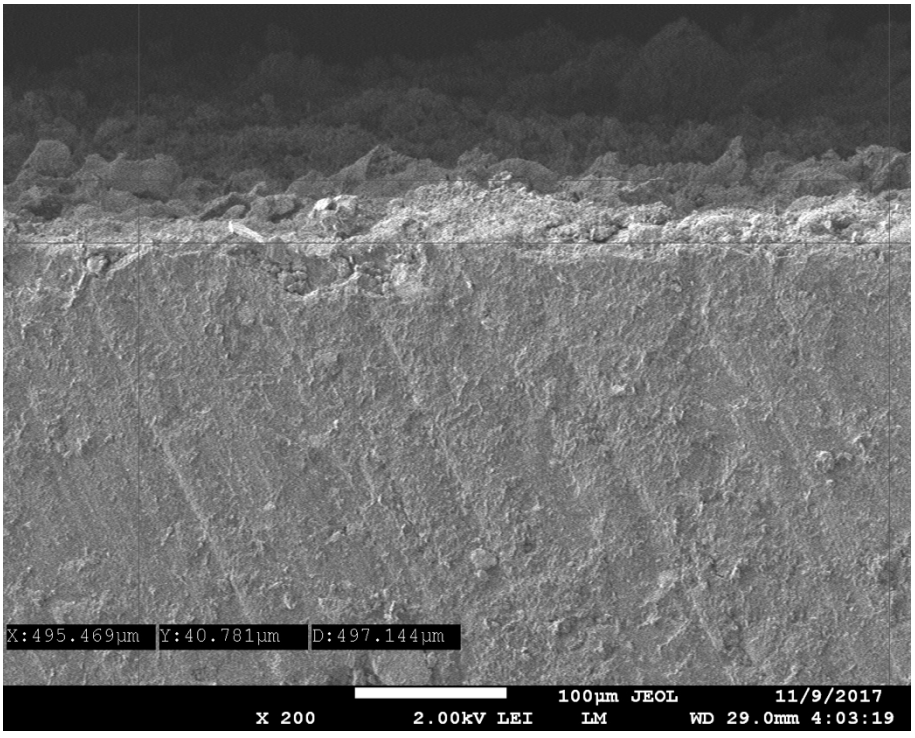
X:495.469µm Y:40.781µm D:497.144µm
100µm JEOL 11/9/2017
X 200 2.00kV LEI LM WD 29.0mm 4:03:19

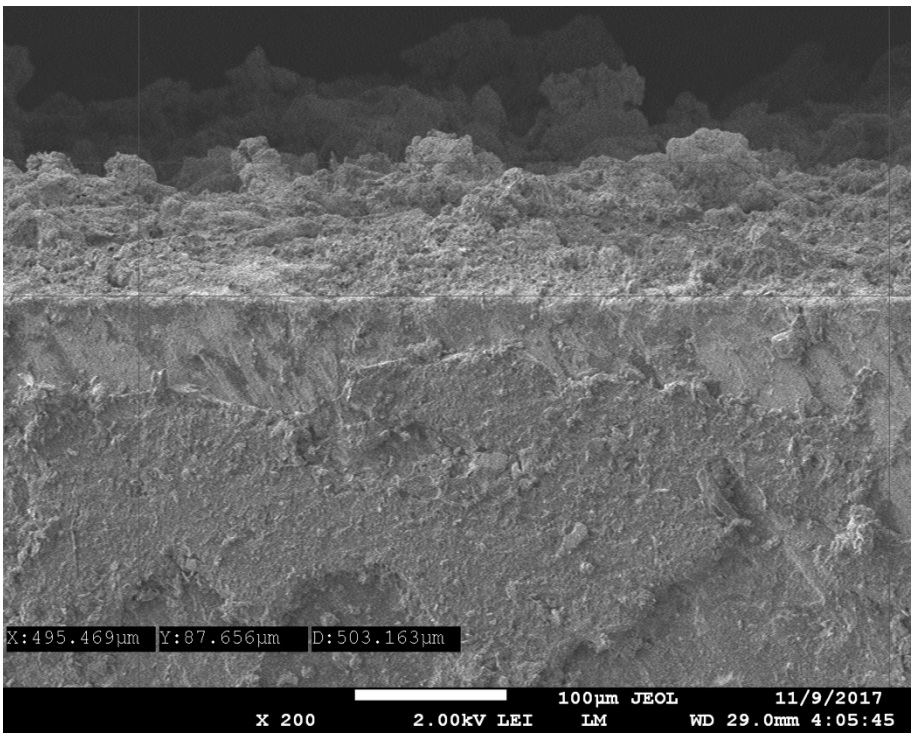
X:495.469µm
Y:87.656µm
D:503.163µm
100µm JEOL
11/9/2017
X 200
2.00kV LEI
LM
WD 29.0mm 4:05:45

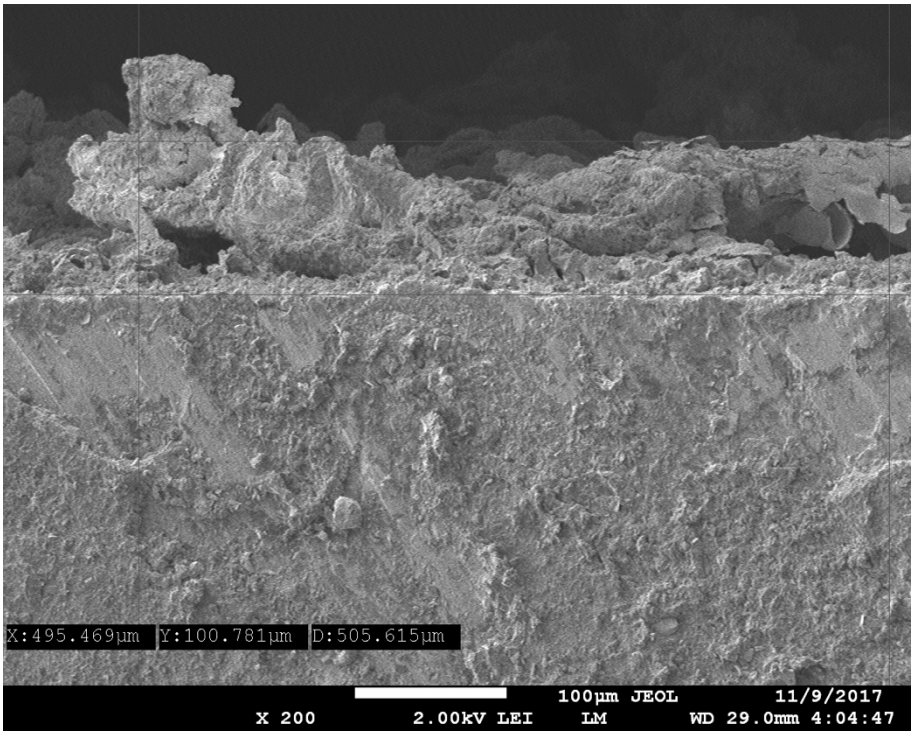
X:495.469µm
Y:100.781µm
D:505.615µm
100µm JEOL
11/9/2017
X 200
2.00kV LEI
LM
WD 29.0mm 4:04:47

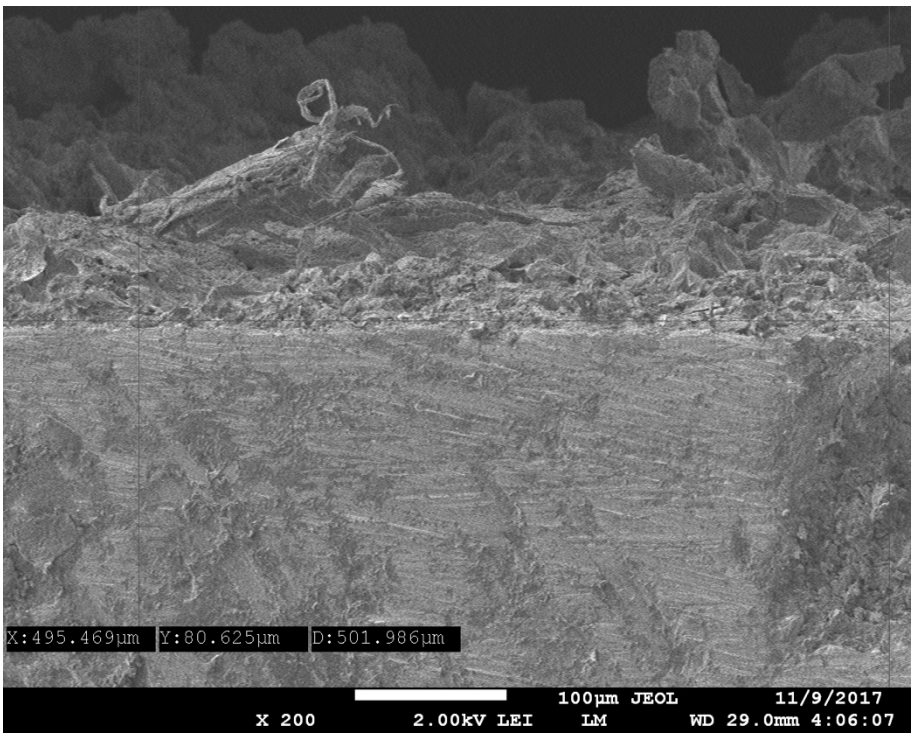
X:495.469µm
Y:80.625µm
D:501.986µm
100µm JEOL
11/9/2017
X 200
2.00kV LEI
LM
WD 29.0mm 4:06:07

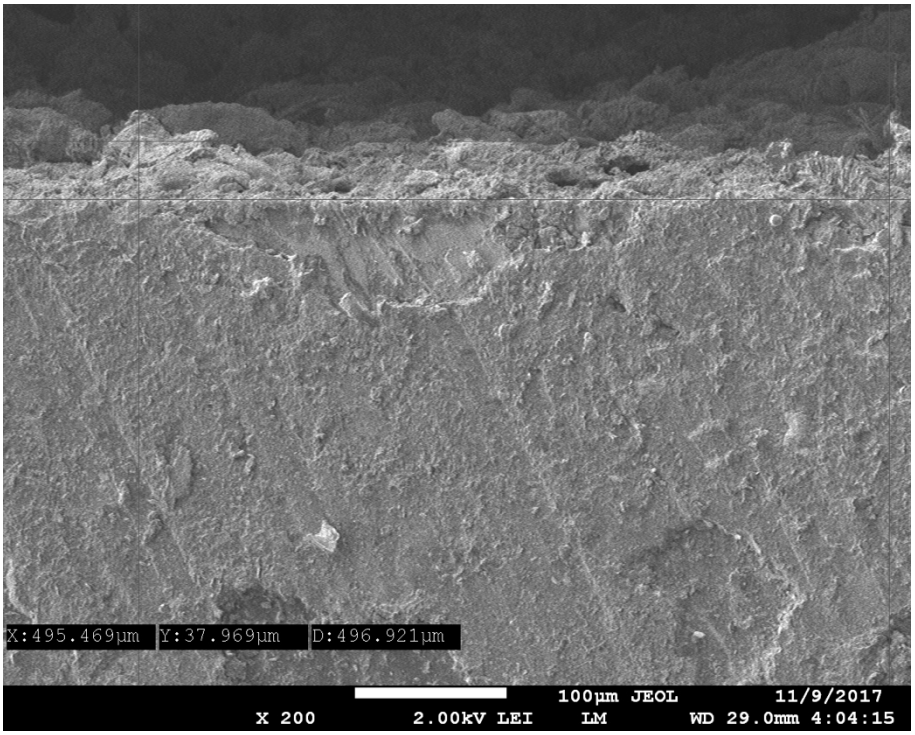
X:495.469µm
Y:37.969µm
D:496.921µm
100µm JEOL
11/9/2017
X 200
2.00kV LEI
LM
WD 29.0mm 4:04:15

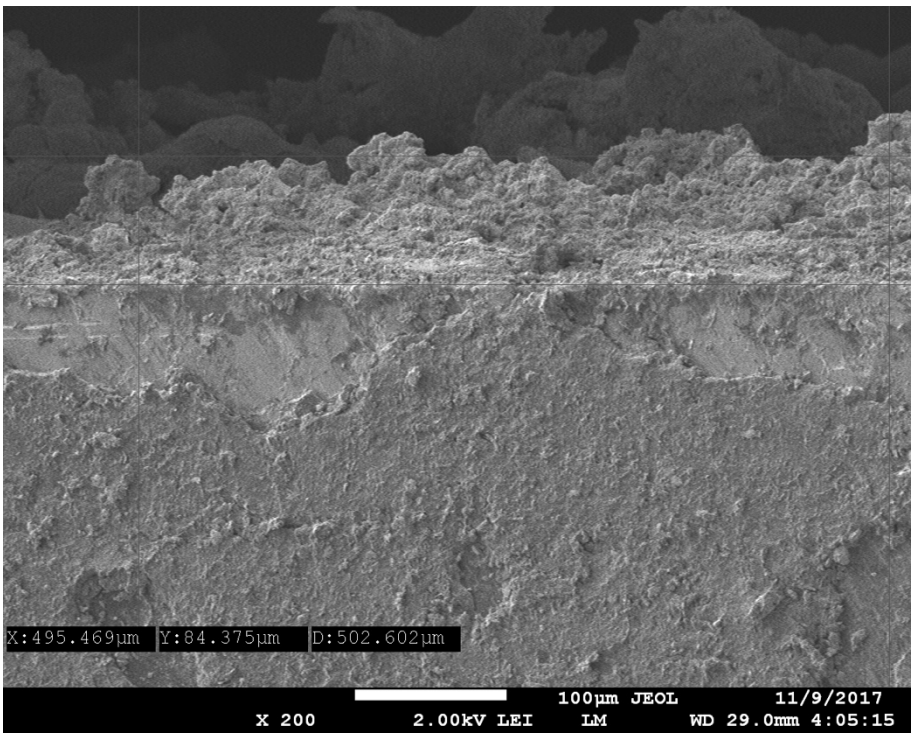
X:495.469µm
Y:84.375µm
D:502.602µm
100µm JEOL
11/9/2017
X 200
2.00kV LEI
LM
WD 29.0mm 4:05:15

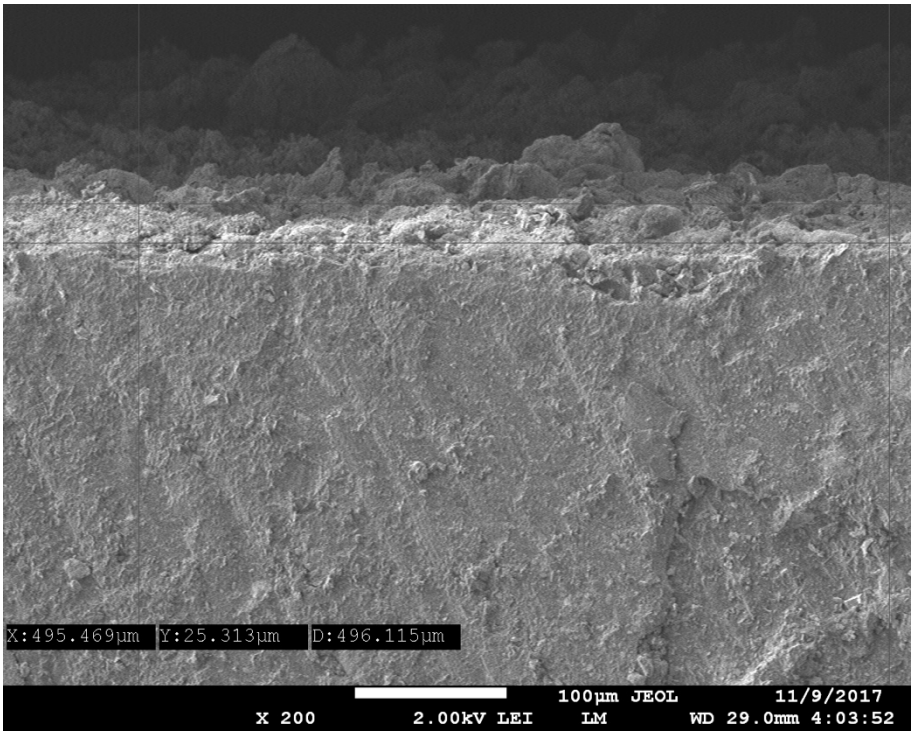
X:495.469µm
Y:25.313µm
D:496.115µm
100µm JEOL
11/9/2017
X 200
2.00kV LEI
LM
WD 29.0mm 4:03:52

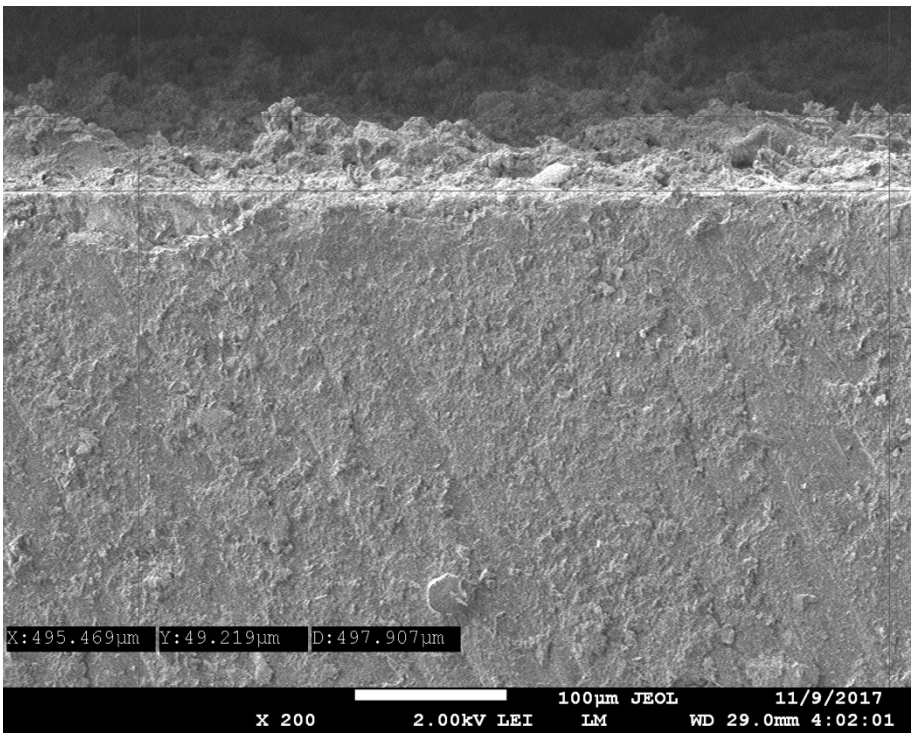
X:495.469µm
Y:49.219µm
D:497.907µm
100µm JEOL
11/9/2017
X 200
2.00kV LEI
LM
WD 29.0mm 4:02:01

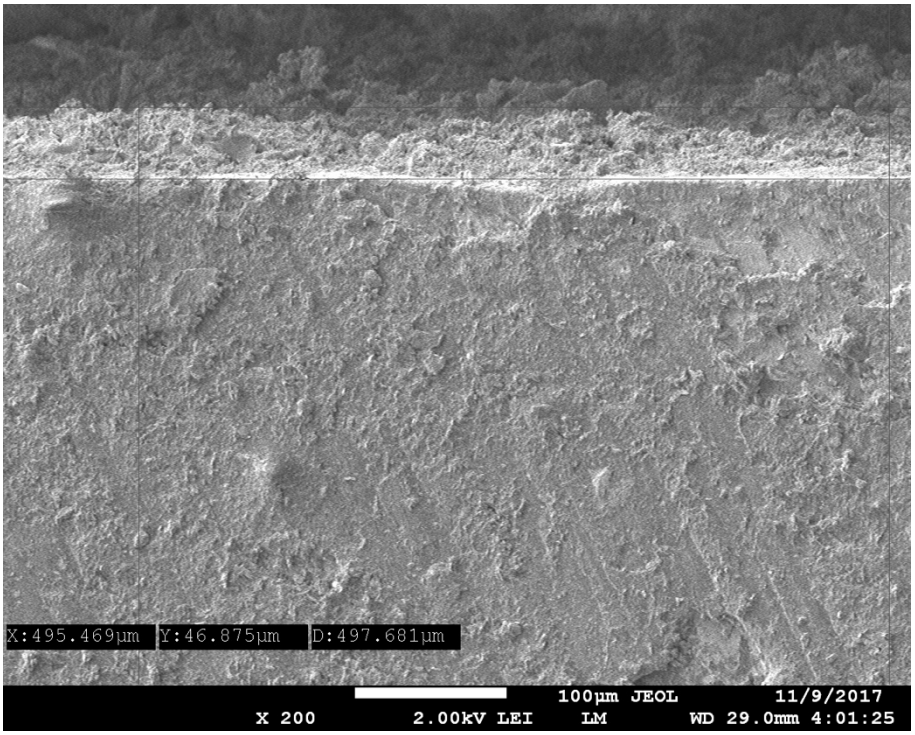
X:495.469µm
Y:46.875µm
D:497.681µm
100µm JEOL
11/9/2017
X 200
2.00kV LEI
LM
WD 29.0mm 4:01:25

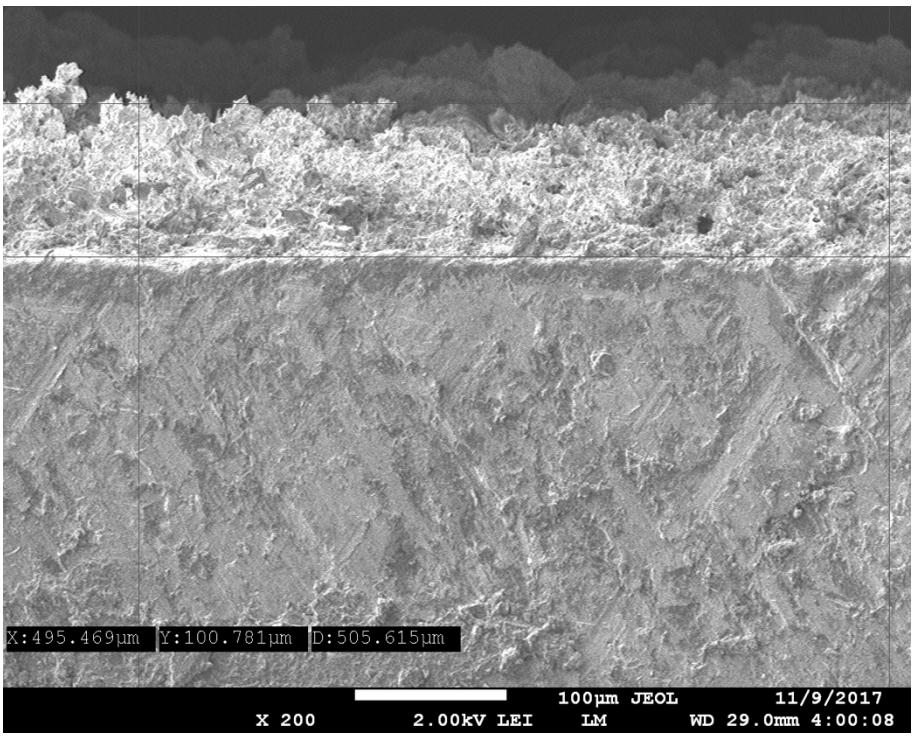
X:495.469µm
Y:100.781µm
D:505.615µm
100µm JEOL
11/9/2017
X 200
2.00kV LEI
LM
WD 29.0mm 4:00:08

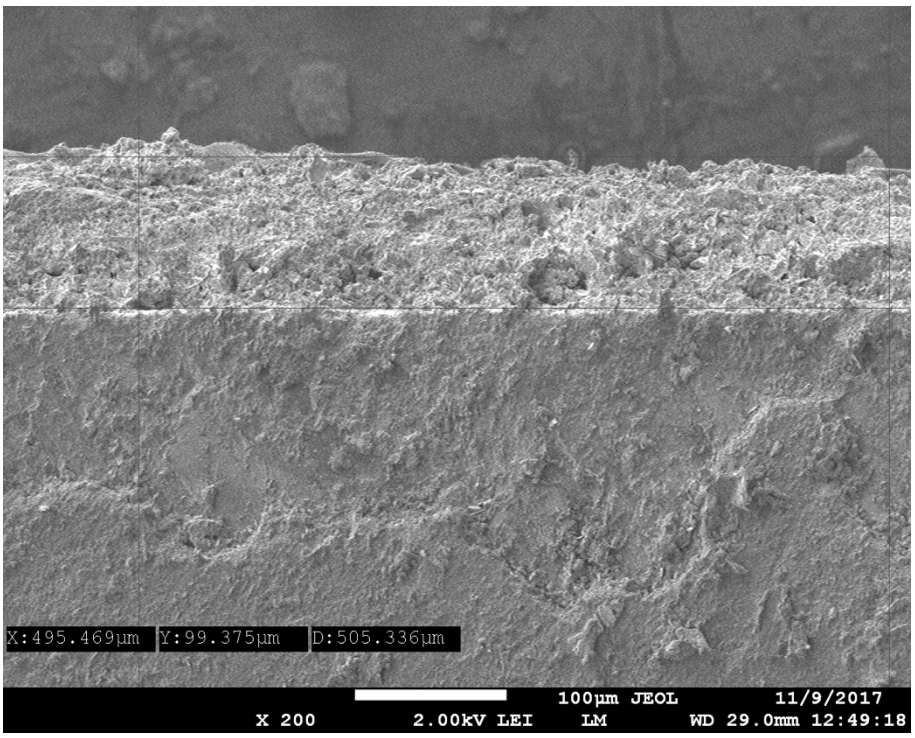
X:495.469µm
Y:99.375µm
D:505.336µm
100µm JEOL
11/9/2017
X 200
2.00kV LEI
LM
WD 29.0mm 12:49:18

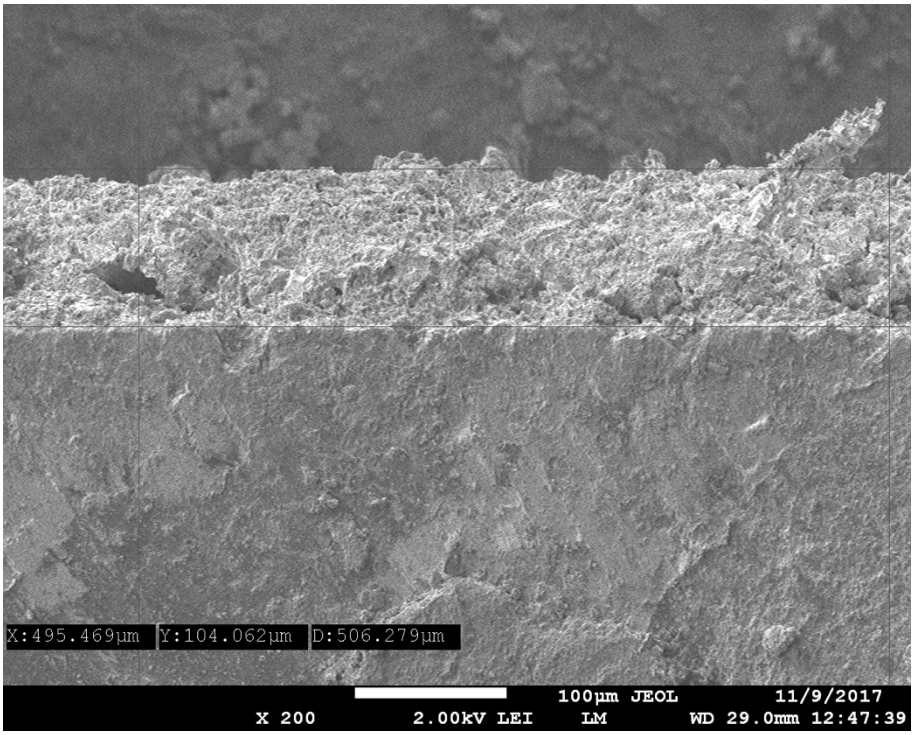
X:495.469µm
Y:104.062µm
D:506.279µm
100µm JEOL
11/9/2017
X 200
2.00kV LEI
LM
WD 29.0mm 12:47:39

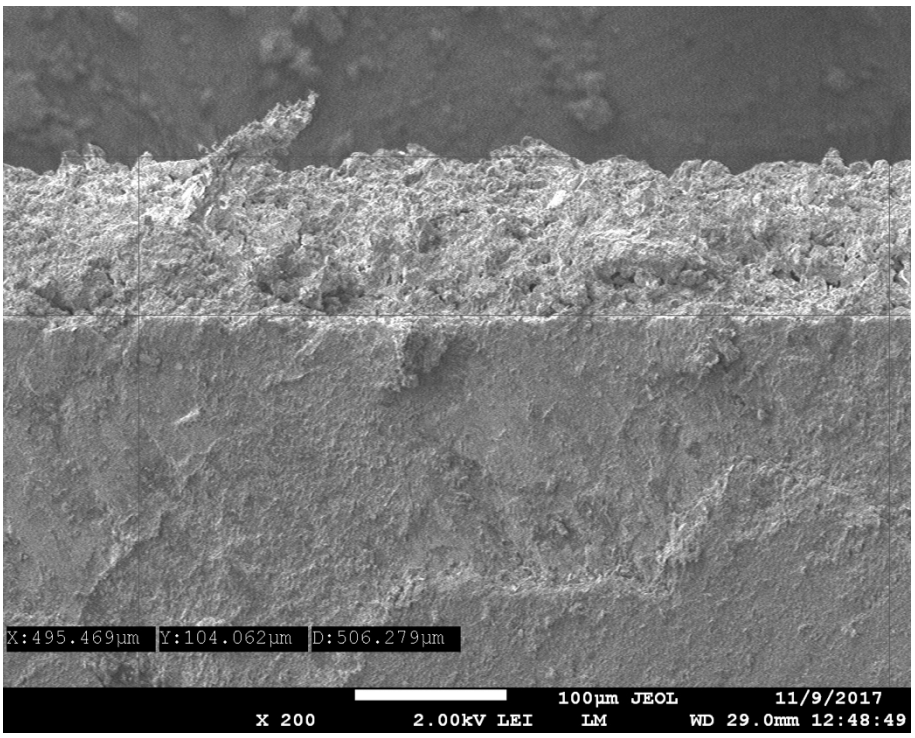
X:495.469µm Y:104.062µm D:506.279µm
100µm JEOL 11/9/2017
X 200 2.00kV LEI LM WD 29.0mm 12:48:49

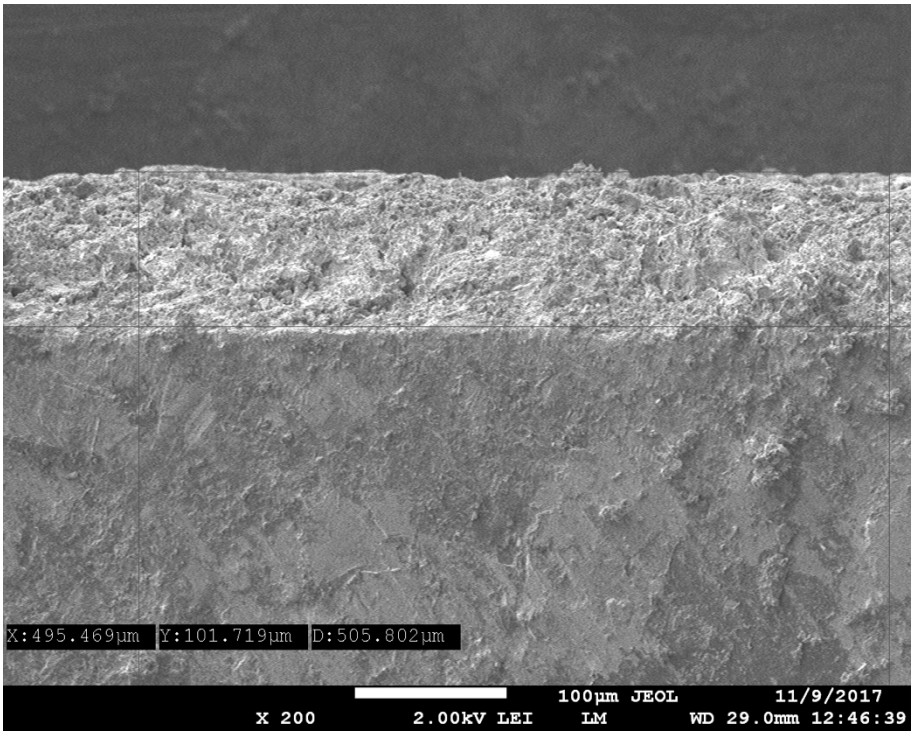
X:495.469µm Y:101.719µm D:505.802µm
100µm JEOL 11/9/2017
X 200 2.00kV LEI LM WD 29.0mm 12:46:39

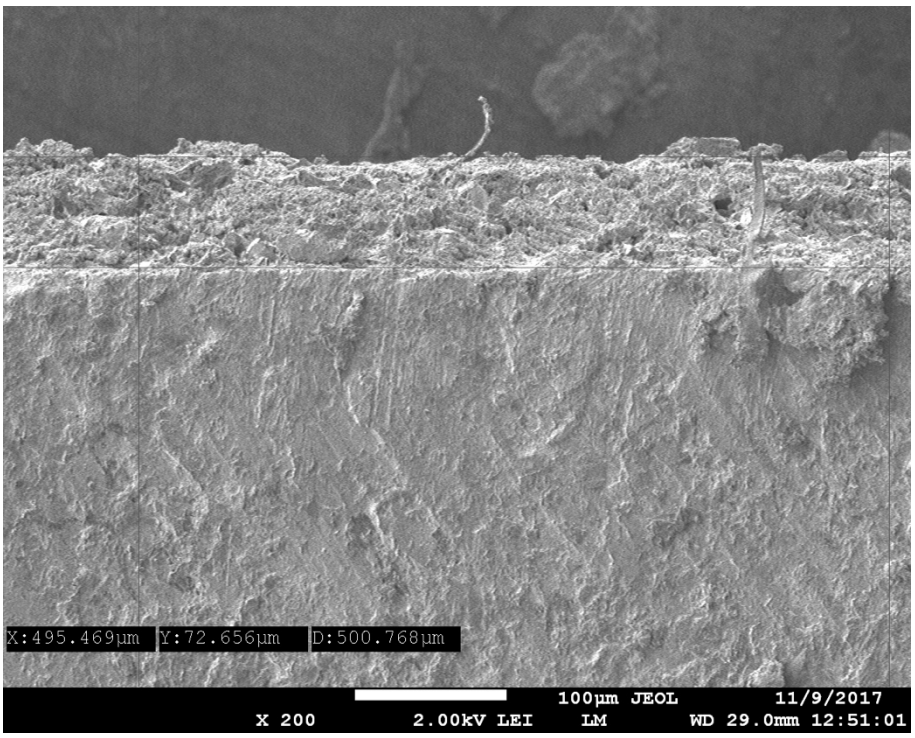
X:495.469µm
Y:72.656µm
D:500.768µm
100µm JEOL
11/9/2017
X 200
2.00kV LEI
LM
WD 29.0mm 12:51:01

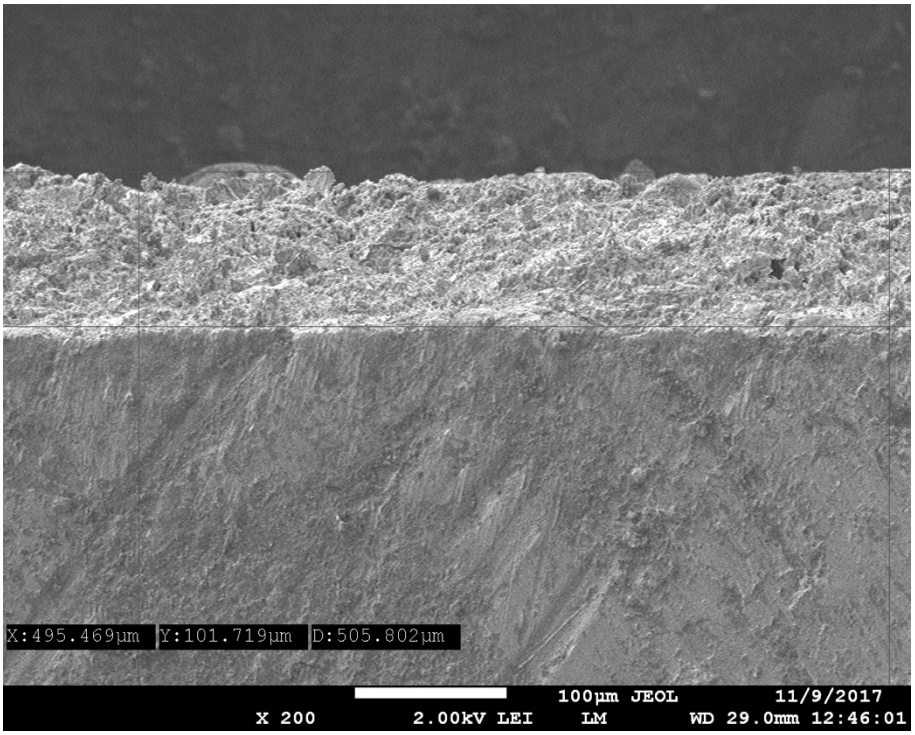
X:495.469µm
Y:101.719µm
D:505.802µm
100µm JEOL
11/9/2017
X 200
2.00kV LEI
LM
WD 29.0mm 12:46:01

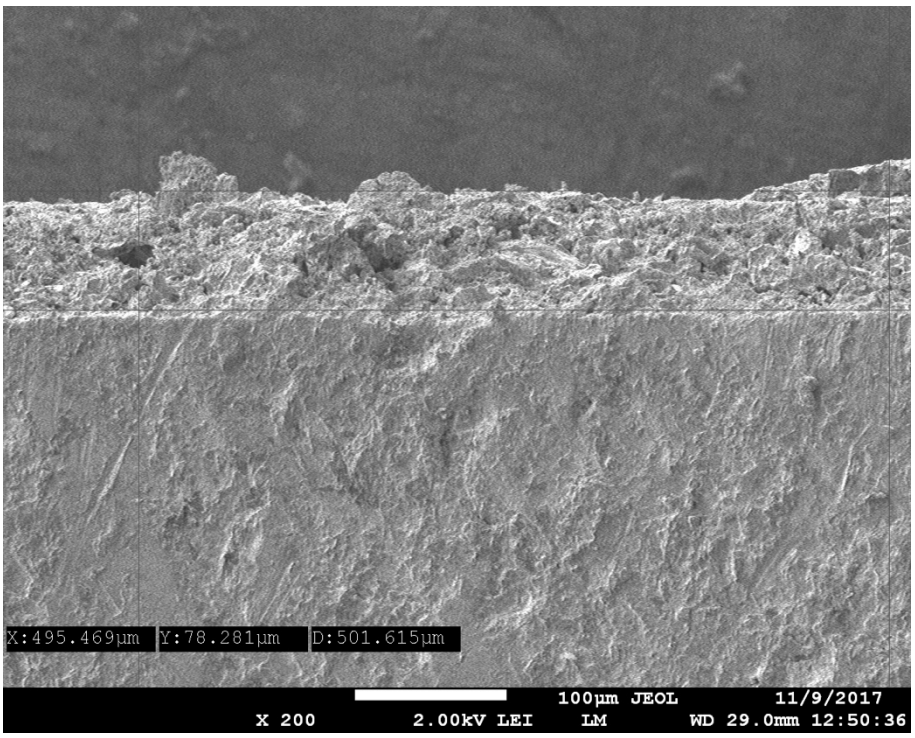
X:495.469µm
Y:78.281µm
D:501.615µm
100µm JEOL
11/9/2017
X 200
2.00kV LEI
LM
WD 29.0mm 12:50:36

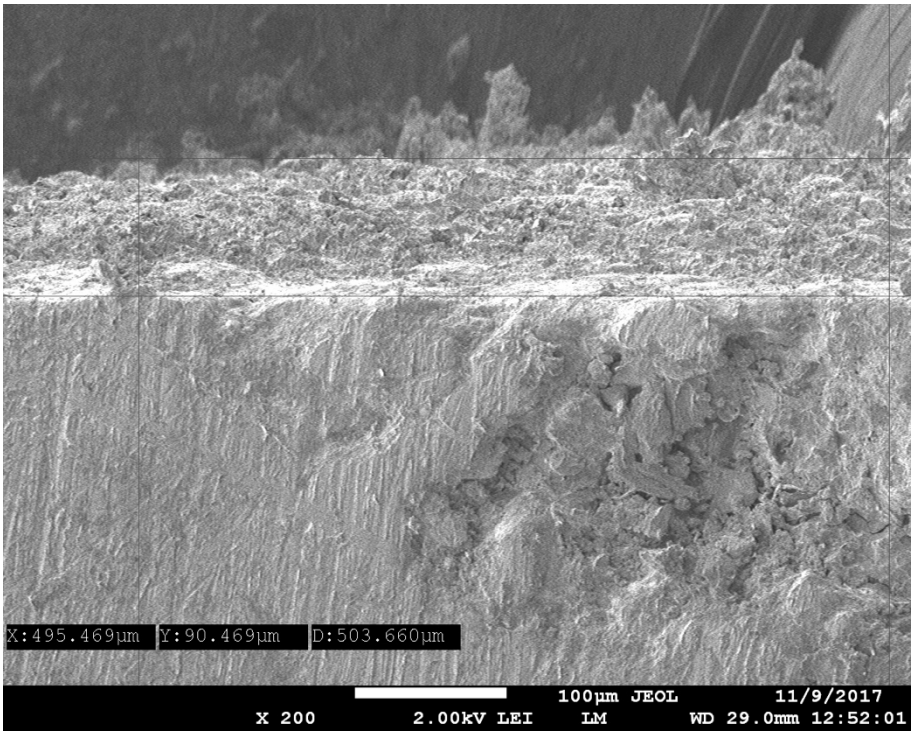
X:495.469µm
Y:90.469µm
D:503.660µm
100µm JEOL
11/9/2017
X 200
2.00kV LEI
LM
WD 29.0mm 12:52:01

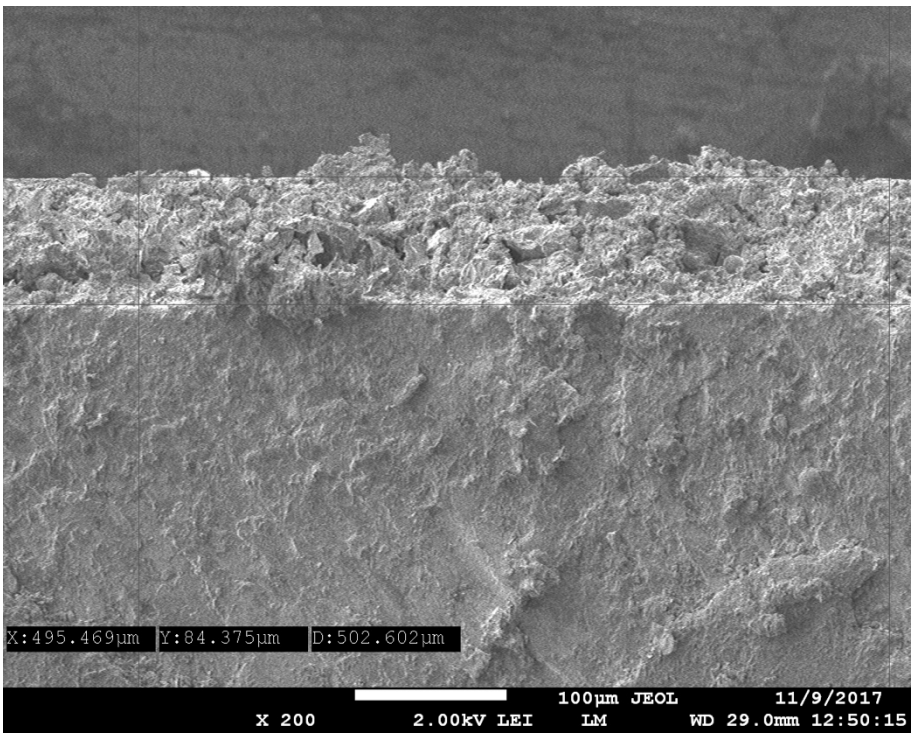
X:495.469µm
Y:84.375µm
D:502.602µm
100µm JEOL
11/9/2017
X 200
2.00kV LEI
LM
WD 29.0mm 12:50:15

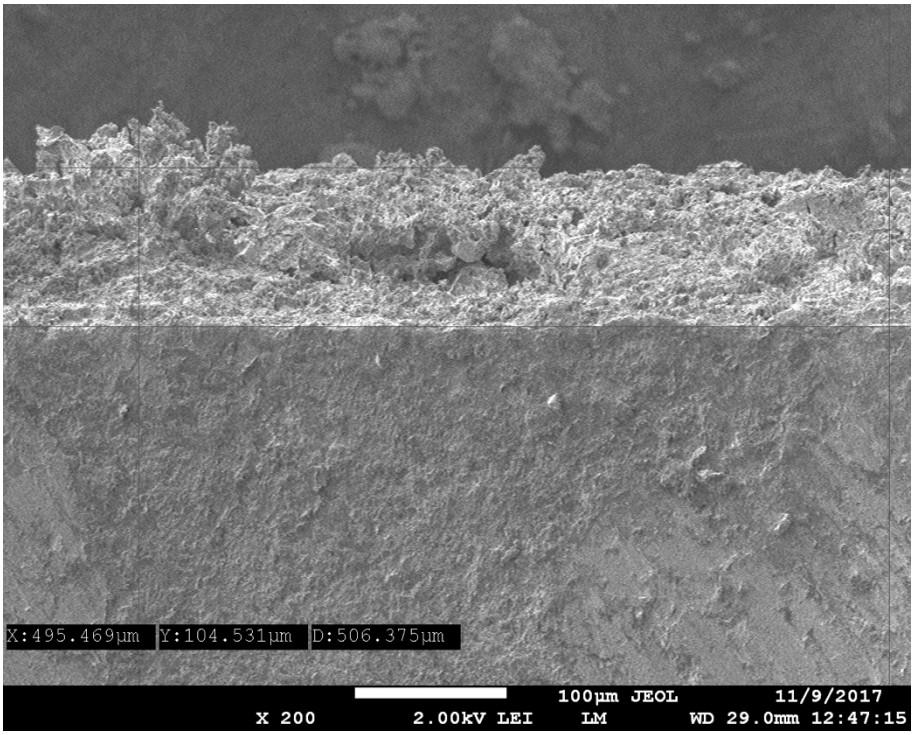
X:495.469µm
Y:104.531µm
D:506.375µm
100µm JEOL
11/9/2017
X 200
2.00kV LEI
LM
WD 29.0mm 12:47:15

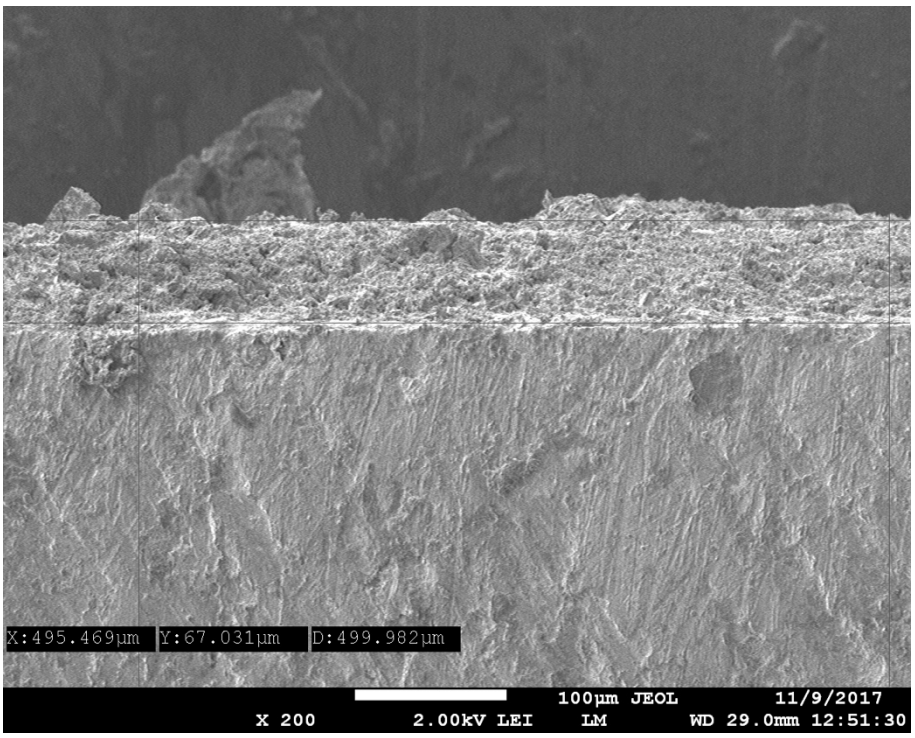
X:495.469µm
Y:67.031µm
D:499.982µm
100µm JEOL
11/9/2017
X 200
2.00kV LEI
LM
WD 29.0mm 12:51:30

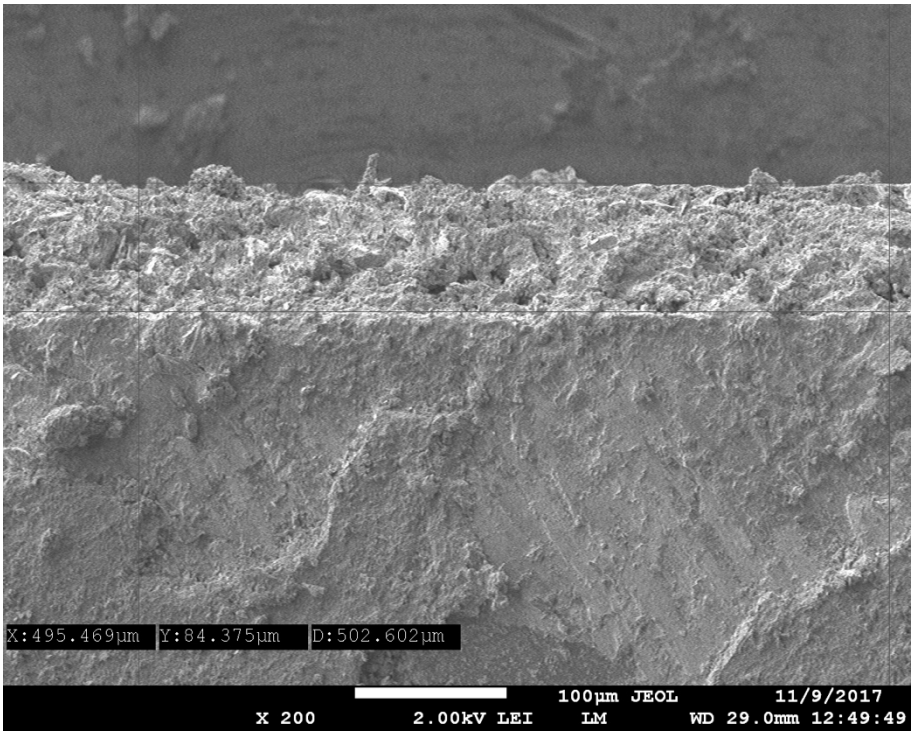
X:495.469µm
Y:84.375µm
D:502.602µm
100µm JEOL
11/9/2017
X 200
2.00kV LEI
LM
WD 29.0mm 12:49:49

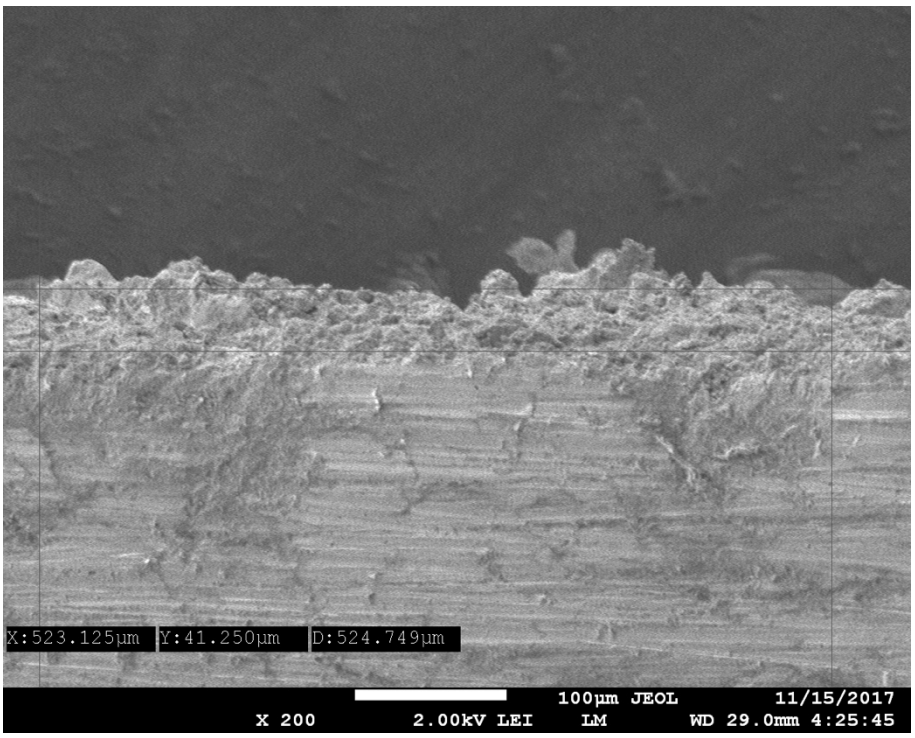
X:523.125µm Y:41.250µm D:524.749µm
100µm JEOL 11/15/2017
X 200 2.00kV LEI LM WD 29.0mm 4:25:45

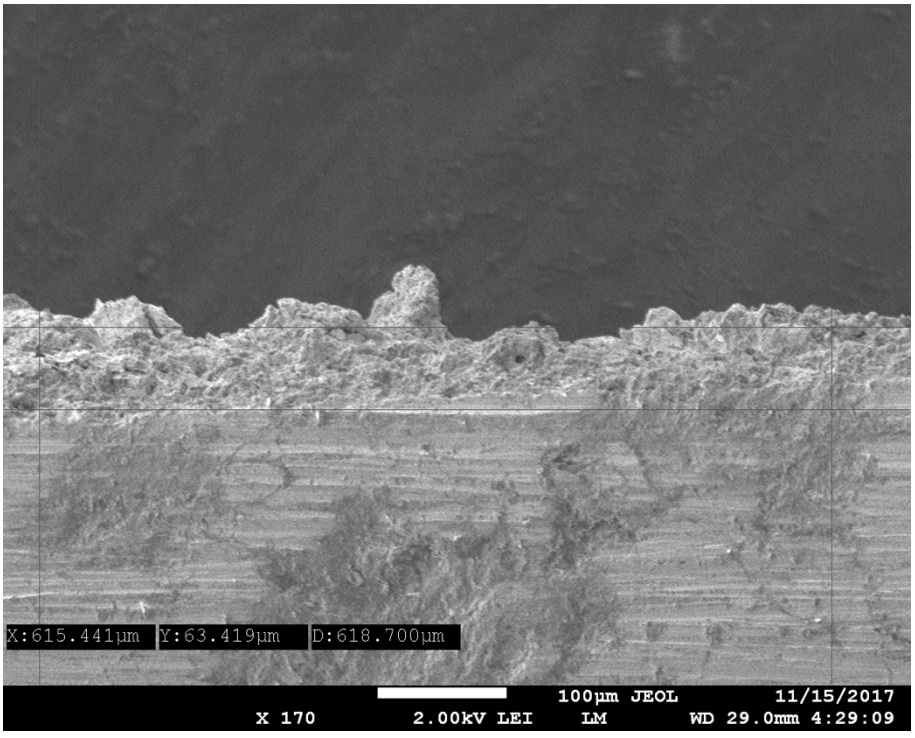
X:615.441µm Y:63.419µm D:618.700µm
100µm JEOL 11/15/2017
X 170 2.00kV LEI LM WD 29.0mm 4:29:09

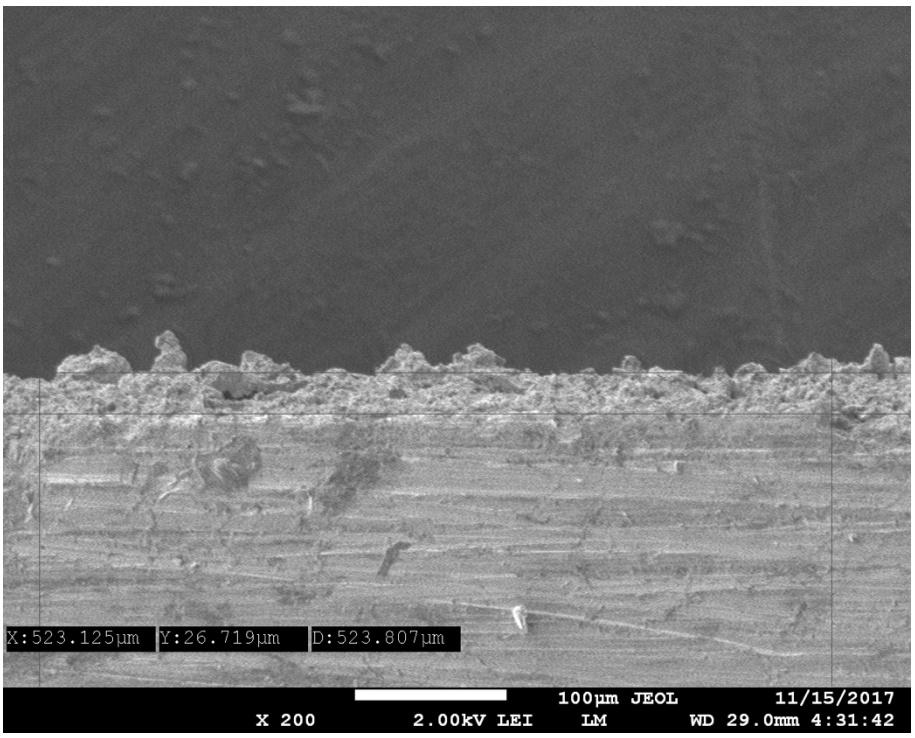
X:523.125µm Y:26.719µm D:523.807µm
100µm JEOL 11/15/2017
X 200 2.00kV LEI LM WD 29.0mm 4:31:42

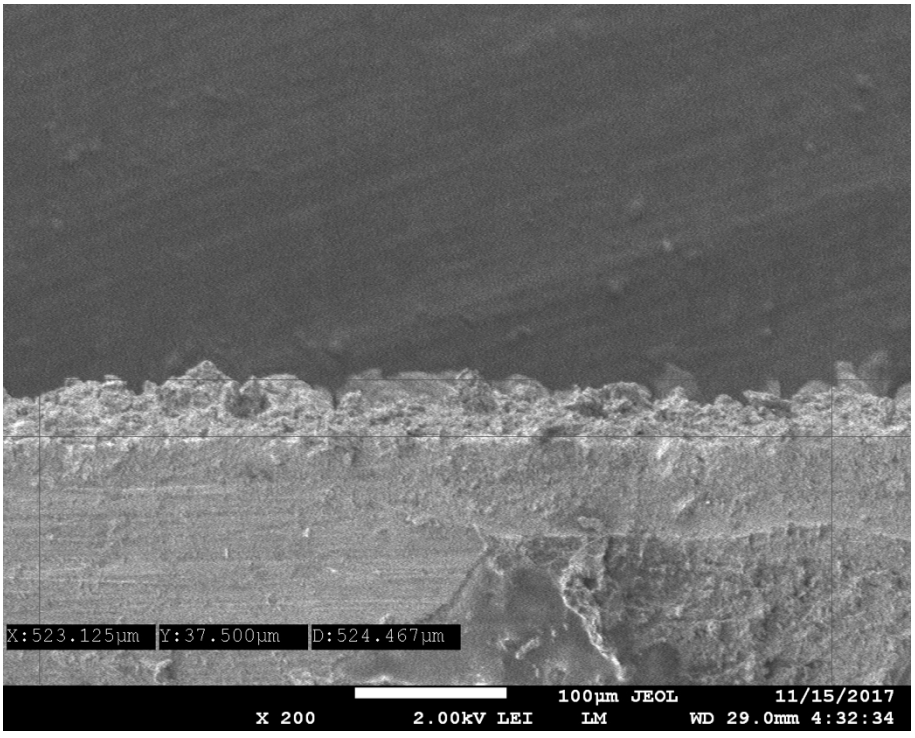
X:523.125µm Y:37.500µm D:524.467µm
100µm JEOL 11/15/2017
X 200 2.00kV LEI LM WD 29.0mm 4:32:34

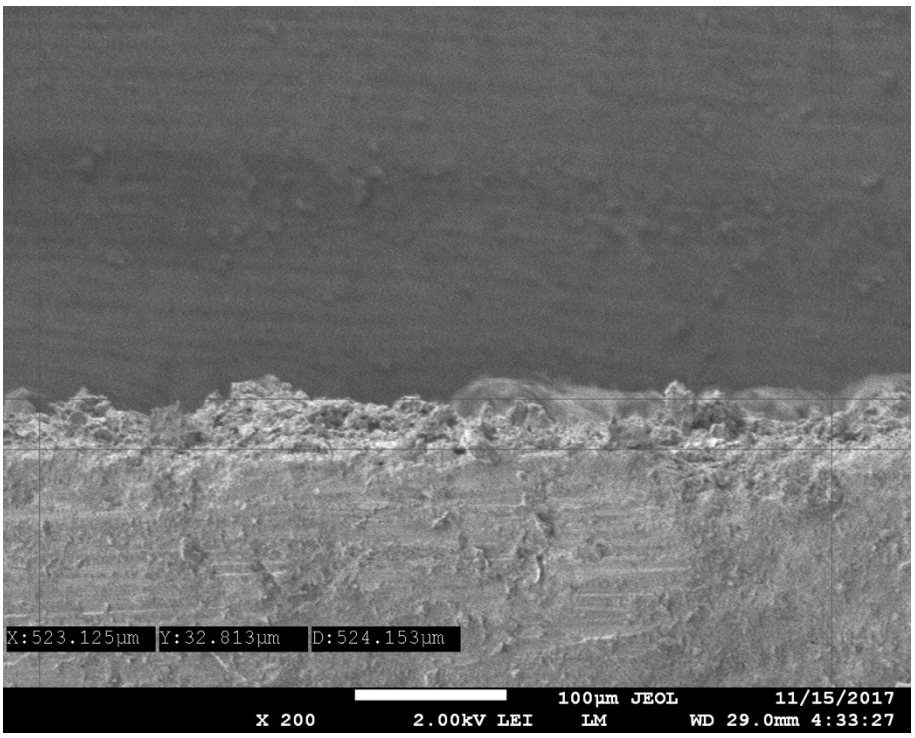
X:523.125µm
Y:32.813µm
D:524.153µm
100µm JEOL
11/15/2017
X 200
2.00kV LEI
LM
WD 29.0mm 4:33:27

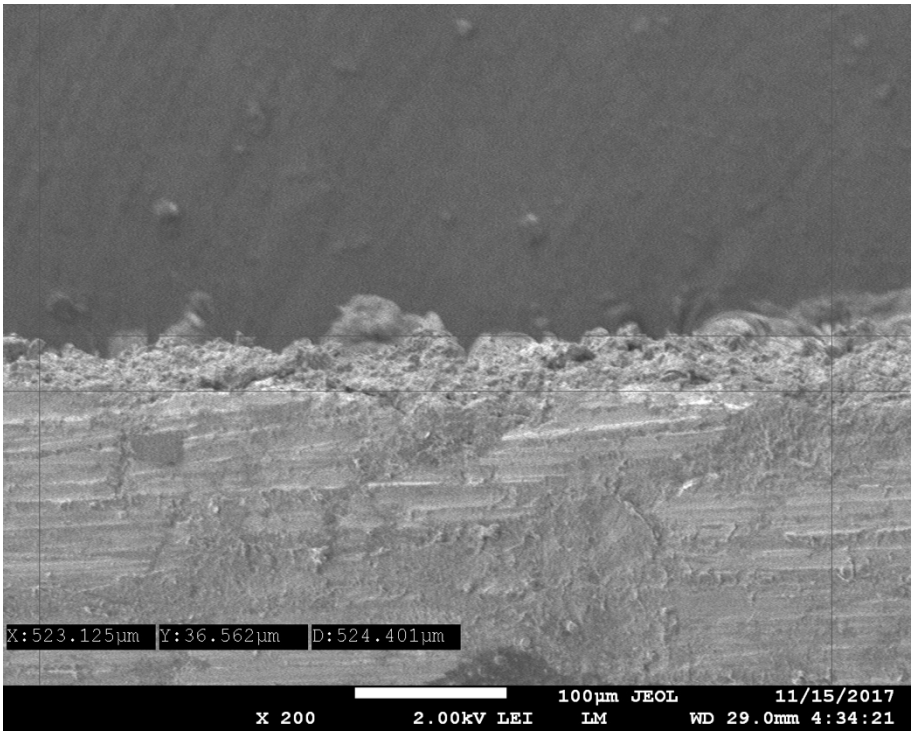
X:523.125µm
Y:36.562µm
D:524.401µm
100µm JEOL
11/15/2017
X 200
2.00kV LEI
LM
WD 29.0mm 4:34:21

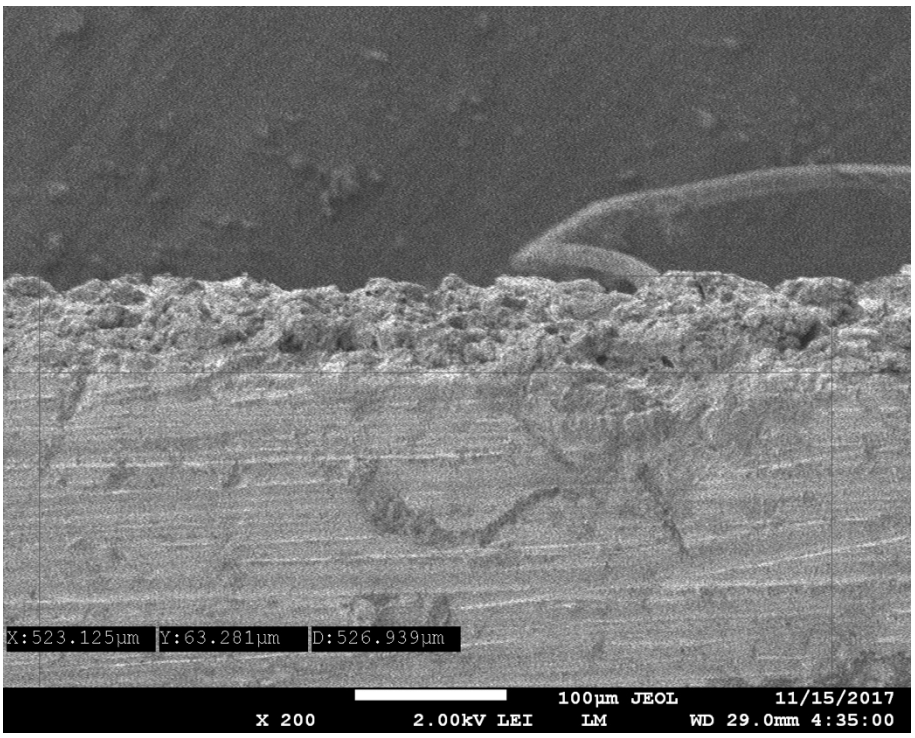
X:523.125µm Y:63.281µm D:526.939µm
100µm JEOL 11/15/2017
X 200 2.00kV LEI LM WD 29.0mm 4:35:00

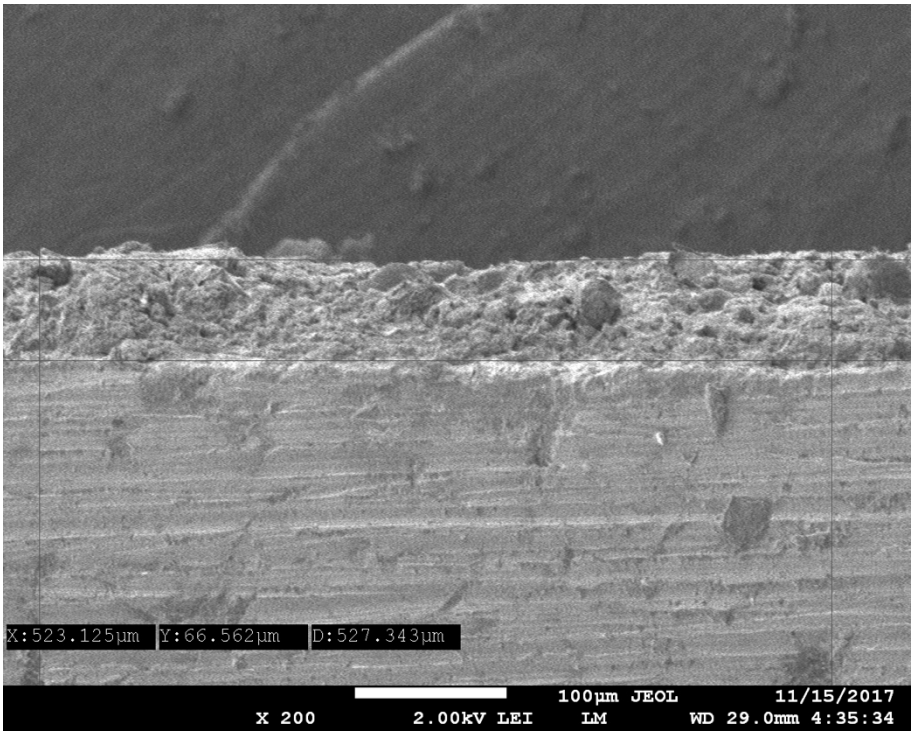
X:523.125µm Y:66.562µm D:527.343µm
100µm JEOL 11/15/2017
X 200 2.00kV LEI LM WD 29.0mm 4:35:34

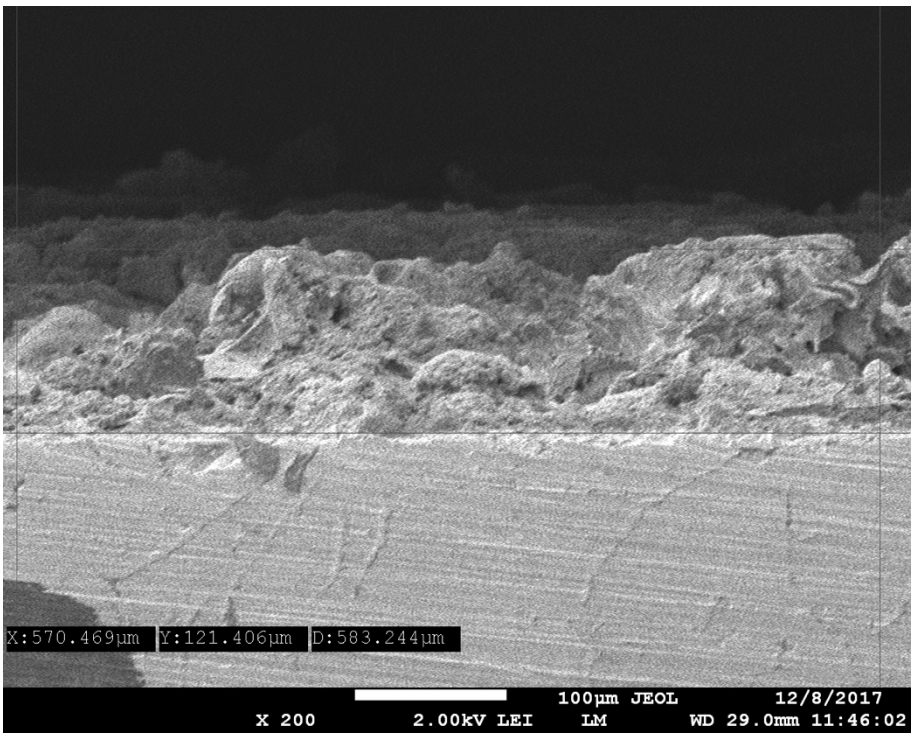
X:570.469µm Y:121.406µm D:583.244µm
100µm JEOL 12/8/2017
X 200 2.00kV LEI LM WD 29.0mm 11:46:02

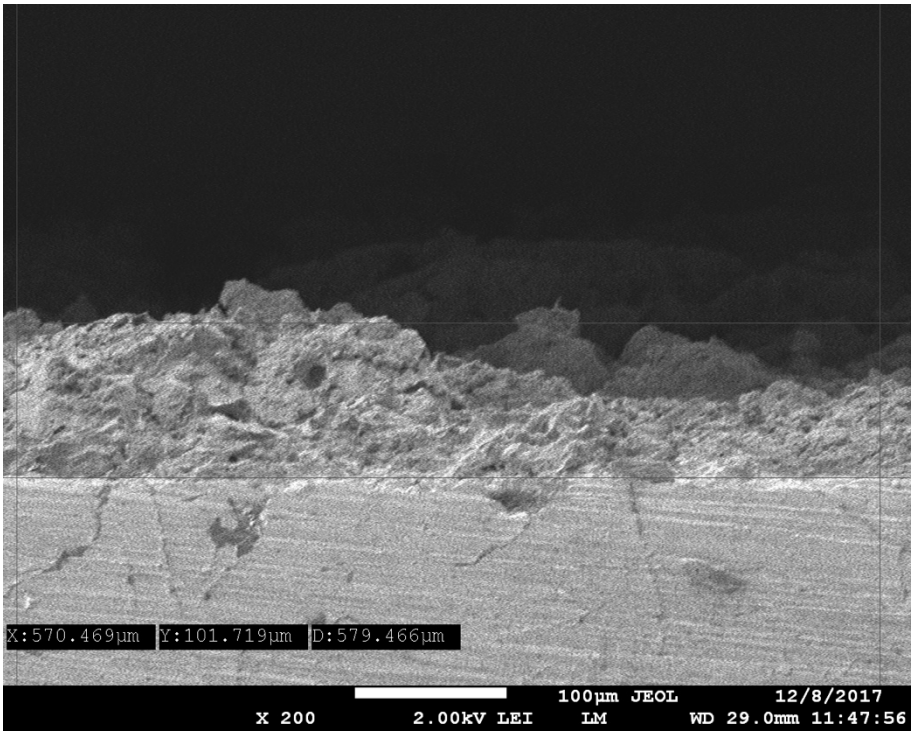
X:570.469µm Y:101.719µm D:579.466µm
100µm JEOL 12/8/2017
X 200 2.00kV LEI LM WD 29.0mm 11:47:56

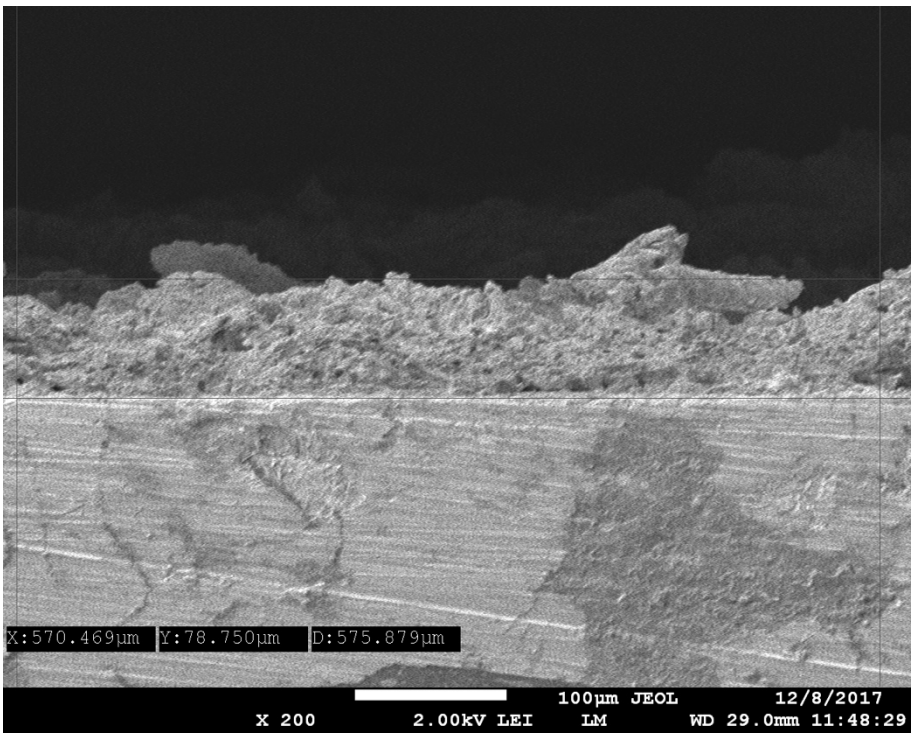
X:570.469µm
Y:78.750µm
D:575.879µm
100µm JEOL
12/8/2017
X 200
2.00kV LEI
LM
WD 29.0mm 11:48:29

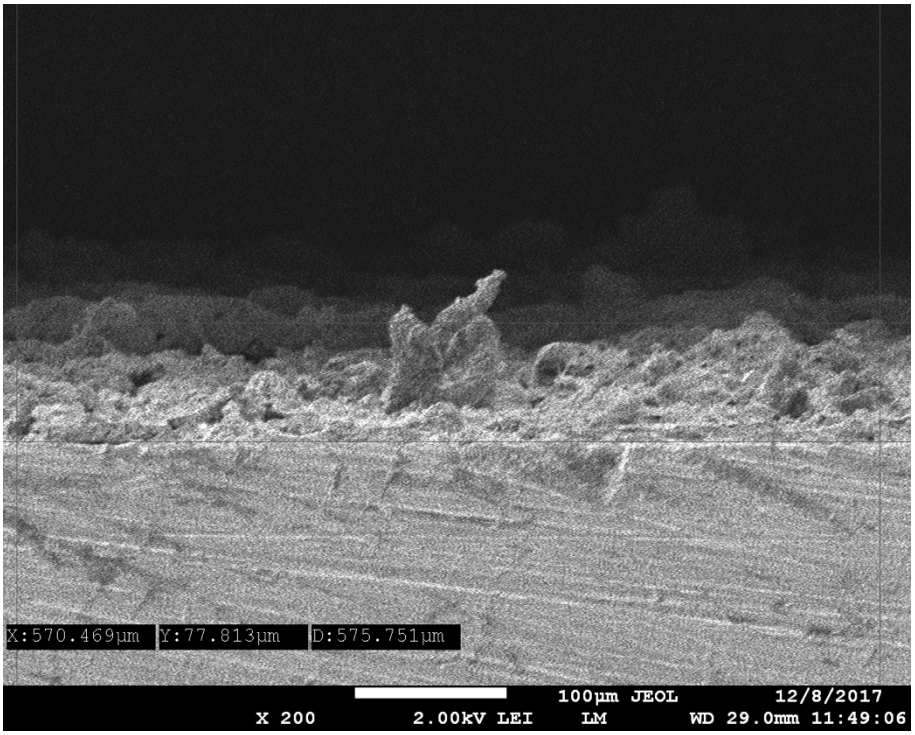
X:570.469µm
Y:77.813µm
D:575.751µm
100µm JEOL
12/8/2017
X 200
2.00kV LEI
LM
WD 29.0mm 11:49:06